PB86-117629

REPORT NO.
UCB/EERC-84/07
AUGUST 1984

EARTHQUAKE ENGINEERING RESEARCH CENTER

BEHAVIOR OF INTERIOR AND EXTERIOR FLAT PLATE CONNECTIONS SUBJECTED TO INELASTIC LOAD REVERSALS

by

HOWARD L. ZEE
JACK P. MOEHLE

Report to the National Science Foundation

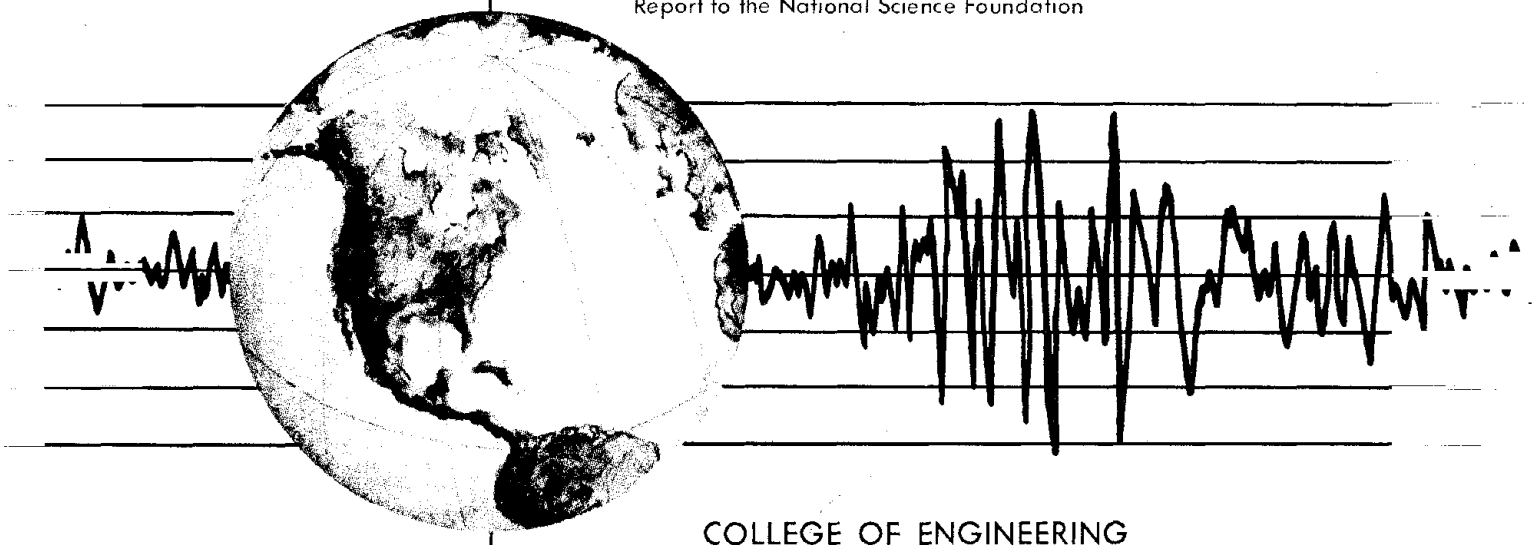

COLLEGE OF ENGINEERING

UNIVERSITY OF CALIFORNIA · Berkeley, California

For sale by the National Technical Information Service, U.S. Department of Commerce, Springfield, Virginia 22161.

See back of report for up to date listing of EERC reports.

DISCLAIMER

50272-101

REPORT DOCUMENTATION PAGE	1. REPORT NO. NSF/CEE-84029	2.	3. Recipient's Accession No. PB86 117629
4. Title and Subtitle: Behavior of Interior and Exterior Flat Plate Connections subjected to Inelastic Load Reversals			5. Report Date: August 1984 6.
7. Author(s): Howard L. Zee and Jack P. Moehle			8. Performing Organization Rept. No. UCB/EERC-84/07
9. Performing Organization Name and Address: Earthquake Engineering Research Center University of California, Berkeley 1301 So. 46th Street Richmond, Calif. 94804			10. Project/Task/Work Unit No. 11. Contract(C) or Grant(G) No. (C) (G) CEE 8110050
12. Sponsoring Organization Name and Address: National Science Foundation 1800 G. Street, N.W. Washington, D.C. 20550			13. Type of Report & Period Covered 14.

15. Supplementary Notes

16. Abstract (Limit: 200 words)

Typical interior and exterior plate column connections occurring in a prototype reinforced concrete flat plate structure were modeled with three-tenths scale test specimens. The test specimens were subjected to both gravity loads and statically imposed lateral loads with reversals.

Design was in accordance with gravity load requirements of the ACI Building Code and the seismic lateral forces associated with Zone 2 of the 1982 Uniform Building Code. Reinforcement details satisfied the provisions of the 1983 ACI Code including special requirements for structures in regions of moderate seismic risk.

Deflection and deformation responses of the test specimens to the gravity and lateral loadings were monitored and recorded throughout the experiments. Existing analytical models for strengths and lateral load stiffnesses of plate column connections were studied by comparing model results with observed behavior. Stiffness models included equivalent beam width and equivalent frame models. Plate column connection strengths were calculated by the procedure suggested in ACI 318-83 and by beam analogies.

Conclusions are drawn in the last chapter regarding the deformation responses of the specimens and the effectiveness of the analytical models.

17. Document Analysis a. Descriptors

b. Identifiers/Open-Ended Terms

c. COSATI Field/Group

18. Availability Statement: Release Unlimited	19. Security Class (This Report)	21. No. of Pages: 143
	20. Security Class (This Page)	22. Price: A07

BEHAVIOR OF INTERIOR AND EXTERIOR FLAT PLATE CONNECTIONS SUBJECTED TO INELASTIC LOAD REVERSALS

by

Howard L. Zee
Research Assistant
University of California, Berkeley

Jack P. Moehle
Assistant Professor of Civil Engineering
University of California, Berkeley

Report to Sponsor:
National Science Foundation

Report No. UCB/EERC-84/07
Earthquake Engineering Research Center
College of Engineering
University of California
Berkeley, California

August 1984

ABSTRACT

A typical interior and exterior plate column connection occurring in a prototype reinforced concrete flat plate structure were modeled with three-tenths scale test specimens. The test specimens were subjected to both gravity loads and statically imposed lateral loads with reversals.

Design was in accordance with gravity load requirements of the ACI Building Code [3] and the seismic lateral forces associated with Zone 2 of the 1982 Uniform Building Code [8]. Reinforcement details satisfied the provisions of the 1983 ACI Code (ACI 318-83) [3] including special requirements for structures in regions of moderate seismic risk.

Deflection and deformation responses of the test specimens to the gravity and lateral loadings were monitored and recorded throughout the experiments. Existing analytical models for strengths and lateral load stiffnesses of plate column connections were studied by comparing model results with observed behavior. Stiffness models included equivalent beam width and equivalent frame models. Plate column connection strengths were calculated by the procedure suggested in ACI 318-83 and by beam analogies.

Conclusions are drawn in the last chapter regarding the deformation responses of the specimens and the effectiveness of the analytical models.

ACKNOWLEDGEMENTS

This study was sponsored by the National Science Foundation under grant No. CEE 8110050. The support is gratefully acknowledged. Opinions, findings, and conclusions or recommendations expressed in this publication are those of the authors and do not necessarily reflect the views of the National Science Foundation or the Earthquake Engineering Research Center, University of California, Berkeley.

The advice and assistance of John Diebold throughout this study is greatly appreciated. The assistance of Roy Stephen with instrumentation and testing is also appreciated. Data reduction software was developed by Christopher Thewalt. Figures were drafted by Mary Edmunds. Their contributions are acknowledged and appreciated. Finally, acknowledgement is due to George Hayler and the Civil Engineering machine shop staff for their contributions to this study.

TABLE OF CONTENTS

LIST OF TABLES

LIST OF FIGURES

LIST OF NOTATION

A_c = area of concrete at critical section

b = larger dimension of rectangular portion of lateral torsional member cross section

c, c_2 = column width

C = torsional constant

d = effective slab depth

E = Young's modulus

f'_c = concrete compressive strength

f_y = yield stress of longitudinal reinforcement

f_{wy} = yield stress of transverse reinforcement

h = slab thickness

I_g = gross section inertia

I'_g = modified inertia

J_c = section property similar to polar moment of inertia

K_t = torsional stiffness of lateral torsional members

l = distance between pinned ends of reaction link

L = transverse slab dimension

L_2 = clear span between adjacent exterior columns

M_f = moment capacity of flexural beam

M_s = unbalanced moment capacity

$\gamma_v M_s$ = moment transferred by eccentricity of shear about centroid of the critical slab section

P_{max} = lateral load capacity

t_1 = smaller dimension of rectangular portion of lateral

torsional member cross section

T_{co}, T_{uo} = torsion capacity in absence of shear

T_u = ultimate torsional capacity

v_c = concrete shear stress capacity

v_u = maximum shear stress

V_u = ultimate direct shear force on connection

V_{uo} = shear capacity

δh = horizontal deflection of reaction link at slab level

δv = vertical deflection of reaction link at slab level

β = effective inertia coefficient

1. INTRODUCTION

1.1 The Flat Plate

The flat plate is a popular structural system for carrying gravity loads because of economies in design and construction permitted by its use. However, the flat plate system, which consists of reinforced concrete slabs supported directly on reinforced concrete columns without beams, capitals, or drop panels at interior supports, by itself may not be a viable structural system when lateral loads must be resisted. The slab-column connections are relatively flexible under lateral loads, a condition which may result in severe structural and nonstructural damage as excessive lateral drifts occur. Also, transfer of shear and unbalanced moment between column and slab is inefficient when connections lack capitals, drop panels, and beams. The concentration of shear and unbalanced moment could result in a brittle punching shear failure leading to, in the worst case, a progressive collapse of the entire structure.

Despite the apparent deficiencies of the flat plate system when subjected to lateral loads, flat plates have been used frequently in regions with low to moderate seismicity. The adequacy of flat plates to resist seismic loads, either alone or in parallel with more rigid elements, has not been adequately proved or disproved through field observation or laboratory research. Due to this lack of information on the performance of flat plates, a research project was undertaken.

1.2 Objectives and Scope

Objectives of the research documented in this report are (1) to study the behavior of typical flat plate slab-column subassemblies under imposed lateral interstory drifts, and (2) to assess the applicability of selected relatively simple analytical models by comparing strength and stiffness estimates with experimentally obtained values. Results of this research can be used to provide insight into the local behavior of a complete flat plate structure.

The test specimens constructed for study are three-tenths of full scale models of typical interior and exterior slab-column subassemblies of a prototype flat plate structure studied by Diebold and Moehle [6] (Fig. 1.1). The prototype structure is a two-story reinforced concrete flat plate frame having three bays along one principal axis and multiple bays along the other. A three-tenths of full scale test structure was constructed to model the prototype structure. The seismic response of the prototype was studied by conducting shaking-table experiments on the test structure shown in Fig. 1.1. Those experiments are detailed in the report by Diebold and Moehle.

The subassemblies for our study were loaded by gravity loads and statically imposed lateral loads with reversals. Dynamic loads were not imposed. Deflection and deformation responses of the subassemblies to the loadings were monitored and recorded throughout the experiments, as was the extent of surface cracking.

The observed behavior of the subassemblies is presented in

Chapter 4 and interpreted in Chapter 5. Comparisons are also made between observed responses and responses predicted by selected analytical models. Finally, conclusions are summarized in Chapter 6.

2. DESIGN

2.1 Introduction

The research presented in this report is part of an overall program designed to study the seismic behavior of reinforced concrete flat plate construction. The overall program involved (1) design of a multi-story, multibay, prototype structure; (2) testing of a three-tenths scale shaking table model of the prototype; and (3) testing of interiorandexterior slab-column connections that were nominally identical to those used in the three-tenths scale shaking table model. The primary objective of this report is to document tests of the connections. However, to obtain a good perspective of the connection behavior, it is important to understand the design procedure used for the prototype structure. This chapter presents a brief outline of that design procedure. Further details are given elsewhere [6].

2.2 Description of the Shaking-Table Structure

The connections described in this report are direct representations of interior and exterior slab-column connections ofthe shaking table structure (Fig. 1.1a) which was tested by Diebold and Moehle [6]. The shaking table structure modeled a fictitious prototype building at three tenths of full scale. The prototype had two stories, with three bays in one direction and multiple bays in the transverse direction. The shaking table structure (Fig. 1.1a) models the prototype in all but the

transverse direction, where only two bays of the multibay direction are modeled.

Each bay in the shaking table model measures 1.83 m (6 ft). Floor heights are 0.914 m (3 ft). The slabs are 61 mm (2.4 in.) thick. Columns have 137-mm (5.4-in.) square cross sections. A spandrel beam measures 107 mm (4.2 in.) deep (from top of slab) and 137 mm (5.4 in.) wide.

The shaking table structure is loaded to simulate a slab dead load of 4800 Pa (100 psf). A design service live load of 2900 Pa (60 psf) is not represented in the tests. The shaking table model is subjected to simulated earthquake base motions having a vertical component and a horizontal component parallel to the three-bay direction (Fig. 1.1a). The structure is considered to be located in a region that may be expected to experience a design seismic event having Intensity VII in the Modified Mercali Intensity Scale.

2.3 Design of the Shaking Table Structure

The shaking table structure is designed to satisfy serviceability and strength requirements of ACI 318-83. Gravity load effects are determined using the Direct Design Method. Seismic design forces are prescribed by the Uniform Building Code [8], assuming the structure to be located in Zone 2 of that code. The structure is proportioned and detailed to satisfy requirements of ACI 318-83 for structures located in regions of moderate seismicity.

Major aspects of slab, spandrel, and column design are outlined in the following subsections.

2.3.1 Slab

Slab thickness is established based on the minimum thickness requirements of ACI 318-83. This minimum thickness is found to be adequate for all strength requirements of ACI 318-83 for both gravity and combined gravity and seismic loads.

Design total moments are described in Fig. 2.1. It is noted that seismic design moments are assumed to be resisted by the slab column strip. As indicated in Fig. 2.1d, the maximum design moments are predominated by factored gravity loads. The relatively low influence of seismic design loads on total moments arises because of the relatively low height of the structure. As a consequence, the total amount of slab flexural steel is determined by gravity load requirements.

Seismic loads have a more significant influence on connection unbalanced moments, that is, the moment that must be transferred from the slab to the column. Table 2.1 presents the total shears and unbalanced moments for various load combinations. The first and second columns in that table present effects due to gravity and combined seismic and gravity loads. The third column is a load combination involving a seismic effect that is twice that of the second column. This last load combination is in accordance with ACI 318-83, which requires that shear capacities for frames in regions of moderate seismic risk be checked for (1) development of flexural hinges, or (2) twice the seismic design shear. Because flexural hinges are not easily defined for slab-column frames, the latter option, involving twice the seismic effect, is used in design.

Slab reinforcement is arranged as required by ACI 318-83 for

beamless slabs in regions of moderate seismic risk. Complete details are in Chapter 3. Briefly, the specified details require that reinforcement be banded near the columns and that minimum top and bottom bar continuity be provided. For the connections described in this report, the requirements are satisfied by banding the top steel required for gravity loads, and by adding a few extra continuous bottom bars. By satisfying these detailing requirements alone, the provided capacities for unbalanced moments (as per ACI 318-83) are in excess of the required capacities of Table 2.1.

2.3.2 Edge Beam

The edge beam is required [3] to resist transverse gravity moments, shears, and torsion from the slab framing into the exterior connection. Gravity moments are determined using the Direct Design Method. One third of the connection shear is assigned arbitrarily to each spandrel beam on either side of a column. The remaining third is assigned to the slab framing into the column. As required by ACI 318-83, the edge connection must be capable of developing the provided flexural strength of the slab column strip. In this regard, the slab framing into the column is assured to transfer moment to the column directly. The spandrel beams must develop in torsion the remaining slab column strip strength. The design procedure of ACI 318-83 for combined flexure, shear, and torsion is used to ensure proper spandrel strength.

Details of edge beam transverse reinforcement (described fully in Chapter 3) were determined from minimum transverse steel

requirements of ACI 318-83 for beams of frames located in regions of moderate seismic risk. Using these details, the required combined flexure, shear, and torsion strengths are automatically provided.

2.3.3 Column

Columns were designed to ensure that their strengths would exceed the unbalanced moment capacity of the slabs at all connections of the shaking table model. Details follow recommendations of ACI 318-83 for frames in regions of moderate seismicity.

3. SPECIMEN DESCRIPTION

3.1 Introductory Remarks

This chapter presents detailed descriptions of interior and exterior slab-column test specimens and of the experimental setup used to test them. The chapter begins by describing the relationship between the shaking-table model, described in Chapter 2, and interior and exterior slab-column connections. This is followed by detailed descriptions of overall configurations, reinforcement details, and material properties of the test specimens. Finally, the experimental setup is described, detailing overall setup, connection hardware, instrumentation, and data acquisition.

3.2 Relation of Connections to Shake-Table Model

The experimental program was designed to study the response of typical interior and exterior slab-column connections of the shaking-table model when subjected to lateral loading. The overall configuration of the shaking-table model is depicted in Fig. 1.1a. Under lateral loading, a simple portal frame analysis model for an elastic structure has points of inflection at column midheights and lines of zero moment running transverse to the direction of lateral loading at slab midspans. Interior and exterior connections can be obtained by cutting at these inflection points and along these zero moment lines. Figure 1.1 shows the interior and exterior subassemblies selected for study

and their relation to the shaking-table model.

The subassemblies are idealized as shown in Fig. 3.1. Columns extend above and below the slab to story midheights, where they are pinned. Slabs have roller supports along the edges corresponding to the lines of zero moment in the portal frame model (transverse edges in Fig. 3.1). In the ideal case, the longitudinal edges should coincide with lines of zero shear and twist and should be restrained against rotation about the longitudinal direction. In the experiments, this edge was left unrestrained. Previous research [1] has shown that this does not have significant effect.

In the shaking-table model, lateral inertial loads are developed primarily in the slab at each floor level. Hence, a "true" portal frame model of the connections shown in Fig. 3.1 should have lateral load applied at the upper column, representing the inertial load developed in upper floors, and at the slab level, representing the additional inertial load developed in the slab. To simplify the loading for the experiments, lateral load was applied at the upper column only.

Gravity load effects were approximated by distributing lead weights on the slab. Details of the placement are described later in this chapter.

3.3 Details of Specimens

3.3.1 Overall Dimensions

The interior and exterior test specimens and the experimental setups are depicted in Fig. 3.2. Slab thickness is 61 mm (2.4 in.). Slab plan dimensions for the interior specimen

are 1828 mm (72 in.) and 2034 mm (80 in.) in the transverse and longitudinal directions, respectively. The longitudinal span between roller supports is 1828 mm (72 in.). An additional 103 mm (4 in.) which overhangs at each edge is required to accommodate the support assemblies. Slab plan dimensions for the exterior specimen are 1828 mm (72 in.) and 1017 mm (40 in.), in the transverse and longitudinal directions, respectively. Again, there is a 103 mm (4 in.) slab overhang from the roller supports, so the longitudinal span between supports is 914 mm (36 in.).

Columns for both specimens have 137-mm (5.4-in.) square cross sections. The point of lateral load application in the upper column is 427 mm (16.8 in.) above the top surface of the slab, whereas the pinned support in the lower column is 427 mm (16.8 in.) below the bottom surface of the slab. These points correspond to column midheights in the shaking table model (Fig. 1.1a).

The cross section of the transverse edge beams of the exterior specimen is 137 mm (5.4 in.) wide and 107 mm (4.2 in.) high, measured from bottom of beam to top of slab.

3.3.2 Reinforcement

The details of slab reinforcement, Figs. 3.3 and 3.4, follow closely those used in the shaking-table model. Slab reinforcement for both specimens consists of two layers of deformed 4.5-mm (0.178-in.) nominal diameter bars. Each layer comprises steel running in the longitudinal and transverse directions. Bars running in the longitudinal direction were placed with the smaller cover; a nominal clear cover of 5 mm (0.25 in.).

For the interior slab-column specimen, all bars running in

the longitudinal direction from edge to edge of slab (Fig. 3.3a) were provided with 180 degree hooks for anchorage. Bars running to the edge in the transverse direction were not provided with hooks.

Details of individual bar lengths and spacings for the interior specimen are in Fig. 3.3. Bar cuts were made on the basis of positive and negative moment considerations. Longitudinal and transverse top bars are spaced at 38 mm (1.5 in.) on centers within a 229 mm (9 in.) wide slab strip centered about the column, then at 57 mm (2.25 in.) on centers for 114 mm (4.5 in.) to either side of the strip, and then, finally, at 114 mm (4.5 in.) on centers for the rest of the slab. All bottom longitudinal and transverse bars are spaced at 114 mm (4.5 in) on centers, with the exception of additional bars placed near the column region. This mat of additional bars was used to improve ductility. All longitudinal bars passing through the column and across the column lines were continuous without splices. Bar cutoffs outside the column region are in the same locations as in the shaking table model.

Spacings of slab reinforcement in the exterior specimen parallel the spacings used in the interior specimen, with the exception that the more closely spaced mat of bottom reinforcement described for the interior specimen was not used for the exterior specimen (Fig. 3.4). Bar lengths and cutoffs are generally different for the interior and exterior slabs. In particular, not all top longitudinal steel in the exterior slab was continuous as it was in the interior specimen. However,

bottom longitudinal bars were continuous in the exterior slab but not in the interior slab, the same arrangement used in the shaking table model. In addition, all slab longitudinal bars were provided with 180 degree hooks as detailed in Figs. 3.3 and 3.4. Slab reinforcement in the transverse direction is nominally the same in the exterior and interior specimens.

Steel conduits were placed in the slab along the roller supported edges. The conduits are necessary for bolting of support hardware when the specimen is ready to be tested.

Edge beam reinforcement consists of longitudinal deformed No. 2 bars, nominal diameter of 6.4 mm (0.25 in.), and 3-mm (0.12-in.) diameter plain wire for closed stirrups (Fig. 3.5). Clear cover is 15 mm (0.6 in.) to the longitudinal bars. Four longitudinal bars are tied to the corners of the closed stirrups and are continuous to the end of the edge beam, where they are terminated without hooks. Single discontinuous bars alternate between a top center position and a bottom center position, as indicated in Fig. 3.5a. Stirrups are spaced at 19 mm (0.75 in.) near the column face and then at 38 mm (1.5 in.) to the end of the beam, as shown in Fig. 3.5b.

Column reinforcement consists of longitudinal No. 2 bars and transverse hoops from 3-mm diameter plain wire. A single longitudinal bar was positioned at each corner and at the center of each face, for a total of eight bars (Fig. 3.6). All longitudinal bars are continuous and are provided with hooks at column ends (Fig. 3.6b). The hoop configuration (Fig. 3.6c) assures that each longitudinal bar is contained in a hoop corner. Hoop spacing is 51 mm (2 in.). Spirals of hoop steel at 19-mm

(0.75-in.) pitch were provided around hollow steel conduits placed in the upper and lower columns at locations corresponding to the applied lateral load and the pinned support, respectively. The ends of the longitudinal bar at the center of each of the transverse column faces were bent around the two conduits, as shown in Fig. 3.6a. Clear cover over the column ties is 11 mm (0.45 in.).

3.3.3 Construction

The two specimens were cast individually in single pours, with the exterior specimen not being cast until after the interior specimen had been tested. The same plywood formwork, with minor modifications, was used for both. To avoid gravity load effects while each specimen cured in the forms, the slab portion of the formwork was uniformly supported atop a table and the lower column portion was supported by a pedestal.

Concrete was placed with the slabs horizontal. The slab concrete was vibrated using form vibrators clamped to the underside of the formwork. The column forms were vibrated by applying a hand held tamping device to the sides.

A wet cure was achieved by covering the specimens with wet burlap and plastic, and lasted 14 and 20 days for the interior and exterior specimens, respectively. Forms were stripped at the end of the wet cures.

Test cylinders and prisms were cast with each specimen, and were subjected to the same curing conditions as the specimens.

3.3.4 Materials and Material Properties

Materials were selected to be representative of conventional

reinforced-concrete materials. Target concrete compressive strength was 28 MPa (4 ksi). Slab and column longitudinal reinforcement was nominally Grade 60 deformed bars with nominal diameters of 4.5 mm (0.18 in.) and 6.4 mm (0.25 in.), respectively. Transverse column and edge beam reinforcement was 3-mm (0.12-in.) diameter plain wire with a nominal yield strength of 620 MPa (90 ksi). Typical stress-strain curves for reinforcement and concrete are in Figures 3.7 through 3.9.

3.3.4.1 Reinforcing Bars

The 4.5-mm (0.178-in.) nominal diameter deformed rebars used for slab reinforcement were fabricated at the University of California at Berkeley. The steel was originally 4.8-mm (0.188-in.) diameter 1064 hard drawn wire, having a yield stress of 1325 MPa (190 ksi) by the 0.2 percent offset method, and an ultimate stress of 1440 MPa (210 ksi). The steel had a fracture strain of 3.5 percent. Young's modulus was 200000 MPa (29000 ksi).

A schedule of heat treatment and cold rolling was developed to transform the 1064 wire into small-diameter deformed reinforcement having characteristics similar to those of full scale Grade 60 rebars. Stress-strain characteristics of the final product are depicted in Fig. 3.7. Nominal strengths are 434 MPa (63 ksi) at yield and 671 MPa (97 ksi) at ultimate, with strains of 0.25 percent at yield, 0.7 percent at onset of strain hardening, 10.8 percent at ultimate, and 12.5 percent at fracture. Young's modulus is estimated at 200000 MPa and initial strain hardening modulus at 8300 MPa (1200 ksi).

Longitudinal column and edge beam reinforcement was deformed 6.4-mm (0.25-in.) diameter rebar (No. 2) having a yield strength

of 470 MPa (68 ksi) by the 0.2 percent offset method, and an ultimate strength of 690 MPa (100 ksi) at 9.2 percent strain. The elastic and strain hardening moduli for these bars are nominally the same as for the slab rebars. A typical stress-strain relation appears in Fig. 3.8.

3.3.4.2 Concrete

Concrete for each specimen was cast from a single batch. Mix proportions by weight were 1:2.7:2.4 (cement : fine aggregate : coarse aggregate), with a water-cement ratio of 0.6. Cement used was Type I-II Permanente brand portland cement donated by Kaiser Sand and Gravel Company, Oakland, California. Fine aggregate was an 82:18 percent mixture by weight of Radum top sand and Tidewater blend sand, respectively. Coarse aggregate was Radum pea gravel having a maximum size of 9.5 mm (0.37 in.). Measured slumps were 130 mm (5 in.) and 190 mm (7.5 in.) for the interior and exterior specimens, respectively.

Fifteen 75-mm by 150-mm (3x6-in.) test cylinders and nine 75-mm by 75-mm by 280-mm (3x3x11-in.) prisms were cast with each specimen and served as control specimens. The cylinders and prisms were stored with the test specimens and were subjected to nominally identical curing conditions.

The interior and exterior slab-column specimens were cured for 14 and 20 days, respectively, under wet burlap and plastic, after which time forms were stripped. The control specimens were removed from their molds two days after casting and were subsequently cured with the slab-column specimens. Upon completion of wet cure, all specimens were stored in the

laboratory until the day of testing. Total age at testing was 124 days for the interior slab-column connection and 48 days for the exterior slab-column connection. Control specimens were tested immediately following the tests of their respective slab-column specimens.

Of the fifteen control cylinders cast with each test specimen, ten were tested in compression and five were tested in splitting tension. Loading rates corresponded to those specified in ASTM C39-72 and C496-71. The prisms were tested in flexure by applying load at the third points of a 229 mm (9 in.) simple span, as specified in ASTM C78-75.

Typical stress-strain relations obtained from the compression tests are plotted in Fig. 3.9. Mean compressive strengths were 26.2 MPa (3.8 ksi) and 19.3 MPa (2.8 ksi) for concrete of the interior and exterior specimens, respectively. Initial tangent moduli were measured as 21700 MPa (3100 ksi) and 21000 MPa (3000 ksi), and the secant moduli at 45 percent of the compressive strength were measured at 21800 MPa (3200 ksi) and 18400 MPa (2700 ksi) for the interior and exterior specimens, respectively. Measured concrete properties are tabulated in Table 3.1.

It should be noted that the compressive properties given above are for 75-mm by 150-mm cylinders, and that adjustments should be made to convert the obtained compressive strengths to values for standard 150-mm by 305-mm (6x12-in.) cylinders. Experiments conducted on nominally identical concretes indicate that the adjustment factor should be 0.955. For this report, no adjustment factor was used.

Splitting tension strengths were obtained following the guidelines of ASTM C496-71. Mean splitting strengths are 3.6 MPa (0.52 ksi) and 3.2 MPa (0.46 ksi) for the interior and exterior specimens, respectively. Values are tabulated in Table 3.1.

Mean values of 4.7 MPa (0.68 ksi) and 3.4 MPa (0.49 ksi) were obtained for moduli of rupture for the interior and exterior specimens, respectively, as tabulated in Table 3.1.

3.4 Test Setup

3.4.1 Supports

Hardware used to support the slab-column specimens in the test setups is shown in Fig. 3.2. The idealized pinned support at the lower column was modeled by a "pin" and clevis assembly, while the roller supports were modeled by "pin-ended" link assemblies. Another "pin" and clevis assembly was used at the point of lateral load application in the upper column. These will be discussed in detail in the following paragraphs.

The clevis for the lower column support (Fig. 3.2) was "fixed" to the laboratory floor by cementing with hydrostone and, subsequently, by bolting. The "pinned" connection was achieved by passinga 19-mm (0.75-in.) diameter steel rod through the clevis arms and through a conduit which was cast into the column. To reduce friction and to ensure a close fit, the pin was passed through ball bearings which were press-fitted into the clevis arms. A similar pin and clevis arrangement was used at the point of lateral load application in the upper column (Fig. 3.2).

The roller supports were modeled by four pin-ended link assemblies along each transverse edge (Fig. 3.2). A typical

linkage is shown in Fig. 3.10. Two lengths of ASTM A519 C1018 cold drawn seamless carbon mechanical tubing with threaded ends are joined by a coupler to form a unit. Spherical rod-ends (bearings) are threaded onto both ends of the unit. Pins passing through the rod-ends connect to clevises bolted to the floor and clevises bolted to the underside of the slab (Figures 3.2 and 3.10). The C1018 tubing used had an outside diameter of 19 mm (0.75 in.) and a thickness of 3 mm (0.12 in.).

The linkages were designed to offer negligible resistance to sway in the longitudinal direction, resisting primarily vertical forces. Ideally, when the slab displaces in the longitudinal direction, the links pivot about the floor clevises with negligible lateral resistance and negligible vertical displacement. However, the linkages will impose vertical slab deflections along the edges as they pivot. The ratio of vertical to horizontal deflections, assuming rigid links, is given by equation 3.1.

$$\frac{\delta v}{\delta h} = \frac{1 - \sqrt{1 - (\delta h/l)^2}}{\delta h/l} \qquad 3.1$$

where, δh = horizontal displacemnt of link (at slab level)

δv = vertical displacement of link

l = length of link between pins

To evaluate the magnitude of vertical deflections given by equation 3.1, representative values of $\delta v/\delta h$ obtained during the tests are given below.

$\delta h/l$	$\delta v/\delta h$
0.01	0.005
0.02	0.01
0.03	0.015
0.04	0.02

The drift measurement $\delta h/l$ is similar to the interstory drift of the test specimen, so when $\delta h/l = 0.01$, the interstory drift of the specimen is about one percent. At one percent interstory drift, the ratio $\delta v/\delta h$ is small enough that the imposed vertical slab deflections do not affect the overall behavior of the slab-column specimens. At greater drifts the imposed vertical deflections increase in magnitude, but since the specimens are cracked and behave non-linearly at these drifts, there is no significant effect on overall behavior.

An additional error due to modeling slab roller supports with links arises because the link reactions become inclined as the links pivot about their base. As a consequence, a horizontal component is created. The ratio of the horizontal to vertical components of the link reactions is approximately equal to the imposed drift. For drifts less than three percent, the ratio between the total horizontal component of reactions in all links to the total applied lateral load is approximately equal to the drift for the interior connection and twice that value for the exterior connection. Because the horizontal component is relatively small, it will not be further considered.

Another error introduced by the links results because of axial deformation of the links. At one percent lateral drift of

a test specimen, the maximum vertical compression or elongation of a link is approximately 0.09 mm (0.004 in.). This corresponds to an equivalent rigid body joint rotation of 0.0001 radians. The total measured joint rotation at this stage of testing was 0.01 radians. At interstory drifts greater than one percent, connection behavior is nonlinear and the equivalent rigid body joint rotation is negligible compared to the total measured joint rotation. Thus, this effect can be ignored.

3.4.2 Loading

3.4.2.1 Dead Load on Slab

For the specimens to accurately model typical connections in the shaking-table model, shear and moment in the slab at the column face should simulate that occurring in the shaking-table model. Because shear transfer from slab to column is usually critical in flat plate structures, and because of difficulty in modeling both shear and moment, the dead load for the specimens was arranged to simulate primarily the shear in the slab at the column face.

Calculation of this shear in the shaking-table model was based on a uniformly distributed slab dead load of 4.79 MPa (0.1 ksf), excluding slab self-weight. Using tributary load ideas, longitudinal slab spans were approximated as beams fixed at both ends with uniformly distributed loading. The clear span of the slab in the longitudinal direction in the shaking-table model was used for the span between fixed ends. Similarly, the slab of the slab-column specimen was idealized as two propped cantilever beams fixed to a column. The shear at the fixed end of each

propped cantilever was obtained by statics, in terms of an unknown distributed loading over the propped cantilever, and set equal to the shear occurring in the shaking-table model. Solving for the unknown distributed loading to produce this shear in the propped cantilever results in a required uniformly distributed slab load of 7.66 MPa (0.16 ksf) for the slab-column specimen.

Lead ingots were distributed symmetrically over the slab to simulate a distributed loading. Sixty ingots, with mean unit weight of 0.43 kN (97 lbs), were arranged symmetrically atop the slab of the interior specimen for a total load of 25.8 kN (5820 lbs). The exterior specimen was loaded by thirty ingots in an arrangement consistent with that used for the interior specimen, as shown in Fig. 3.11.

The effectiveness of the lead weights in simulating gravity load effects in the shaking table model is discussed in Section 5.2.

3.4.2.2 Lateral Loading

Lateral load was applied at the upper column by a hand pumped hydraulic actuator. The actuator was reversible, so load could be applied or gradually relieved in either direction as the actuator arm extended or retracted. A constant load could be achieved by maintaining a constant hydraulic pressure.

3.5 Instrumentation

Lateral load was applied to the interior and exterior specimens as described above. The magnitude of lateral loading was measured by a load cell in the actuator arm.

Deflection of the upper column in the direction of lateral

loading was measured by a linear potentiometer attached to concrete at the level of lateral load application. A linear voltage displacement transducer (LVDT) was used to measure lower column displacements in the direction of lateral loading at the pinned support. Small displacements were measured there because of clearance between the pin and the hole in the column receiving the pin. Interstory drift of the specimens is obtained by subtracting the displacement at the lower column pinned support from the deflection of the point of lateral load application in the upper column.

Linear potentiometers (instruments 2 and 3 in Fig. 3.12) were used to measure displacement in the direction of lateral loading of slab mid-depth. For the exterior connection, instrument 3 was attached to the edge beam at the slab mid-depth.

Reaction forces in the pin-ended links were measured by strain gages affixed to the links. Foil gages were arranged in a four-arm bridge on each link.

Weldable strain gages having 25-mm (1-in.) gage lengths were welded onto top and bottom layer slab reinforcement bars running in the longitudinal direction on the west side of the column in both specimens. All gages were welded to the sides of the bars so as to minimize readings due to bar flexure. The strain gages are attached just beyond the north column face to bars located at the center of the column, and at distances of 114 mm (4.5 in.), 229 mm (9 in.), 457 mm (18 in.), and 686 mm (27 in.) from the center of the column.

These strain gages measured the variation of strain along a transverse slab section at the column face extending from the

longitudinal slab centerline to a longitudinal edge. The strain variations thus obtained provide clues to the distribution of bending moment along that section.

Rotations of the slab-column joint were measured approximately using LVDTs. For these measurements, square steel collars were mounted directly on the concrete of the upper and lower columns at locations 20 and 150 mm above the slab surface and 14 and 155 mm below the slab surface of the interior specimen (Fig. 3.12). Collars were mounted on the concrete of the exterior specimen columns at locations 20 and 150 mm above the slab surface and 25 and 150 mm below the bottom surface of the edge beam. The amount of rotation was approximated by measuring the rotation of the collar mounted on the upper column just above the slab surface. Measurement was by LVDTs mounted to a fixed reference frame above the specimen. Rotation of the collar mounted on the lower column was not measured.

Slab rotations relative to the north and south column faces were measured by LVDTs nos. 8, 10, 7, and 9 for the interior specimen, and LVDTs nos. 7 and 9 for the exterior specimen (Fig. 3.12). The instruments were mounted to the top and bottom slab surfaces at distances of a column width from their respective column faces. They were targeted on the collars closest to the slab.

Slab rotations about a transverse axis along the transverse column line were measured by LVDTs mounted to a reference frame above the specimen. The LVDTs measured vertical slab deflections along two parallel transverse lines (Figs. 3.12). Given the

distance between the lines, average slab rotations can be obtained.

3.6 Data Acquisition

All experimental data was recorded on a Data General Nova Computer high speed data acquisition system, and stored on both magnetic tape and hard disk. Throughout the experiment, selected instruments were monitored on a Tektronix terminal. In addition, an X-Y plotter was used to monitor lateral load and deflection at the upper column lateral load point.

3.7 Test Chronology

The test chronologies are given in the following table:

Event	Date	
	Interior Specimen	Exterior Specimen
Specimens Cast	Jan. 21, 1983	June 28, 1983
Forms Stripped	Feb. 2, 1983	July 18, 1983
Instrument Calibration	May 19, 1983	Aug. 10, 1983
Testing Begins	May 25, 1983	Aug. 15, 1983
Testing Ends	May 26, 1983	Aug. 16, 1983
Cylinder & Prism Tests	May 27, 1983	Aug. 17, 1983

4. OBSERVED BEHAVIOR

4.1 Introduction

This chapter presents the observed behavior of the interior and exterior slab column specimens when subjected to lateral load reversals. Topics to be covered in this chapter include load-deflection relationships, measured slab rotations, and strains in slab longitudinal reinforcement. Observed crack patterns and apparent failure modes are presented also. Interpretations of observed behavior are presented in Chapter 5.

4.2 Test Prodedure

Similar procedures were followed for testing the interior and exterior specimens. The first step was to move the specimen from the casting area to the test set-up location. This was accomplished by lifting the specimen at its upper column pin hole with an overhead bridge crane. When positioned in the test set-up, and before the application of dead load, the interior specimen was balanced so that the links, which simulated roller supports (Fig. 3.2), carried negligible loads. Therefore, the specimen was loaded by the weight of the slab cantilevering from the columns. The exterior specimen, however, could not be balanced since it was not symmetric like the interior specimen, so the links of that specimen carried an initial load of half the slab weight. Additional lead weights simulating gravity load effects were not placed on the slab surfaces of the two specimens

until after testing began.

Instruments were calibrated and positioned during the week before the start of testing.

Preliminary tests were conducted on each specimen before they were loaded with lead weights. Preliminary testing involved reversed lateral loadings at drift levels equal to approximately 0.0005 times the specimen height. After a few cycles of low magnitude lateral loading, the lead weights were placed and testing was resumed. Lateral loading was displacement controlled, with each cycle of loading corresponding to a specific percentage of interstory drift. Upon attaining the desired peak interstory drift for each cycle, the deflected shape was maintained while the specimen was inspected and cracks were marked.

Testing spanned two days for each specimen with no testing during the night. Testing concluded with failure of the specimen. Control cylinders and prisms were promptly tested for compressive and splitting tension strengths, and modulus of rupture following conclusion of specimen tests.

4.3 Sign Convention

Lateral load on the upper column is positive when it is directed towards the north (Fig. 3.1) and negative when it is directed towards the south. The north-south direction coincides with the longitudinal direction in plan views of the specimens. Flexural moment about a transverse axis of the slab is positive when it produces tension in the bottom layer of slab rebars and compression in the top layer. Moment is negative when tension is

induced in the top layer and compression in the bottom layer.

When viewed from east to west along a transverse axis, clockwise slab and column rotations are considered positive.

4.4 Imposed Lateral Deflections

Lateral loads applied to the interior and exterior test specimens were displacement (or deflection) controlled. They were applied slowly and were cycled with reversals. Histories of the lateral deflections imposed on the interior and exterior test specimens after application of full dead load are shown in Fig. 4.1.

4.5 Preliminary Tests (Prior to Dead Load)

Prior to application of full dead loads on the interior and exterior slab-column specimens, each was subjected to low magnitude lateral loads with reversals. The deflection histories of Fig. 4.1 do not include these preliminary tests. The lateral loads and the amounts of upper column deflections, or interstory drifts, never exceeded values corresponding to the first cycles of testing following application of full dead load. The measured load-deflection curves from these preliminary tests are presented in Fig. 4.2. The stiffnesses of the specimens without dead load can be approximated by measuring the slope of the line which best describes the overall shape of these preliminary curves. The figure indicates a small amount of hysteresis which is negligible compared to the hysteretic behavior observed throughout the experiments.

4.6 Tests With Full Dead Load

4.6.1 Load-Deflection Curves

For this report, interstory drift will be defined as the deflection in the longitudinal direction of the upper column point of lateral load application relative to the deflection at the lower column pinned support. For the remainder of this report, unless stated otherwise, deflection of the upper column, or simply the term "deflection", is intended to be synonymous with interstory drift. When presented as a percentage, the term interstory drift is the ratio between column deflection and column height.

Measured load-deflection curves are presented for both interior and exterior specimens in Fig. 4.3 and 4.4. Figure 4.3 shows response for interstory drifts less than approximately one-half percent. Fig. 4.4 presents the entire response history to failure (drifts to approximately five percent).

For drift ratios less than or equal to one-half percent (Fig. 4.3), a "modest" amount of hysteresis is present. The presence of a small amount of hysteresis during the first cycles suggests the presence of either friction in the experimental apparatus, initial cracking, or both. Although no cracks were visible to the unaided eye before testing, the presence of hairline cracks is likely. To drifts of approximately two mm (0.2 percent interstory drift) the hysteresis is relatively stable with little degradation in stiffness and no pronounced "pinching".

Beyond drifts of approximately two mm (0.2 percent), a gradual reduction in average stiffness is apparent for both

specimens (Fig. 4.3 and 4.4). The reduction becomes most apparent at drifts of approximately 15 mm (1.5 percent drift) for the interior specimen and five mm (0.5 percent drift) for the exterior specimen. Beyond these drift levels, each specimen exhibits a gradual increase in resistance as drifts increase toward failure (Fig. 4.4).

The hysteretic behavior becomes more pronounced with increasing drift level (Fig. 4.4). Pinching of the curves is apparent. In addition, degradation in the response (failure to reach the same resistance when cycled to a given displacement a second time) is apparent.

4.6.2 Slab Rotation Profiles Along Transverse Axis

Average slab rotations about a transverse axis were inferred from relative displacement measurements of LVDTs attached to slabs and columns as described in Section 3.5. Records of rotation versus time were used to construct rotation profiles along the transverse axis of a specimen at various times during each test. Representative profiles are plotted in Fig. 4.5.

A general trend which is apparent in the slab rotation profiles (Fig. 4.5) is that rotations increase roughly in proportion to the increase of interstory drift. At any level of interstory drift, slab rotations are largest at the column and tend to decrease with increasing distance from the column. The rate of decrease near the column is larger for the interior specimen than for the exterior specimen (with the edge beam).

4.6.3 Slab Reinforcement Strains

Strains in selected slab longitudinal reinforcing bars were

measured throughout each test with weldable strain gages. Representative profiles of bar strains obtained at various stages of testing are presented in Figures 4.6 and 4.7. Top reinforcing bar strains (Fig. 4.6) are plotted for instances when top bars were in tension, that is, when the specimen was pushed to the south. Bottom strains (Fig. 4.7) are plotted for times when bottom bars were in tension, that is, when the specimen was pushed to the north.

Strain profiles for top reinforcing bars (Fig. 4.6) indicate that, for interstory drifts to one percent, strains were largest near the column with a gradual tapering to small strains near the slab edge. Beyond one percent drift, slab bar strains increased most rapidly near the slab edge, although strains near the column exceeded those near the edge for each specimen. Yield in top layer slab reinforcing bars was not detected until interstory drifts reached 2.5 percent. Yield was limited to bars passing near the column.

Strain profiles for bottom reinforcing bars (Fig. 4.7) followed the same general trend as described for the top bars with exceptions noted below. For the interior specimen, strains in the bottom slab bars near the edge exceeded corresponding strains near the column for drifts exceeding 2.5 percent. At maximum drift levels, measured strains in all bottom bars were near or beyond the yield strain.

4.6.4 Slab Rotations Along Longitudinal Axis

Slab rotation relative to the column was measured by LVDTs attached to the top and bottom slab surfaces at a distance of one column width (137 mm), which is approximately two slab depths,

from the column face and targeted to the column face as described in Section 3.5.

Representative histories of rotations of the slab on the north side of the columns are presented in Fig. 4.8. Relative slab rotation histories followed trends nearly identical to trends described for load-displacement histories (Section 4.6.1).

4.7 Slab Shear

Strain gages in the links which simulated roller supports (Fig. 3.2) enabled link reactions to be inferred. The axial load carried by the column can be computed by subtracting the measured link reactions from total specimen weight including superimposed slab loads. By further subtracting the column weight from the column reaction, the total slab shear around the column is obtained. This shear was monitored throughout each test.

Measured slab shear histories are plotted in Fig. 4.9. The histories indicate that slab shears remained relatively constant throughout a test for the interior specimen. Shears cycled up and down in phase with imposed lateral loads for the exterior specimen.

4.8 Visible Cracking and Other Damage

Visible cracks on top and bottom slab surfaces, on edges of the edge beam, and on column faces were traced on specimens and sketched on paper at the peak interstory drift of each half cycle. Only surface cracks visible to the unaided eye were marked. Observation of cracks on top slab surfaces was hampered by the presence of lead weights which had been added to increase

dead loads. Therefore, recorded patterns for the top surface are likely to be incomplete. Recorded crack patterns at representative stages of each test are presented in Fig. 4.10.

Surface cracking of the interior specimen slab initiated near the column as short and straight small cracks. As larger drifts were imposed, these cracks widened, lengthened, and started curving toward the transverse centerline. Relatively straight cracks running in the transverse direction on the top slab surface away from the column initiated at about 1.5 percent interstory drift, whereas similar cracks on the bottom surface initiated at about one percent drift. The spacing of these relatively straight transverse cracks corresponds roughly to the spacing of slab rebars running in the transverse direction.

The sequence of surface cracking for the exterior specimen slab differed from that for the interior specimen in that the straight transverse cracks appeared earlier in the exterior specimen test. Transverse cracks first appeared on the bottom surface at about (0.05 percent) interstory drift. Curved cracks near the column and diagonal cracks on the south face of the edge beam near the column appeared at about one percent drift. Again, spacing of transverse surface cracks corresponds roughly to the spacing of transverse slab rebars. Cracking of the edge beam was predominantly "diagonal", and was most severe near the column.

Cracking in the columns of both the interior and exterior specimens was similar, with horizontal cracks spaced roughly at the hoop reinforcement spacing. Column cracks were predominantly located on the north and south faces.

The interior slab-column connection failed under negative

lateral load by a punching shear failure of the slab. The top surface of the slab ruptured in a crescent shaped crack about 100 mm from the north face of the column (Fig. 4.11a). The failure was sudden.

The failure mode of the exterior specimen was of a more gradual nature and can be considered a torsional failure of the edge beam. As the connection was failing, cracks along the base of the column and diagonal cracks on the south side of the edge beam near the column opened significantly, and column deflection increased with essentially constant negative load. Failure was declared as concrete of the edge beam began to spall, exposing its reinforcement. Photographs of specimen damage after failure are reproduced in Fig. 4.11.

5. INTERPRETATION OF RESPONSE

5.1 Introduction

Interpretations of observed behavior are made in this chapter. The chapter begins with a study of the state of the test specimens under gravity loads alone. Sources of deformation of the slab-column assemblies are subsequently identified. Results obtained by conventional analytical methods are compared with observed behavior. Methods used to interpret lateral load stiffnesses include the effective beam width and the equivalent frame models [2,5,12,14,15]. Methods of interpreting strengths include moment-curvature analyses as well as the procedure suggested by ACI 318-83 [3].

5.2 Effects of Gravity Loads

The slabs of the slab-column assemblies were loaded initiallyby their selfweight and by subsidiary lead weights supported atop the slab surface, as described in section 3.4.2.1. This section briefly describes the loading and its likely effect on internal forces of the specimens. A comparison is made between internal forces of the slab-column assemblies and internal forces expected in a complete structure.

5.2.1 Interior Slab-Column Specimen

During the experiments, the interior slab-column assembly was initially set in the testing apparatus such that the entire vertical weight of the specimen was supported by the bottom

column. In this condition, the slab "hung" from the column as a cantilever. After positioning the specimens, the reaction links which simulated roller supports (Fig. 3.2) were connected such that they carried negligible vertical loads. Following low-intensity (elastic) lateral loading, the subsidiary lead weights were added. At this stage, the weights were supported in part by the edge links, with the remainder being carried through slab shear to the column.

Distribution of internal slab forces in the interior slab-column specimen were investigated using a linear elastic finite element analysis. Plate bending elements available in SAP-80 [16] were arranged in the grid shown in Fig. 5.1. The grid represents one quarter of the slab-column specimen, with the effects of the remaining slab modeled by selecting appropriate boundary conditions. The finite element model was loaded analytically in the same manner as the test specimen. The calculated distribution of slab moments is in Fig. 5.2. Calculated internal forces are compared with those anticipated for the prototype structure in the following paragraphs so that the adequacy of the test setup can be gaged.

In the prototype structure which the specimen is intended to model, anticipated slab forces can be obtained from available analytical solutions [10]. Considering gravity load equal to slab self weight, the anticipated slab shear on the critical section one half slab depth from an interior column is 15.8 kN (3.6 kip). The corresponding shear expected from the finite element solution, 21.3 kN (4.8 kip), exceeds the prototype value by 35 percent. The anticipated prototype slab negative moment is

two-thirds of the static moment, resulting in a negative moment of 1.95 kN-m (17 kip-in.) acting across the full slab width at the column face. This value differs by only four percent from the corresponding value of 2.03 kN-m (18 kip-in.) calculated by the finite element method. Hence, the finite element analysis indicates that under gravity loads the test specimen was more heavily loaded in shear than would be the case in the prototype (by 35 percent). However, it was loaded similarly in flexure. Because initial lateral load response is likely to be affected mostly by initial flexural stresses, and less influenced by initial shear, it appears likely that the interior test specimen will give a representative indication of behavior under low magnitude lateral loads. The capacity under more severe lateral loads will probably be reduced because of the higher initial shears.

The validity of the finite element model in representing the interior test specimen can be checked by comparing measured and calculated total slab shears and moments. In the experiments, slab shear on a critical section a distance of one half slab depth from the column could be deduced from known weights and measured link reactions. The measured slab shear after loading with the lead weights was 19.8 kN (4450 lb) on the critical section. This corresponds to a nominal shear stress of $0.0943\sqrt{f'_c}$ MPa ($1.14\sqrt{f'_c}$ psi). The measured shear is seven percent less than calculated for the finite element model. The measured slab moment across the entire width at the column face is 1.3 kN-m (11.5 kip-in.). This value is 36 percent less than the calculated

value.

The discrepancy between measured and calculated slab moments at the column face can be attributed to slab cracking. The calculated cracking moment of a unit slab width is 2.91 kN-m/m (0.654 kip-in./in.). The peak moment indicated by the finite element model occurs near the column and has a value of 3.92 kN-m/m (0.882 kip-in./in.). Because this value exceeds the calculated capacity, cracking is credible. In the presence of induced tensile stresses attributable to differential shrinkage in this region, cracking is almost certain. The reduction of stiffness associated with cracking near the column results in migration of bending moment away from the column, hence, the specimen develops negative moment less than that predicted by the analysis.

Because similar moments are anticipated in both the prototype structure and the finite element model, as previously discussed, cracking and corresponding redistributions of moment are also indicated for the prototype structure. It is not unreasonable to deduce from the preceeding discussion that the test specimen represented the prototype with reasonable accuracy insofar as flexure is concerned. It may have been more heavily loaded in shear than the prototype.

5.2.2 Exterior Slab-Column Specimen

The exterior specimen was loaded vertically in a manner similar to the interior specimen. However, since the exterior specimen was statically determinate, the slab did not project as a cantilever from the column, and zero moment was initially induced at the column centerline. This was verified, within

small experimental error, by experimental data. Calculated shear on a section one slab depth from the column face was 7.5 kN (1.7 kip).

Because of complexities involved in modeling the edge beam of the specimen, a finite element analysis was not performed. However, tabulated elastic solutions for edge panels are available [10]. These indicate that the edge moment is relatively small, being on the order of 20 percent of the static moment for connections having proportions similar to the test specimen. Hence, the absence of moment in the exterior specimen is reasonable. Using tributary areas concepts, the shear at the exterior connection should be approximately half that at the interior connection, or about 7.9 kN (1.8 kip). This value differs from the measured by five percent.

From the above the discussion, it can be concluded that the exterior slab-column specimen adequately represents the exterior connection of the prototype structure.

5.3 Sources of Slab-Column Specimen Deformations

There are primarily two sources from which measured specimen interstory drifts arise, from the column and from the slab. The contribution of column deformation to measured interstory drift is investigated by analyzing the analytical moment-curvature response of the column. The contribution of slab deformation is analyzed by studying experimentally obtained slab deformation measurements.

5.3.1 Column Deformation

Moment-curvature relations were calculated for the columns

of the interior and exterior specimens using MOMCUR, an interactive computer program developed for use on micro-computers. MOMCUR is designed to analyze the inelastic, monotonically-increasing, moment-curvature response of reinforced concrete beams and columns in flexure with axial load. Idealized material properties used by the program are in Fig. 5.3.

Load-deflection responses for tip loaded columns fixed at their bases to completely rigid slabs are presented in Fig. 5.4, and are based on moment-curvature relations obtained by MOMCUR. The measured lateral load capacity of the interior specimen was 11.2 kN (2.5 kip). This value corresponds to 66 percent of the calculated column capacity of 17 kN, which was obtained from the calculated moment-curvature response. The measured lateral load capacity of the exterior specimen, 8 kN (1.8 kip), corresponds to 47 percent of the calculated column capacity of 17 kN. Based on this discussion, it can be concluded that the columns remained essentially in the elastic range of response and that column deformations were a small fraction of the total measured specimen deformation.

5.3.2 Slab Deformation

The distribution of slab deformations can be determined by examining measured deformations along the slab longitudinal and transverse axes. By studying these deformations, effective slab widths, and the effectiveness of the spandrel beam, can be inferred qualitatively.

Instruments attached to the slab a column width (approximately two slab depths) from the front and back faces of

the columns (Fig. 3. 12) provide a measure of how the slab deformations were distributed in the longitudinal direction. Measured rotation histories, which were determined from these instruments and are shown in Fig. 4.8, are similar in appearance to the load-deflection plots of Fig. 4.4, suggesting that a sizable portion of the total deformation was attributable to slab deformation near the columns. The portion of total drift attributable to rotation close to the columns can be determined approximately by assuming the slab rotations in Fig. 4.8 are due to uniform curvature along a distance equal to two slab depths from the column, and assuming all other protions of the slab-column assembly to be rigid. The "calculated" and measured total drifts are compared in Fig. 5.5 for several stages of testing.

Examination of the data in Fig. 5.5a indicates that the deflections calculated from rotations alone exceed the measured total deflection for the interior specimen. As this cannot actually occur, it is apparent that an error exists in the rotation measurement (the error is not likely to have been in the deflection measurements, as these were cross checked with redundant measurements). Nonetheless, the closeness between measured and "calculated" results (Fig. 5.5a) suggests the majority of deformations occurred in the slab close to the columns. Similarly, examination of data in Fig. 5.5b indicates that the slab within two slab depths of the column contributed approximately two thirds of the total drift. It is likely that the spandrel beam has resulted in a greater effective width for the exterior specimen, which in turn forces slab deformations to extend further along the longitudinal axis.

Slab rotation profiles (Fig. 4.5) suggest that deformations were greatest in the slab near the column, diminishing in the transverse direction with increasing distance from the column. The lower ratio of decrease in rotations for the exterior specimen supports the conclusion made in the previous paragraph that the edge beam resulted in a greater slab effective width.

Measured distribution of slab bar strains (Figures 4.6 and 4.7) are generally similar to distributions of slab rotations, and support the same conclusions.

It may be noted that bottom layer slab reinforcement strains near the edge of the interior specimen eventually increase at a more rapid rate than do strains near the column. This accumulation of plastic strains is attributed to the experimental setup, which in effect caused the edge of the slab to act as a simply supported beam spanning from one set of "roller" supports (links) to the other (Fig. 3.1).

5.4 Initial Lateral-Load Stiffness

The initial stiffnesses of the two specimens were compared with elastic stiffnesses "predicted" by the effective beam width model [2,12,15] and the equivalent frame method [5,14,15].

In the effective beam width method, slabs are replaced by beams spanning in the direction of lateral loading. The depth of the beam is equal to the slab depth. The width of the beam is equal to the product of an effective width coefficient and the transverse slab dimension.

In the equivalent frame method, the slab-column connection is transformed to an assemblage composed of a column connected to

a lateral torsional member, which is connected to a beam having flexural inertia equal to that of the full slab (Fig. 5.6).

5.4.1 Effective Beam Width Model

Analyses were performed for several effective width coefficients. The resulting stiffnesses are presented in Figures 5.7 and 5.8 for the interior and exterior specimens, respectively. It is noted that the effective beam width model used in this report assumes a beam connected to the column directly without a rigid connection region.

Vanderbilt and Corley [15] present a range of theoretical effective width coefficients for assemblages having square columns, square slabs, and Poisson's ratio of zero. For an interior connection having the dimensions of the test specimen, the coefficients given in their paper range from about 0.65 for a rigid column system to approximately 0.35 for a flexible column system. The rigid column system is generally considered the better for elastic structures, whereas the flexible column system gives a lower bound to the elastic response [15]. Figure 5.7 indicates that the initial stiffness of the interior specimen can be modeled by an equivalent beam with an effective width of about 0.6L, where L is the transverse slab dimension. This value is close to the theoretical value of 0.65L. Figure 5.8 indicates that an effective width coefficient of 0.75 is required for an equivalent width beam to model the initial stiffness of the exterior specimen. By the presence of the edge beam and the contribution of its torsional stiffness to the overall connection stiffness, the slab is more effective in the exterior connection

than in the interior connection, requiring a wider equivalent beam to model the initial stiffness.

5.4.2 Equivalent Frame Model

The equivalent frame model, or lateral torsional member model, assumes that the column and slab of a slab-column connection are joined through a lateral torsional member which can transfer torsion only. Idealizations for the interior and exterior specimens are shown in Fig. 5.6. Although not shown in the Figure, the coluns is assumed rigid over the slab or spandrel depth. Gross section properties are assumed for all members. Details of the torsion member and slab members stiffnesses are described below.

The lateral-torsional member of the interior specimen is formed by a slab strip of width one column width as shown in Fig. 5.6. The torsional member of the exterior specimen is composed of the edge beam and an adjacent slab strip of width 46 mm (1.8 in.), as specified in ACI 318-83 [3]. The literature [3,5,14,15] gives the total torsional stiffness of lateral torsional members in a slab-column connection as K_t, where

$$K_t = 18EC / L_2 (1-c_2/L_2)^3 \qquad (5.1)$$

and C is the torsional constant, where

$$C = (bt_1^3 / 3)(1 - 0.63t_1 / b) \qquad (5.2)$$

E = Young's Modulus

c_2 = square column dimension; Fig 5.6

b, t_1 = larger and smaller dimensions of rectangular portions of cross sections of lateral torsional members.

The gross section inertia, I_g, is used for the slab, except

in the joint region where a modified inertia, I_g', is used according to the ACI Code. The modified inertia is given in equation 5.3 below.

$$I_g' = I_g / (1 - c_2/L)^2 \qquad (5.3)$$

The stiffnesses used in the equivalent frame model are based primarily on gross-section (uncracked) properties. Under working lateral loads that may crack the structure, it is likely that the equivalent frame will be excessively stiff. Vanderbilt and Corley [15] recommend using an effective slab inertia of one third the gross section inertia to estimate the lower bound lateral load stiffness. For comparison, stiffnesses were calculated using both the gross section inertia and an effective inertia equal to one third the gross section value.

Results of equivalent frame modeling using both gross section inertia and an effective slab inertia equal to one-third the gross slab inertia are shown in Figures 5.9 and 5.10 for the interior and exterior specimens, respectively. The initial stiffness of the interior specimen is slightly higher than that indicated by the equivalent frame using the gross section inertia of the slab (β = 1). The initial stiffness of the exterior specimen is modeled well by the gross section equivalent frame.

5.5 Lateral-Load Stiffness at Working Loads

The equivalent beam width and equivalent frame stiffnesses were compared with the stiffnesses of the specimens at working loads. Two arbitrary definitions for working load are used in the following. One definition is that working load is a lateral load equal to approximately 40 percent of the lateral load

strength. The second definition defines the working load as the load producing lateral drift equal to 0.002 times the story height. This drift limit is frequently cited as a limit for wind design. For the test specimens, this corresponds to a lateral deflection equal to 1.8 mm (0.04 in.). The gross section inertias were used in the analyses of all equivalent width beams.

Figure 5.7 indicates that an effective width coefficient of about 0.2 is necessary for an equivalent beam to model the secant stiffness of the interior specimen at $0.4P_{max}$, or about one third the width required to model the initial stiffness. A width coefficient of approximately 0.25 is required at the drift limit of 0.2 percent. The effective width required to model the working load stiffness of the exterior specimen depends on whether the applied lateral load is positive or negative. Recall from Section 4.3 that lateral load on the exterior specimen is positive when it increases tensile stress in the bottom of the slab. A width coefficient of about 0.7 is required for positive lateral loads and a coefficient of about 0.5 is required for negative lateral loads (Fig. 5.8) when using the limit of $0.4P_{max}$. Corresponding widths at the drift limit are 0.6 and 0.5. A possible reason for the different coefficients for the exterior specimen is that longitudinal slab reinforcement is not identical in the top and bottom layers (Fig. 3.4).

An accurate modeling of the secant stiffness of the interior specimen at working loads is provided by an equivalent frame having an effective inertia of about one third of the gross section inertia when considering the load limit of $0.4P_{max}$ (Fig.

5.9). The specimen is stiffer at the drift limit. Figure 5.10 indicates that effective slab inertias of approximately one-half and three-quarters of the gross section value are required for equivalent frames to model the secant stiffness of the exterior specimen at working loads when the top and bottom slab surfaces are in tension, respectively. This indicates that at working loads the exterior specimen is still relatively stiffer than the interior specimen, most likely because of the stiffening effect of the edge beam.

Both the equivalent frame and equivalent beam width models indicate that the exterior specimen continues to be stiffer than the interior specimen at working loads, since greater effective inertias and wider equivalent beam widths are required to model the exterior specimen stiffness.

5.6 Connection Strengths

As discussed in Section 5.3, maximum lateral loads applied to both the exterior and interior subassemblies were substantially less than loads corresponding to column capacities. Thus, lateral load resistance of the subassemblies was apparently limited by capacity of the slab to transfer shear and moment to the column. In the course of the research, several analytical methods were used to determine "theoretical" strengths of the connection regions. Computed "theoretical" strengths are compared with measured strengths in Table 5.1. The analytical methods and resulting theoretical strengths are described in the following paragraphs.

5.6.1 Interior Slab-Column Connection

Four approaches to estimating strength of the slab-column connection region of the interior connection were investigated. These are described in the following subsections.

5.6.1.1 Moment-Curvature Analysis

The program MOMCUR was used to calculate the slab flexural moment capacity. It is noted that the program assumes plane sections remain plane, an assumption which is obviously violated (Figures 4.6 and 4.7). Computed capacities are compared with measured capacities of the slab in negative and positive bending moment in Fig. 5.11. In that figure, the computed and measured moments are the unstressed moment capacities less the initial moments due to gravity loads. The computed capacities are 165 and 110 percent of measured capacities in negative and positive moment, respectively, indicating that it is unlikely for the slab to develop its full flexural yield line capacity.

One possible reason why the computed flexural capacities presented in the previous paragraph do not match the measured capacities is that the program assumes plane sections remain plane, which is contrary to measured slab reinforcement strain distributions (Figures 4.6 and 4.7). In an attempt to account for the nonuniform variation of bar forces, a new moment-curvature analysis was performed assuming that plain sections remain plane but that rebar strains had the distribution shown for two percent drift in Fig. 4.6. The results of the modified analysis are presented in Fig. 5.12. The modified analysis offers little improvement over the original analysis, indicating that the slab capacity is probably reached by some mechanism other than pure

flexure.

5.6.1.2 Linear Shear Stress Variation

Shear and unbalanced moment capacities of slab-column connections can be estimated conveniently by assuming a linear variation of shear stress about a critical section, with maximum shear stress limited to a critical value. The ACI Building Code follows this approach in design of slab-column connections for shear and unbalanced moment.

In the ACI design approach, the unbalanced moment, M_s, is resisted in part by direct flexure in the slab and in part by eccentric shear around a critical section. The critical section is taken to have the same shape as the column with dimensions equal to the column cross section plus the mean depth to slab longitudinal reinforcement, ie., c + d. For the proportions of the interior slab-column connection, the portion of M_s resisted by eccentric shear is $\gamma_v M_s$, where $\gamma_v = 0.4$. The remainder of M_s is to be taken in design by slab flexural reinforcement within a width c + 3h centered about the column, where h = slab thickness. The shear stress caused by the moment $\gamma_v M_s$ is given by Eq. 5.4.

$$v_u = \frac{V_u}{A_c} + \frac{\gamma_v M_s (c + d)}{2J_c} \qquad 5.4$$

where v_u = maximum shear stress, V_u = ultimate direct shear force on the connection, A_c = area of critical section = 4d(c+d), γ_v = 0.4, and J_c = a section property similar to polar moment of inertia as given by Eq. 5.5.

$$J_c = 2d(c+d)[(c+d)/2]^2 + 2[(c+d)^3 d + (c+d)d^3]/12 \qquad 5.5$$

According to ACI 318-83, v_u is limited to the value v_{max}, given by Eq. 5.6.

$$v_{max} = 0.33\sqrt{f'_c}, \text{MPa} = 4\sqrt{f'_c}, \text{ psi} \qquad 5.6$$

Using Eqs. 5.4 through 5.6, with V_u taken equal to 19.2 kN (4.32 kip) as measured during the experiments, the value of $\gamma_v M_s$ is calculated to be 3.01 kN-m (26.6 kip-in.). Accordingly, M_s is 7.53 kN-m (66.6 kip-in.). This value is 73 percent of the measured value of 10.3 kN-m (91.2 kip-in.).

As noted previously, the portion of M_s not carried by eccentric shear is to be carried by direct flexure in the slab. The computed flexural capacities of top and bottom slab reinforcement within a width of c + 3h are 2.63 kN-m (23.3 kip-in.) and 2.36 kN-m (20.9 kip-in.), for a combined capacity of 5.00 kN-m (44.2 kip-in.). For the proportions of the test specimen, this is to be 60 percent M_s, so that M_s based on the flexural reinforcement is found to be 8.33 kN-m (73.7 kip-in.), which is 81 percent of the measured capacity.

It should be noted that the value of 0.4 given to the coefficient γ_v has been set somewhat arbitrarily by the ACI Building Code, and can be considered as a guide to the desired proportions of unbalanced moment to be carried by flexure and eccentric shear. In a given connection, some redistribution of actions can be anticipated, so that it is possible that the capacities in flexure and eccentric shear can be developed simultaneously. In this case, the computed unbalanced moment capacity is given as $\gamma_v M_s + (1 - \gamma_v)M_s = 3.00 + 5.00 = 8.00$ kN-m (70.9 kip-in.). This value is 78 percent of the measured

unbalanced moment capacity, which is not significantly different from the capacities calculated previously for eccentric shear or flexure alone.

It should be noted that the effective flexural width of c + 3h used in the ACI Building Code exceeds the column width, the intention being to account approximately for the torsional strength of slab reinforcement which is otherwise ignored by the method. Beam analogies presented by Hawkins and by Park and Islam [7,11] envision beams of width equal to c + d framing into each face of a column. If torsional cracks extend back from the edges of the front flexural beam, then it appears reasonable that reinforcement within a width of c + d to either side of the column critical section contribute to torsional strength. Accordingly, the effect of the torsional steel can be included in the flexural strength by defining an effective flexural width equal to 3(c + h). Using this width, the sum of positive and negative flexural capacities of the slab is 6.99 kN-m (61.9 kip-in.). Adding this to the eccentric shear capacity of 3.00 kN-m (26.6 kip-in.) obtained previously, the computed unbalanced moment capacity is 10.0 kN-m (88.5 kip-in.), which is 97 percent of measured capacity.

5.6.1.3 Beam Analogy of Park and Islam

Park and Islam [11] present a beam analogy whichenvisions beams of width c + d framing into each face of the column at a connection. Each beam has section properties identical to those of a slab section having the same width. The capacities of the individual beams are summed to obtain the connection strength.

The beam at the front face is presumed to be capable of developing its flexural capacity (top in tension) and the beam at the back face to be capable of its flexural capacity (bottom in tension). Computed capacities for the interior specimen are 1.72 kN-m (15.2 kip-in.) for both front and back beams.

Beams at the side face are each assumed to develop torsional capacities given by Eq. 5.7.

$$T_u = T_{co}\sqrt{1 - \left(\frac{V_u}{V_{uo}}\right)^2} \qquad 5.7$$

where T_u = ultimate torsional capacity of a torsion beam, V_u = shear acting on the torsion beam (assumed to be one-quarter of the total measured connection shear at failure), V_{uo} = shear capacity = $v_c(c + d)$, and T_{co} is the torsion capacity in the absence of shear, given by Eq. 5.8.

$$T_{co} = 0.133\sqrt{f'_c}\, h^2(c + d), \quad \text{N-mm} \qquad 5.8$$

The value of T_{co} is 0.477 kN-m (4.22 kip-in.) for the interior specimen. Taking V_u = 4.80 kN (1.08 kip), the torsional capacity of each beam is found by Eq. 5.7 to be 0.457 kN-m (4.04 kip-in.).

The beam at the front face is assumed to develop its shear capacity in addition to its flexural capacity. With an ultimate shear stress of v_c given by Eq. 5.4, the shear capacity of the front face is 16.5 kN (3.72 kip). Given that the front face is already loaded with a shear of V_u = 4.80 kN (1.08 kip) (one quarter of the gravity load shear), the unbalanced shear that the face can carry is equal to 16.5 - 4.80 = 11.7 kN (2.64 kip). The unbalanced shears on the front and back faces contribute an unbalanced moment equal to the product of the unbalanced shear

and its moment arm, which equals (c + d). The resulting unbalanced moment due to eccentric shear is equal to 2.22 kN-m (19.6 kip-in.).

The total unbalanced moment capacity is thus M_s = 2(1.72) + 2(0.457) + 2.22 = 6.57 kN-m (58.1 kip-in.), which is 64 percent of the measured capacity. The shortcoming of the calculated capacity probably occurs because the torsional capacities do not include a realistic estimate of the effect of slab reinforcement. A similar analogy presented by Hawkins considers explicitly the torsional strength due to slab steel. That method is described in detail in the next section.

5.6.1.4 Beam Analogy of Hawkins

The beam analogy of Hawkins [7] is identical to that of Park and Islam except in the consideration of the torsional strength of the torsional beams. In the Hawkins analogy, torsional strength calculations consider slab reinforcement explicitly, with the torsional strength given by the following expressions.

$$T_u = \left[1 - \left(\frac{V_u}{V_{uo}}\right)^2\right] T_{uo} \qquad 5.9$$

where T_u = torsional strength of single beam in the presence of shear, and T_{uo} = torsional strength without shear, as given by Eq. 5.10.

$$T_{uo} = 0.066 \sqrt{f'_c}\,(c + d)h^2 + \frac{A_t\, t x_1 y_1 f_y}{s}, \text{ N-mm} \qquad 5.10$$

where A_t = cross-sectional area of a slab bar, $_t$ = 0.66 + $0.33y_1/x_1 \leq 1.5$, x_1 = center to center distance between outermost layers of top and bottom slab bars, y_1 = c + d, and s = average spacing of slab bars. The value of T_{uo} is calculated to

be 1.85 kN-m (16.3 kip-in.) assuming an average spacing of s = 57 mm (2.25 in.). The value for T_u is subsequently calculated to be 1.69 kN-m (14.93 kip-in.).

All flexural and shear strengths are as calculated in Section 5.6.1.3 for the beam analogy of Park and Islam. Adding these strengths to the torsional capacity from the previous paragraph results in a calculated unbalanced moment capacity of 9.03 kN-m (79.9 kip-in.), which is 88 percent of the measured capacity.

5.6.2 Exterior Slab-Column Specimen

5.6.2.1 Moment-Curvature

Moment-curvature analyses were performed using the same approaches used for the interior specimen as described in Section 5.6.1.1. As for the interior specimen, selecting a nonuniform strain distribution for the slab reinforcement had negligible effect on computed capacities. Computed negative moment capacity is 7.8 kN-m (69 kip-in.), and computed positive capacity is 5.8 kN-m (51 kip-in.). These values are approximately 15 percent in excess of measured maximum values.

The closeness between measured and calculated capacities indicates that the plane-section capacities were nearly reached, suggesting that unbalanced moment capacities may have been limited by flexural yield across the full slab width. This possibility is investigated further in the next section in which unbalanced moment capacity in combined flexure and torsion is calculated using a beam analogy approach.

5.6.2.2 Beam Analogy Based on Space-Truss Theory

A beam analogy was developed to interpret unbalanced moment strength of the exterior connection. The analogy envisions a flexural beam of width c + d framing into the front face of the column, with transverse torsion beams comprising the spandrel beams.

Flexural strength of the beam at the front face is calculated directly as 1.72 kN-m (15.2 kip-in.) for top layer of reinforcement in tension, and 0.605 kN-m (5.35 kip-in.) for bottom layer in tension.

Torsional strength of the spandrel beam in combined torsion and shear is computed using concepts of the space truss theory [9]. Accordingly, the torsional strength in the absence of shear is given by Eq. 5.11.

$$T_{uo} = 2x_o y_o \sqrt{\frac{A_t f_{wy}}{s} \frac{A_l f_y}{2(x_o + y_o)}} \qquad 5.11$$

where x_o = horizontal center to center spacing of spandrel longitudinal bars, y_o = vertical center to center spacing of spandrel longitudinal bars, A_t = cross-sectional area of spandrel transverse bar, A_l = symmetric portion of total spandrel longitudinal steel, and s = center to center spacing between spandrel transverse bars. In the presence of shear the strength is given by Eq. 5.12.

$$T_u = \frac{T_{uo}}{1 + x_o V_u} \qquad 5.12$$

in which V_u is the shear in the spandrel beam. The shear V_u in each spandrel was not measured directly. Rather, the total shear on the connection at the time of failure was measured. For

simplicity, it was assumed that the proportion of the total connection shear carried by each torsional beam was equal to the ratio R given by Eq. 5.13.

$$R = \frac{T_{uo}}{2T_{uo} + M_f} \qquad 5.13$$

in which M_f = moment capacity of the flexural beam. Using this approximation, the torsion strength in the absence of shear was computed to be 2.66 kN-m (23.5 kip-in.) when the connection was in negative moment, which was reduced in the presence of shear to 2.09 kN-m (18.47 kip-in.). In the presence of positive moment, the corresponding capacities are 2.6 kN-m (23.5 kip-in.) and 2.52 kN-m (22.3 kip-in.).

The shear not carried by the torsion members was assigned to the flexural member at a distance d/2 from the column face. This eccentric shear contributed to the unbalanced moment.

The computed connection unbalanced moment capacities (the sum of the flexural, shear, and torsional components) are 6.28 kN-m (55.5 kip-in.) and 5.64 kN-m (50.0 kip-in.) in negative and positive moment. These values are 86 and 115 percent of maximum measured capacities. It is noted that the connection failed in combined torsion and flexure in negative moment (Fig. 5.14). It is possible that the positive unbalanced moment capacity was not achieved during the experiments. Considering that bottom slab strains were all near yield (Fig. 4.7) and considering that flexural capacity (Section 5.6.2.1) is approximately equal to the combined torsion flexure capacity, it is also possible that positive moment capacity was limited by flexural yield across the full slab width.

Other researchers [11,13] have suggested that torsional cracking in the spandrel results in a tendency for axial growth of the spandrel. As this growth would be restrained by the slab, the spandrel develops axial compression which enhances the spandrel torsion capacity. Considering the close comparison between measured and calculated negative unbalanced moment capacities for the test specimen, it appears unlikely that the effect referred to was significant. It is possible that inelastic load reversals imposed during the experiment dissipated the restraint if indeed there was a tendency for the restraint to develop. Further research is required to develop a firm understanding of this phenomenon.

6. CONCLUSION

6.1 Summary

Two reinforced concrete slab-column connections were subjected to gravity loads and slowly applied lateral loads with reversals. Each connection comprised a column and a full panel width of slab. One of the connections represented an interior connection, the other represented an exterior connection with a shallow spandrel beam. Both connections were three-tenths scale models of typical connections in a prototype flat plate structure designed for combined gravity and seismic loads.

This report documents the experiments, presents measured data and observations, and compares the measured behavior with behavior anticipated by analytical models. Primary conclusions of the study are presented in the following paragraphs.

6.2 Conclusions

Results of a linear elastic finite element analysis of the interior test specimen under gravity loads indicated that the prototype dead load moments were simulated properly, but that the test specimen was probably more heavily loaded in shear than the prototype. It was also concluded that gravity load effects on the exterior slab-column specimen adequately represented those on an exterior connection of the prototype structure.

The primary source of measured interstory drift of the subassemblies under lateral loads was deformation of the slab.

Slab deformations were localized within distances of approximately a column width (two slab depths) from the column faces of the interior connection, whereas the edge beam caused deformations to spread further in the exterior connection. Columns remained relatively rigid and elastic throughout the experiments.

Effective beam width analytical models were used to investigate lateral load stiffnesses at low level loads and at loads corresponding to working loads. Effective width coefficients of approximately 0.6 and 0.75 are required for equivalent width beams to model the initial secant stiffness of the interior and exterior specimens, respectively. Vanderbilt and Corley [15] suggest a value of 0.65 for an interior plate column connection having the same proportions as those tested. The slightly lower stiffness of the interior specimen may be a consequence of cracking in the specimen under gravity loads. The larger coefficient for the exterior connection is necessary because of the stiffening effect of the edge beam.

An effective width coefficient of approximately 0.25 is required to model the secant stiffness of the interior connection at working loads, where working loads are defined at a drift of approximately 0.2% of height, or a lateral load equal to 40% of capacity. The coefficient for the exterior connection depends on how working loads are defined and on whether the top or bottom surface of the slab is in tension. An average value for the coefficient is 0.6.

Equivalent frame models as defined for gravity loads by ACI 318-83 were also used to investigate lateral load stiffnesses.

An equivalent frame having gross section properties slightly underestimates the initial stiffness of the interior connection. The initial stiffness of the exterior specimen was approximated closely by equivalent frames having gross section inertias.

To investigate lateral load stiffnesses at working loads using the equivalent frame model, moments of inertia for slabs were reduced while maintaining gross section properties for columns and edge beams of the equivalent frames. A reduced effective slab inertia of approximately one-third of the gross section value is required to model the stiffness of the interior connection at working loads. An equivalent frame requires an effective slab inertia of approximately two-thirds of the gross section value to model the exterior connection stiffness at working loads. The effect of the edge beam is to lessen the reduction in effective slab inertia necessary for an equivalent frame to model the exterior connection stiffness.

Strength of the interior connection was limited by the capacity of the slab, and the exterior connection strength was limited by the combined flexural strength of the slab and torsional strength of the edge beam. Columns of the subassemblies were not loaded to their capacities in the experiments.

A standard moment-curvature analysis assuming plane sections remain plane in bending was found inapplicable for calculating the flexural capacity of the slabs because of the nonuniform distribution of moments across the slab widths. The localization of slab deformations indicates that slab bending moments are

greatest near the column and decrease away from the column.

A conservative interior connection slab strength estimate is provided by the procedure described in ACI 318-83 [3] for slab-column connections transferring shears and unbalanced moments. The beam analogy approach as described by Park and Islam [11], whereby a slab-column connection is modeled by an assemblage of flexural and torsional beams framing into the column yields a more conservative strength estimate of the interior connection. The analogy proposed by Hawkins yields a computed strength close to the measured strength.

A beam analogy approach was used to estimate the unbalanced moment capacity of the exterior connection. This approach provides a good estimate of the exterior connection strength.

Measured responses indicate that the plate-column subassemblies did not develop significant yield until imposed lateral drifts approached 1.5 percent. For comparison, ATC, in its report [4], recommends a limiting drift of 1.5 percent for seismic design. Hence, flat plates having proportions similar to those reported herein will remain essentially elastic at this drift level and cannot be expected to dissipate significant amounts of energy through hysteretic response. As a consequence, structural damage is expected to be minimal at the code implied drifts. However, the code procedure may not be directly applicable because the implied inelastic behavior will not occur at the prescribed drift.

Maximum displacement ductilities obtained during the experiments cannot be clearly defined because of the gradual yielding behavior exhibited by the connections. However, failure

did not occur until lateral drifts reached approximately four percent of interstory height. It is concluded from this observation that the reinforcement details provided in these connections were adequate.

REFERENCES

1. Aalami, B., "Moment-Rotation Relation Between Column and Slab," ACI JOURNAL, Proceedings V. 69, No. 5, May 1972, pp. 263-269.

2. Allen, Fred, and Darvall, Peter, "Lateral Load Equivalent Frame," ACI JOURNAL, Proceedings V. 74, No. 7, July 1977, pp. 294-299.

3. American Concrete Institute, "Building Code Requirements for Reinforced Concrete," ACI 318-83, Detroit, 1983, 102pp.

4. Applied Technology Council (ATC), "Tentative Provisions for the Development of Seismic Regulations for Buildings," Report ATC3-06, NBS Special Publication 510, NSF Publication 78-08, June 1978.

5. Corley, W. Gene, and Jirsa, James O., "Equivalent Frame Analysis for Slab Design," ACI JOURNAL, Proceedings V. 67, No.11, Nov. 1970, pp. 875-884. Also, discussion by Arthur C. Eberhardt and Edward S. Hoffman, Ti Huang, J. C. Jofriet and V. K. Handa, and Authors, Proceedings V. 68, No. 5, May 1971, pp. 397-401.

6. Diebold, John W., and Moehle, Jack P., "Experimental Study of the Seismic Behavior of a Two-Story Flat Plate Structure," Report No. UCB/EERC-84/08, Earthquake Engineering Research Center, University of California, Berkeley, California, 1984.

7. Hawkins, N. M., "Shear Strength of Slabs with Moments Transferred to Columns," Shear in Reinforced Concrete, ACI Special Publication 42, Vol.2, American Concrete Institute, Detroit, 1974, pp.817-846.

8. International Conference of Building Officials, Uniform Building Code, Whittier, CA, 1982, 780 pp.

9. Onsongo, W. M., and Collins, M. P., "Longitudinally Restrained Beams in Torsion," Publication No. 72-07, Department of Civil Engineering, University of Toronto, May 1972, 35pp.

10. Park, R., and Gamble, W. L., Reinforced Concrete Slabs, John Wiley & Sons, New York, 1980, 618pp.

11. Park, Robert, and Islam, Shamfiqul, "Strength of Slab-Column Connections with Shear and Unbalanced Flexure," Proceedings, ASCE, V. 102, ST9, Sept. 1976, pp. 1879-1901.

12. Pecknold, David A., "Slab Effective Width for Equivalent Frame Analysis," ACI JOURNAL, Proceedings V. 72, No. 4, April 1975, pp. 135-137. Also, discussion by F. H. Allen and P. LeP. Darvall, Robert Glover, and Author, Proceedings V. 72, No. 10, Oct. 1975, pp. 583-586.

13. Rangan, B. Vijaya, and Hall, A. S., "Moment and Shear Transfer Between Slab and Edge Column," ACI JOURNAL, Proceedings V.5, No.5, May 1983, pp. 183-191.

14. Vanderbilt, M. Daniel, "Equivalent Frame Analysis for Lateral Loads," Proceedings, ASCE, V. 105, ST10, Oct. 1979, pp. 1981-1998. Also, discussion by Ziad M. Elias, V. 106, ST7, July 1980, pp. 1671-1672, and closure, V. 107, ST1, Jan. 1981, p. 245.

15. Vanderbilt, M. Daniel, and Corley, W. Gene, "Frame Analysis of Concrete Buildings," Concrete International, ACI, V. 5 No. 12, Dec. 1983, pp. 33-43.

16. Wilson, Edward L., "SAP-80 - Structural Analysis Programs for Small or Large Computer Systems," Presented at CEPA 1980 Fall Conference and Annual Meeting, Newport Beach, California, October 13-15.

Table 2.1 Direct Shears and Unbalanced Moments Used in Design

Location/Action	Load Combination		
	Ug = 1.4D + 1.7L	0.75(Ug + 1.87E)	0.75(Ug + 1.87[2E])
Exterior Shear, kN	19.2	15.2	16.0
Interior Shear, kN	38.3	28.7	28.8
Exterior Moment, kN-m	4.25	3.94	4.69
Interior Moment, kN-m	0.89	2.07	3.48

Table 3.1 - Plain Concrete Properties

	INTERIOR SPECIMEN		EXTERIOR SPECIMEN	
	Mean MPa (ksi)	Std. Dev. MPa (ksi)	Mean MPa (ksi)	Std. Dev. MPa (ksi)
f_c	26.2 (3.8)	1.9 (0.3)	19.3 (2.8)	1.4 (0.2)
f_t	3.59 (0.52)	0.21 (0.03)	3.17 (0.46)	0.074 (0.01)
f_r	4.69 (0.68)	0.30 (0.04)	3.37 (0.49)	0.13 (0.02)
$E_{.45f}$	21793 (3200)	0.69 (100)	18414 (2700)	2760 (400)
$E_{tangent}$	21655 (3100)	0.48 (70)	21007 (3000)	1483 (200)

Table 3.2 - Concrete Mix Composition

Material	Specific Gravity	SSD Wgt
Type I-II Permanente Cement (C1024)	3.15	2.593
Water	1.00	1.557
Radum Pea Gravel (9.5-mm MSA)	2.68	6.347
Radum Top Sand	2.68	5.809
Tidewater Blend Sand	2.60	1.312
Total	--	17.62

Table 5.1 Unbalanced Moment Capacity Estimates

(a) INTERIOR CONNECTION

Measured	10.3 kN-m
Linear Shear Stress Variation	
(a) effective flexural width of c+h	8.33 kN-m
(b) effective flexural width of 3(c+h)	10.0 kN-m
Park and Islam	6.57 kN-m
Hawkins	9.03 kN-m
Moment Curvature	
(a) bottom surface in tension	5.2 kN-m
(b) top surface in tension	7.9 kN-m

(b) EXTERIOR CONNECTION

Measured	
(a) bottom surface in tension	4.9 kN-m
(b) top surface in tension	7.3 kN-m
Moment Curvature	
(a) bottom surface in tension	5.8 kN-m
(b) top surface in tension	7.8 kN-m
Beam Analogy Based on Space Truss Analogy	
(a) bottom surface in tension	5.64 kN-m
(b) top surface in tension	6.28 kN-m

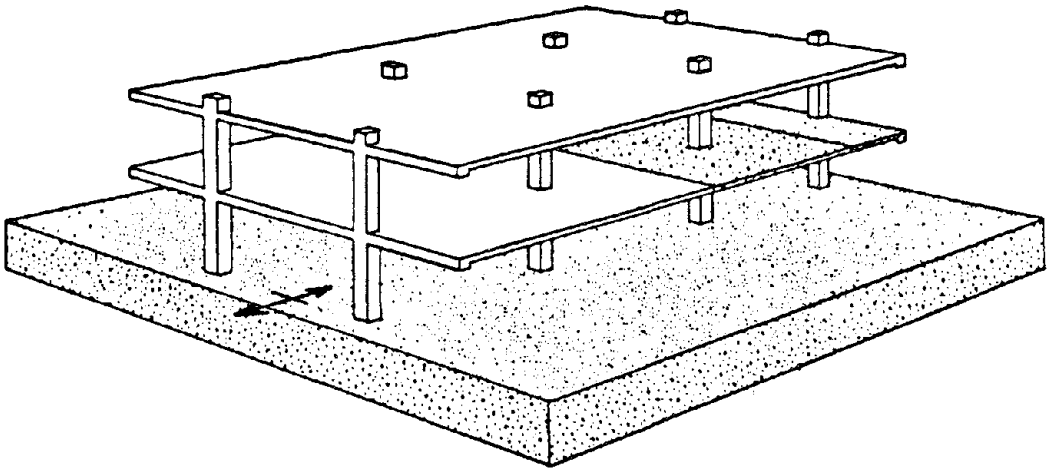

(a) SHAKE-TABLE MODEL

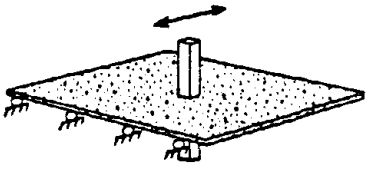

(b) INTERIOR CONNECTION

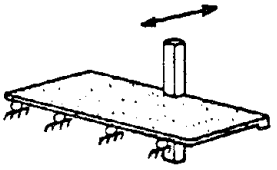

(c) EXTERIOR CONNECTION

FIG. 1.1 Flat Plate Structure Under Study

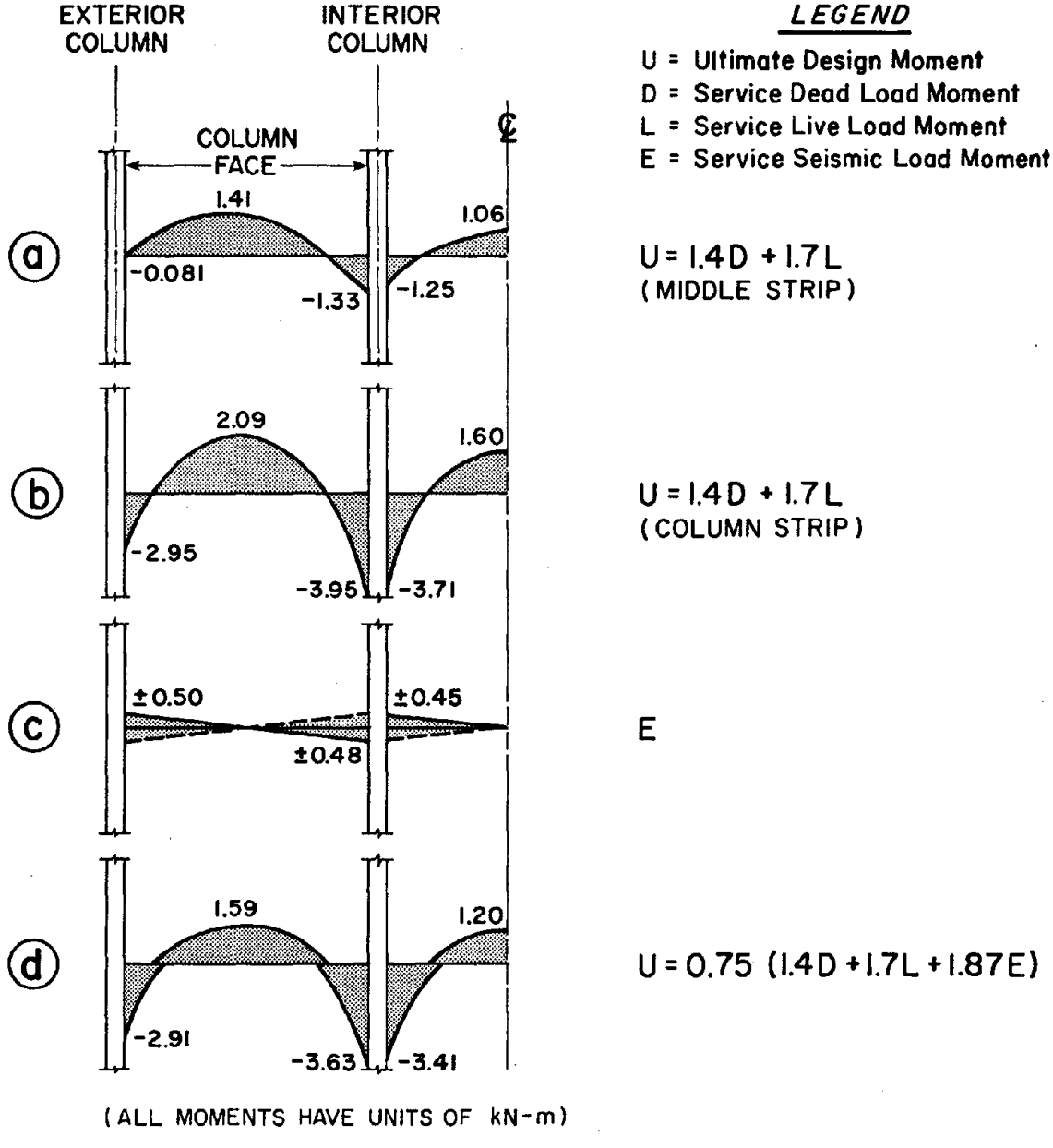

FIG. 2.1 Slab Design Moments

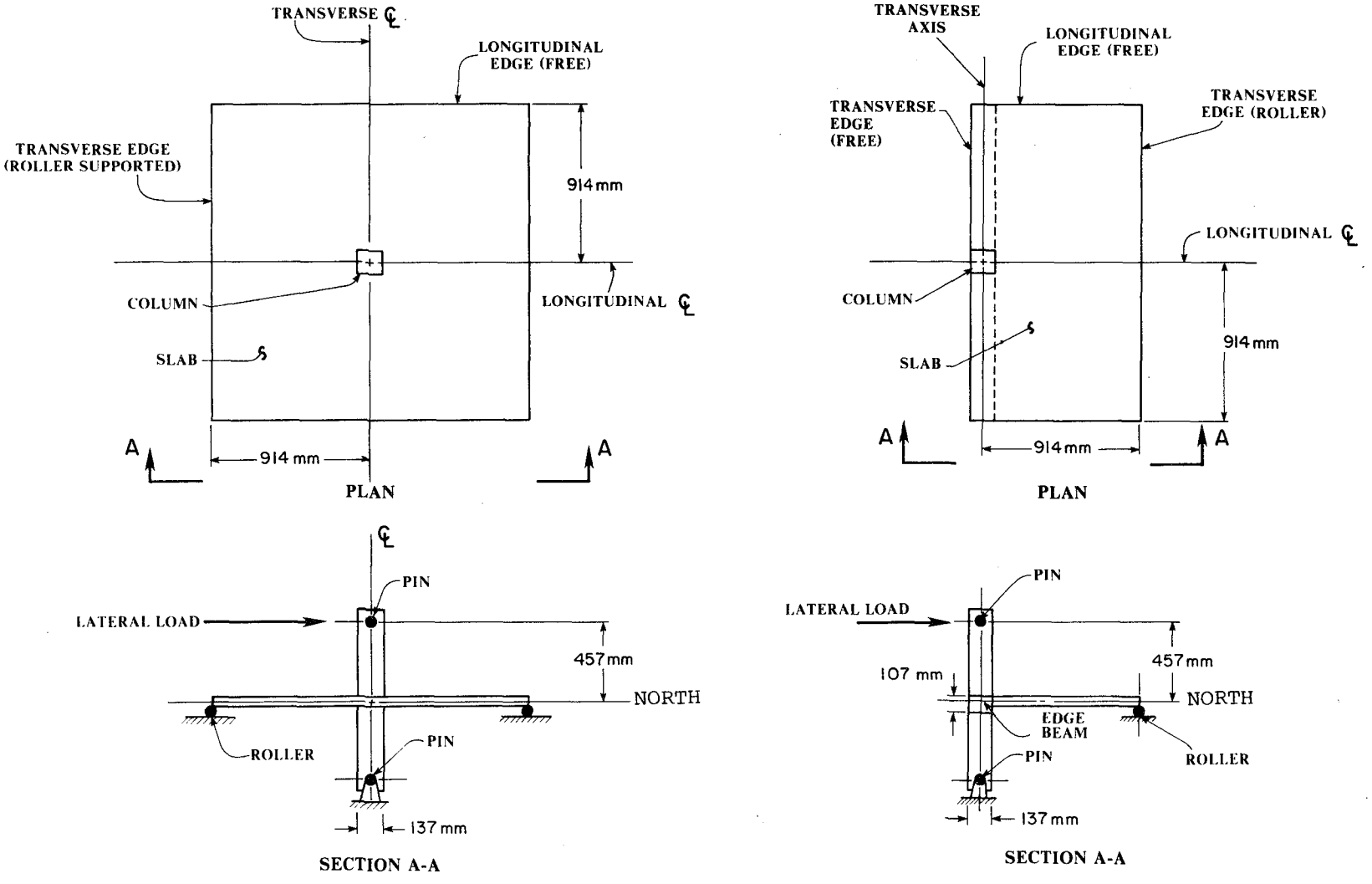

(a) INTERIOR CONNECTION **(b) EXTERIOR CONNECTION**

FIG. 3.1 Idealizations Of Interior And Exterior Subassemblies

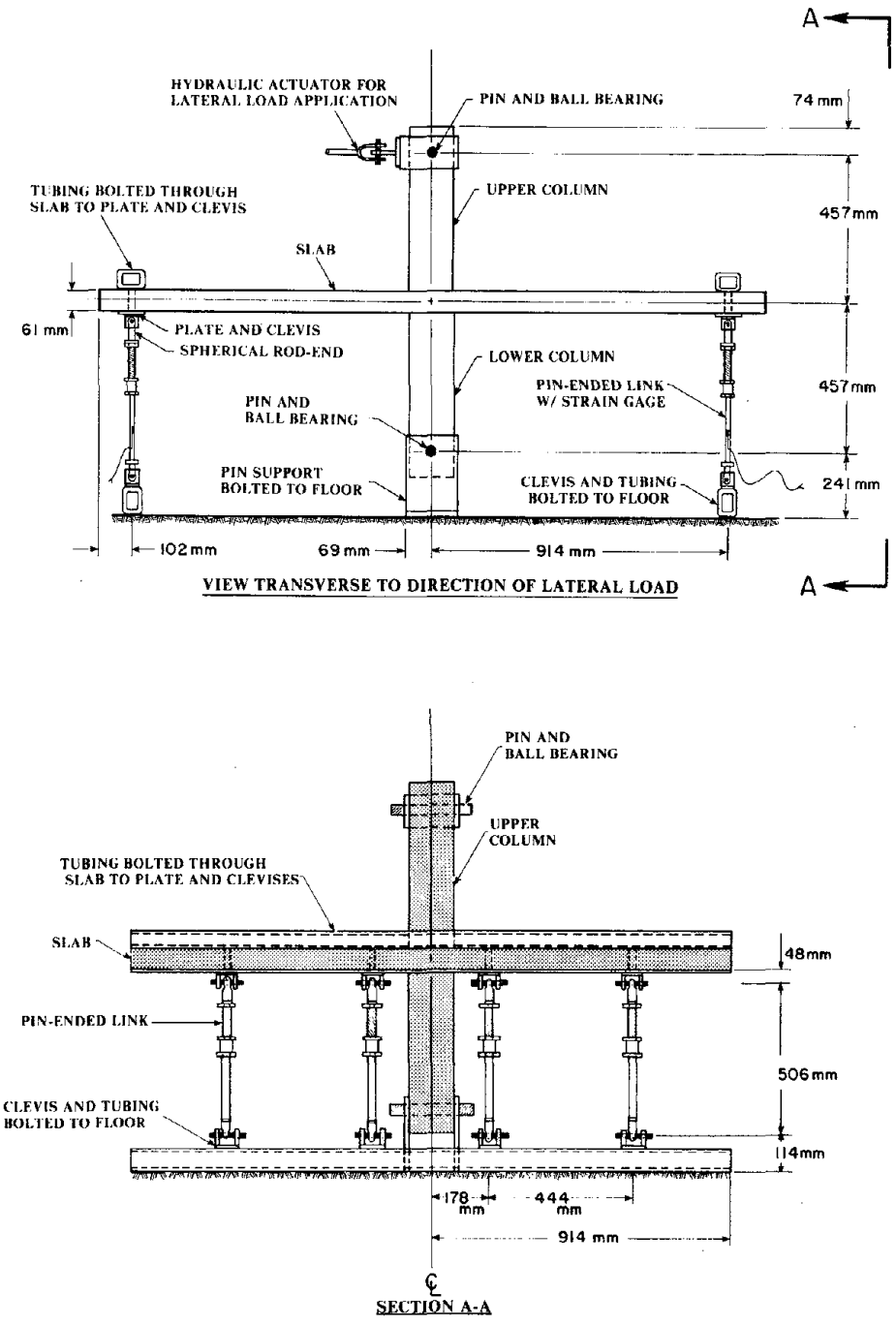

(a) INTERIOR CONNECTION

FIG. 3.2 Interior And Exterior Test Specimens

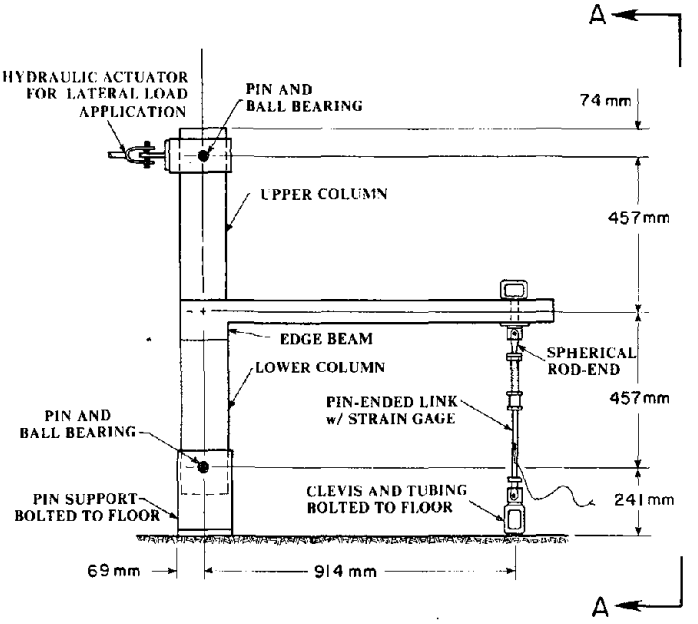

VIEW TRANSVERSE TO DIRECTION OF LATERAL LOAD

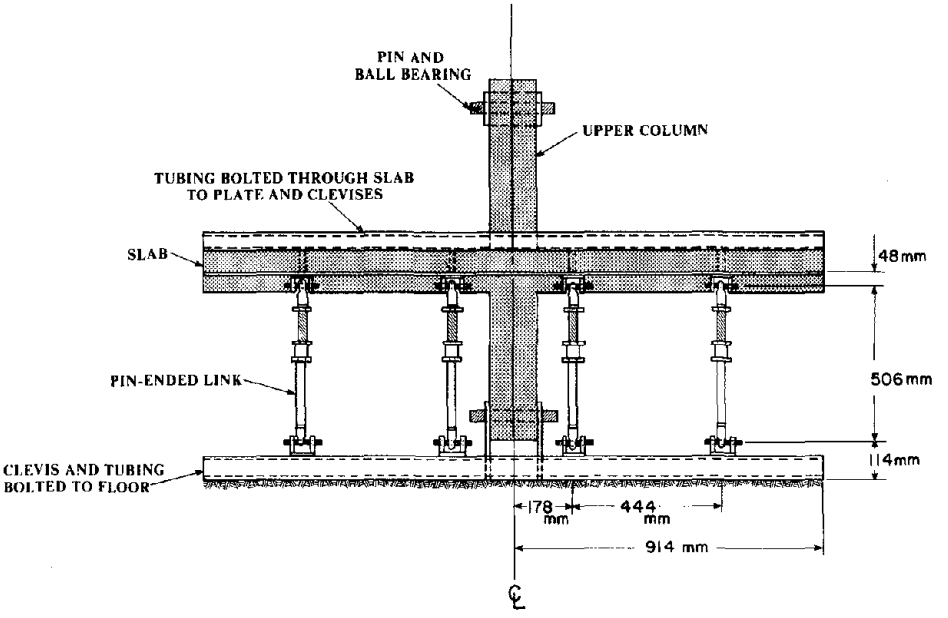

SECTION A-A

(b) EXTERIOR CONNECTION

FIG. 3.2 Continued

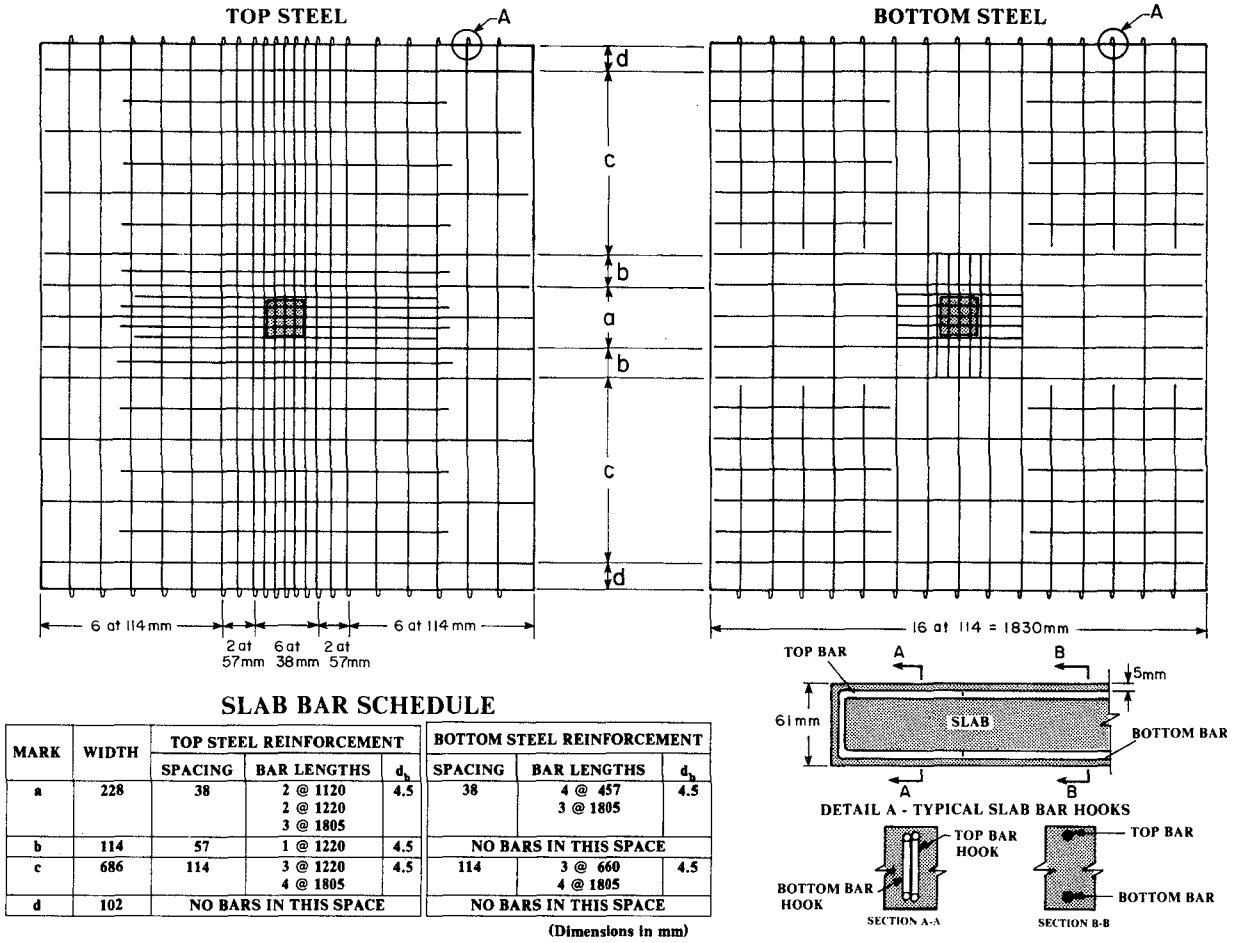

SLAB BAR SCHEDULE

MARK	WIDTH	TOP STEEL REINFORCEMENT			BOTTOM STEEL REINFORCEMENT		
		SPACING	BAR LENGTHS	d_b	SPACING	BAR LENGTHS	d_b
a	228	38	2 @ 1120 2 @ 1220 3 @ 1805	4.5	38	4 @ 457 3 @ 1805	4.5
b	114	57	1 @ 1220	4.5	NO BARS IN THIS SPACE		
c	686	114	3 @ 1220 4 @ 1805	4.5	114	3 @ 660 4 @ 1805	4.5
d	102	NO BARS IN THIS SPACE			NO BARS IN THIS SPACE		

(Dimensions in mm)

FIG. 3.3 Slab Reinforcement Of Interior Connection

SLAB BAR SCHEDULE

MARK	WIDTH	TOP STEEL REINFORCEMENT			BOTTOM STEEL REINFORCEMENT		
		SPACING	BAR LENGTHS	d_b	SPACING	BAR LENGTHS	d_b
a	228	38	2 @ 610 2 @ 660 3 @ 1060	4.5		SEE CORRESPONDING FIGURE	
b	114	57	1 @ 660	4.5			
c	686	114	3 @ 660 3 @ 1060	4.5 4.5			
d	102	NO BARS IN THIS SPACE			NO BARS IN THIS SPACE		
e	686	114	3 @ 1220 4 @ 1805	4.5 4.5	114	3 @ 650 4 @ 1805	4.5 4.5
f	114	57	1 @ 1220 1 @ 1805	4.5	114	1 @ 1805	4.5
g	182	NO BARS IN THIS SPACE			NO BARS IN THIS SPACE		

(DIMENSIONS IN mm)

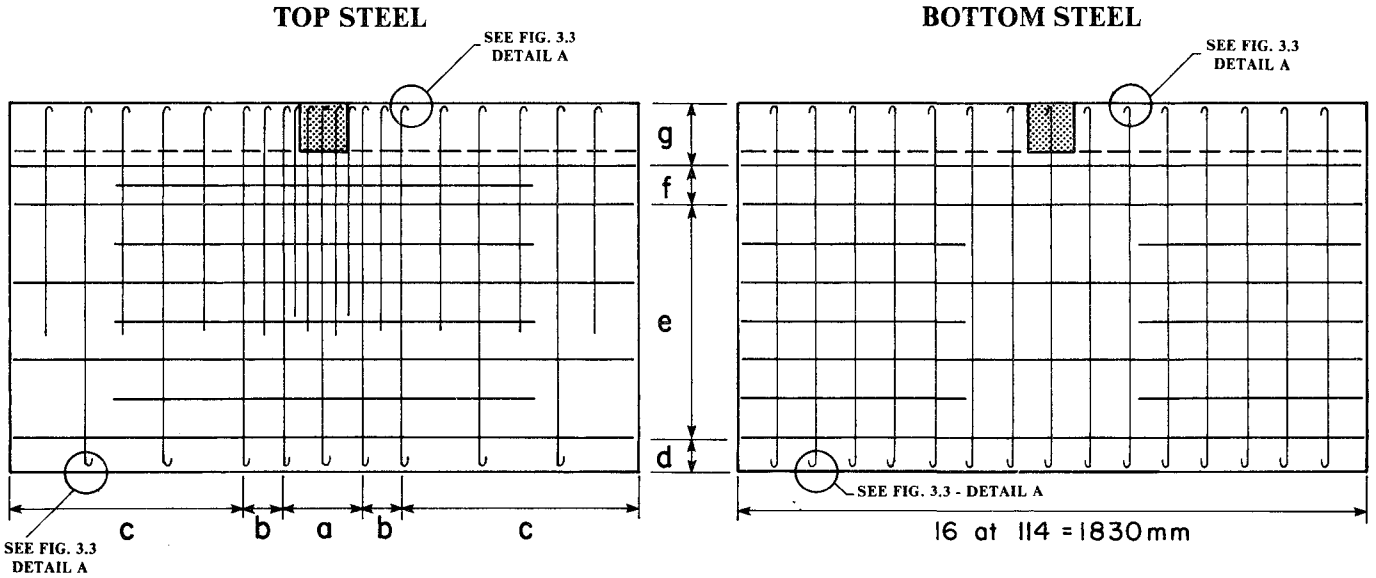

FIG. 3.4 Slab Reinforcement Of Exterior Connection

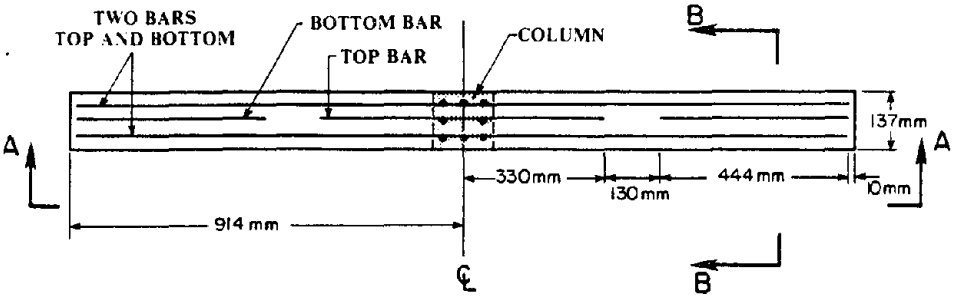

(STIRRUPS NOT SHOWN)

(a) PLAN

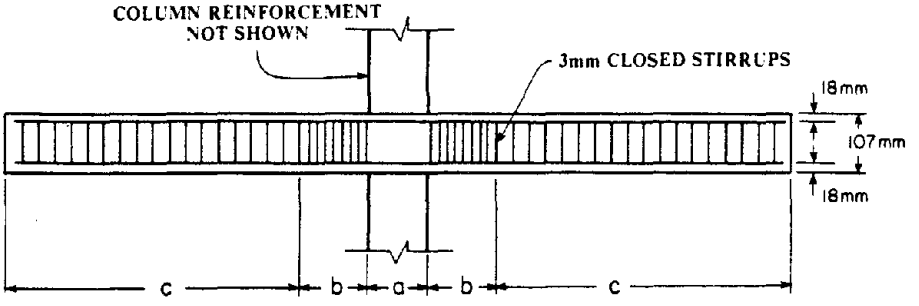

(SEE EDGE BEAM STIRRUP SCHEDULE)

(b) SECTION A-A

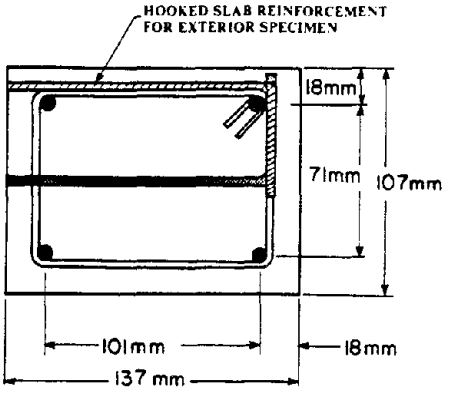

(c) SECTION B-B

MARK	LENGTH (mm)	SPACING (mm)	DIAM. (mm)
a	152	NO STIRRUPS	
b	152	19.1	3.0
c	686	38.1	3.0

(d) EDGE BEAM STIRRUP SCHEDULE

FIG. 3.5 Edge Beam Reinforcement

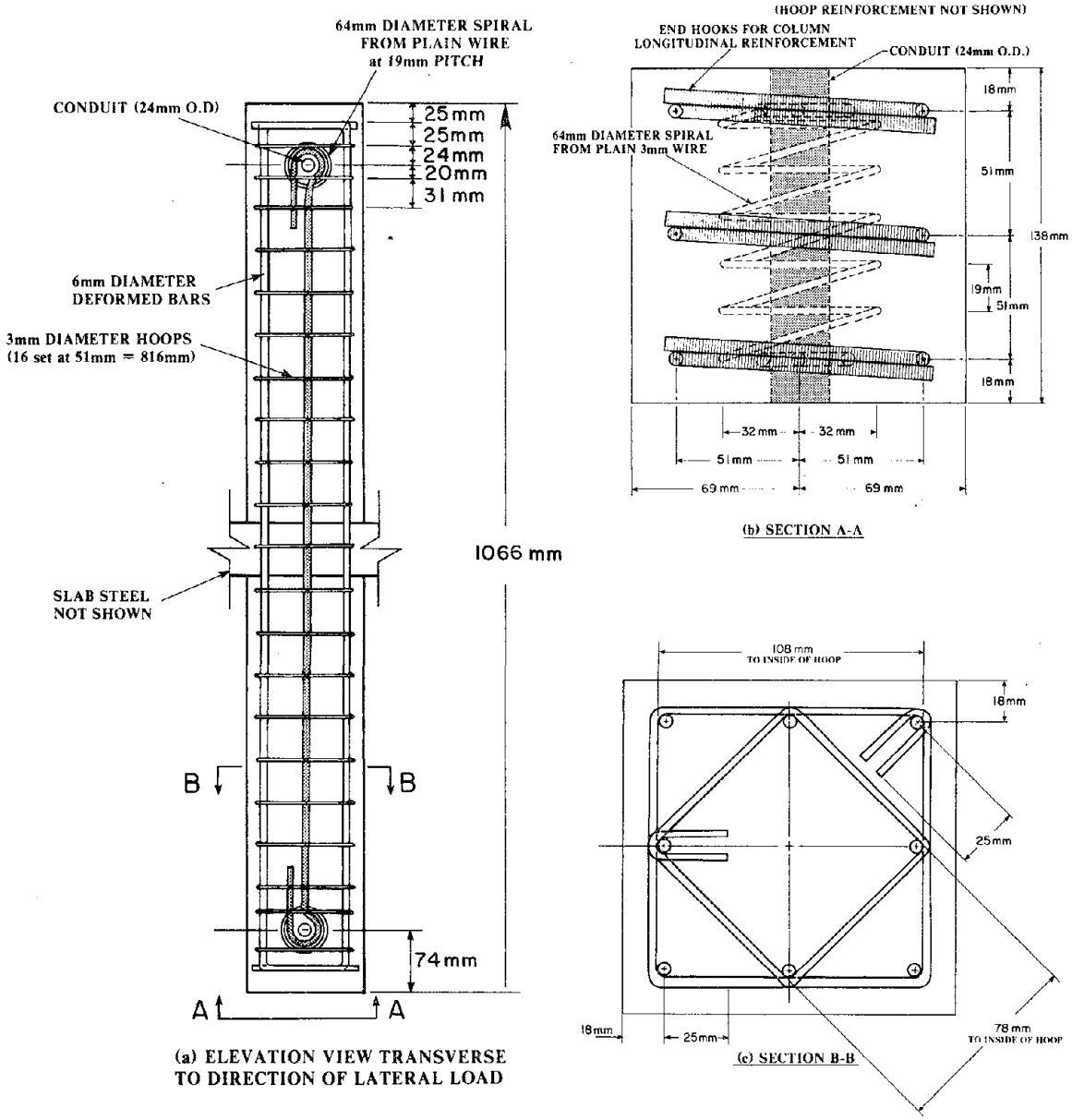

FIG. 3.6 Column Reinforcement

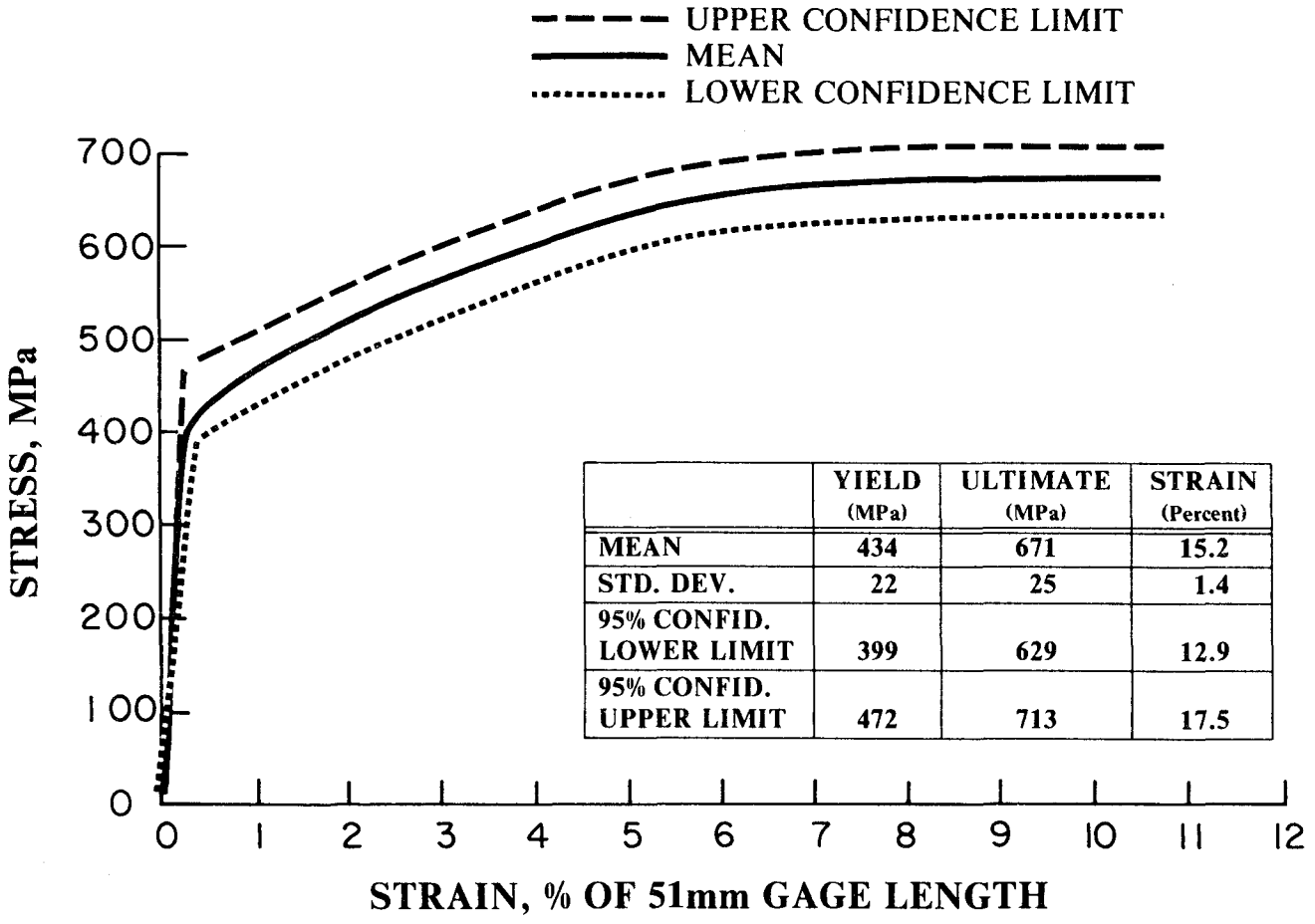

	YIELD (MPa)	ULTIMATE (MPa)	STRAIN (Percent)
MEAN	434	671	15.2
STD. DEV.	22	25	1.4
95% CONFID. LOWER LIMIT	399	629	12.9
95% CONFID. UPPER LIMIT	472	713	17.5

FIG. 3.7 Stress-Strain Relation For 4.5-mm Nominal Diameter Reinforcement

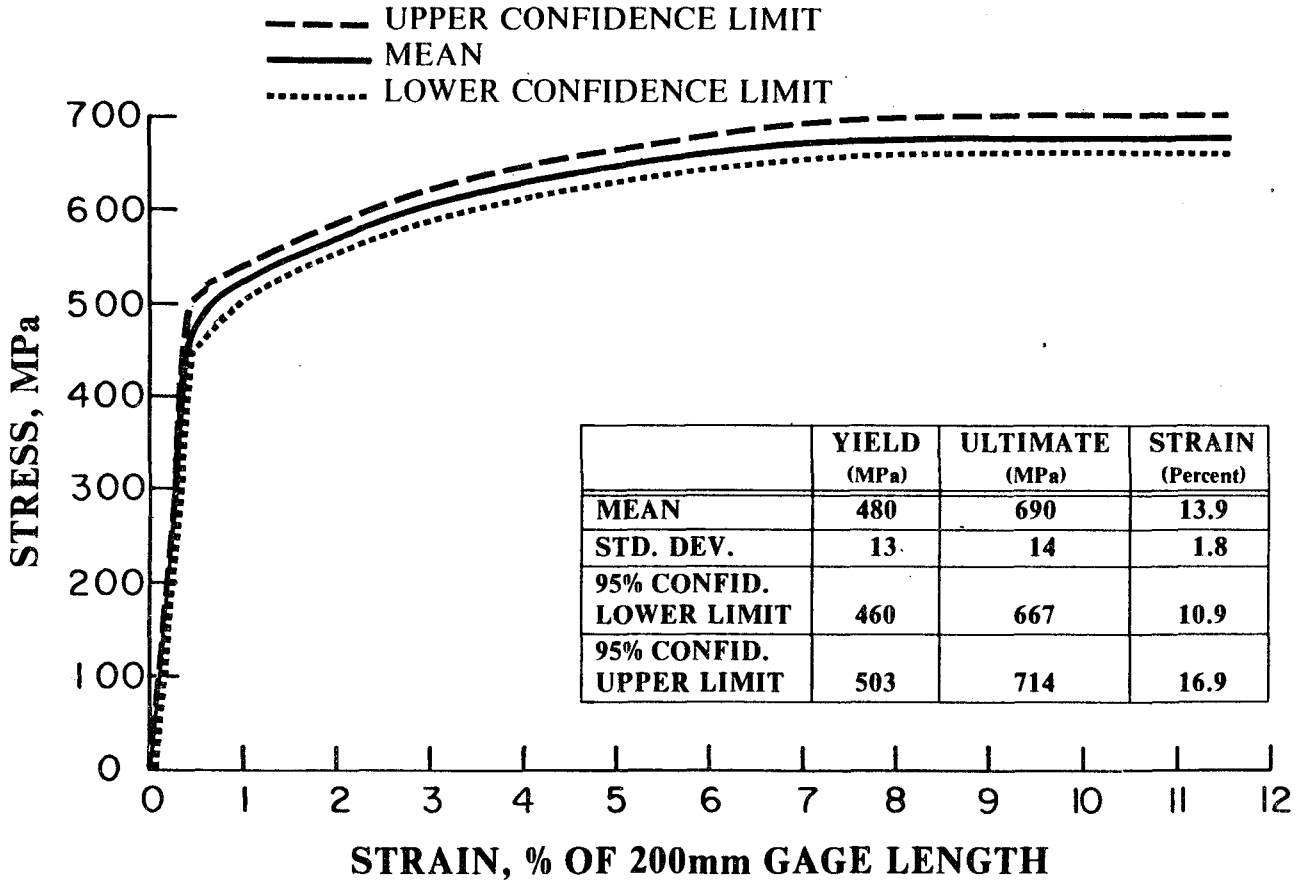

	YIELD (MPa)	ULTIMATE (MPa)	STRAIN (Percent)
MEAN	480	690	13.9
STD. DEV.	13	14	1.8
95% CONFID. LOWER LIMIT	460	667	10.9
95% CONFID. UPPER LIMIT	503	714	16.9

FIG. 3.8 Stress-Strain Relation For 6.4-mm Nominal Diameter Reinforcement

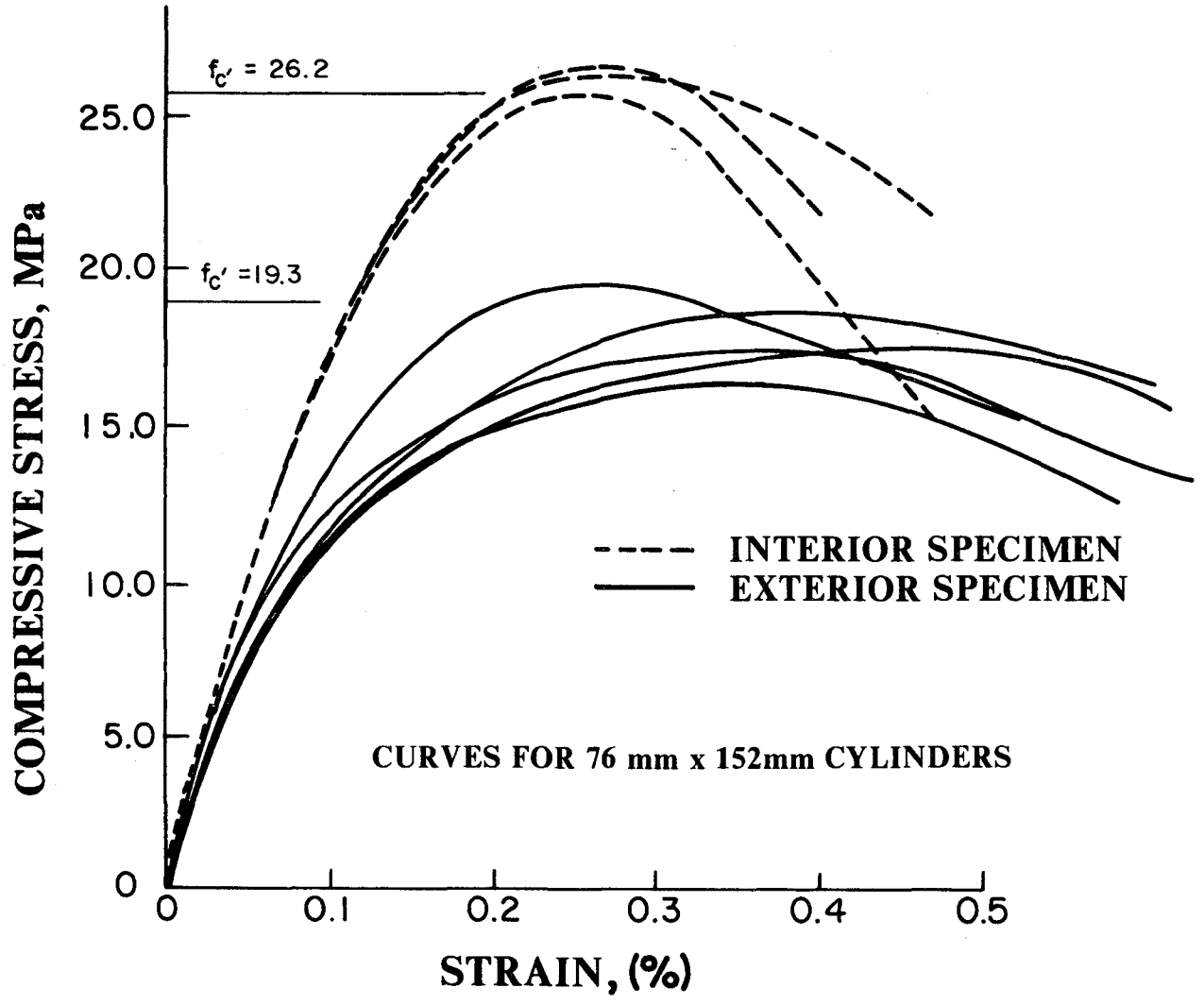

FIG. 3.9 Concrete Stress-Strain Relations

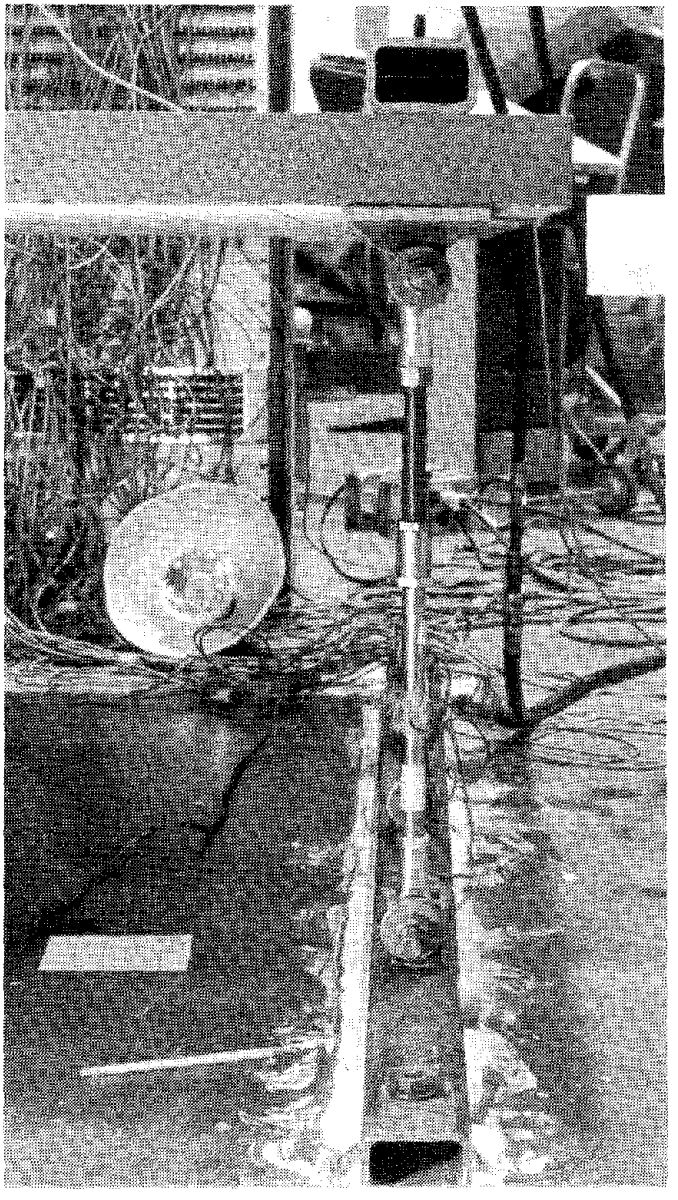

FIG. 3.10 Typical Pin-Ended Link Bolted To Slab And Floor

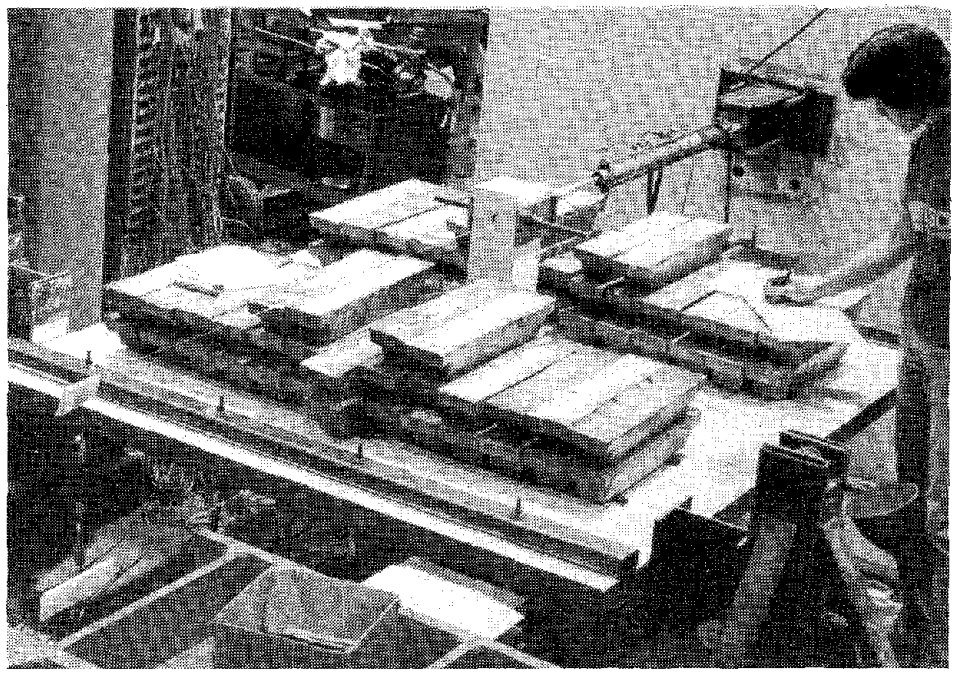

(a) INTERIOR SPECIMEN

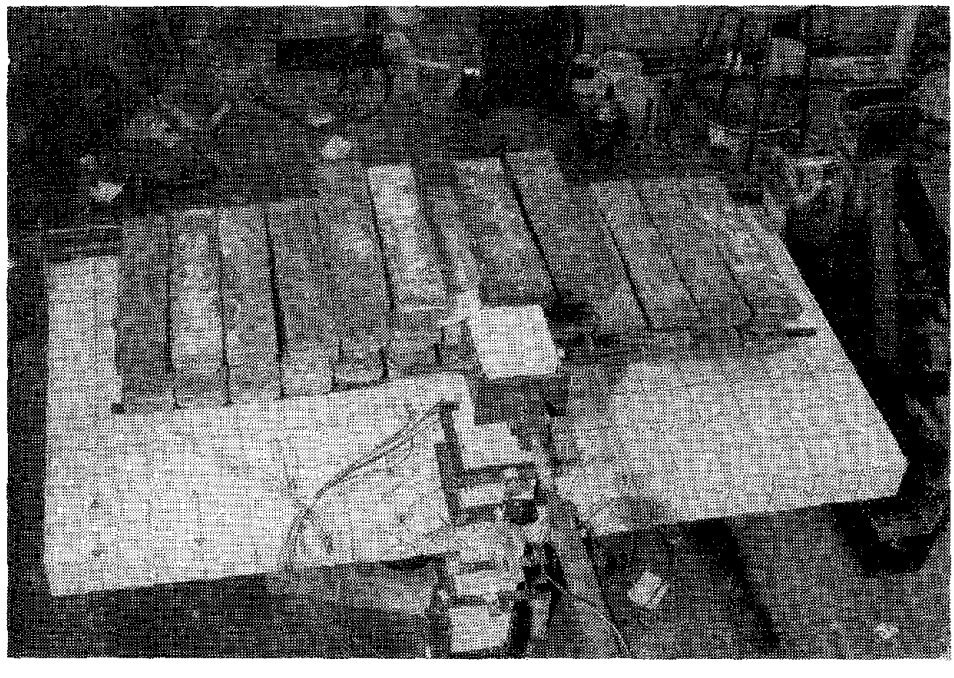

(b) EXTERIOR SPECIMEN

FIG. 3.11 Dead Load On Interior And Exterior Specimens

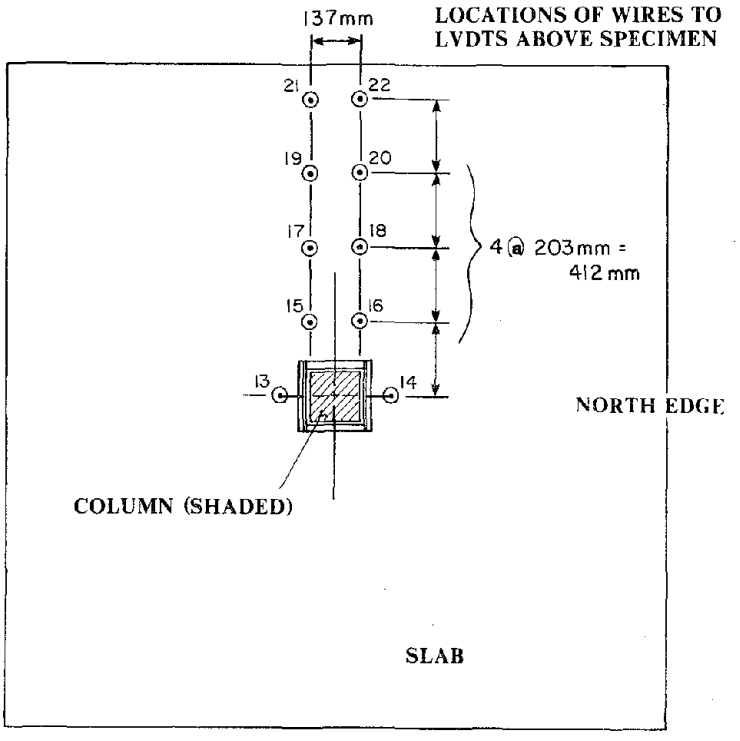

PLAN

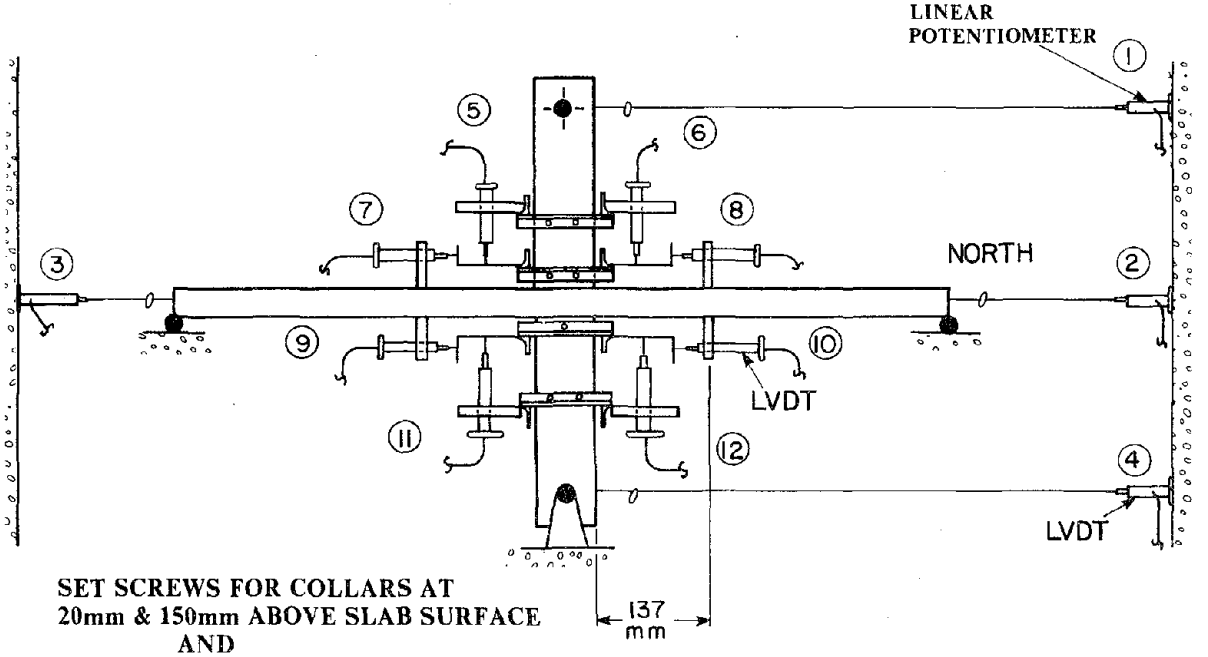

SET SCREWS FOR COLLARS AT
20mm & 150mm ABOVE SLAB SURFACE
AND
14mm & 155mm BELOW SLAB SURFACE

END VIEW

(a) INTERIOR SPECIMEN

FIG. 3.12 Instrumentation Of Test Specimens

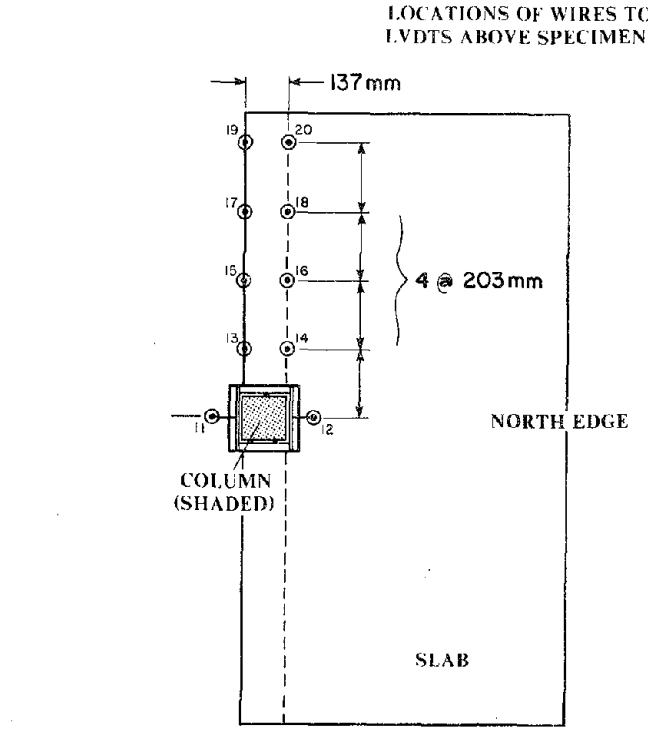

PLAN

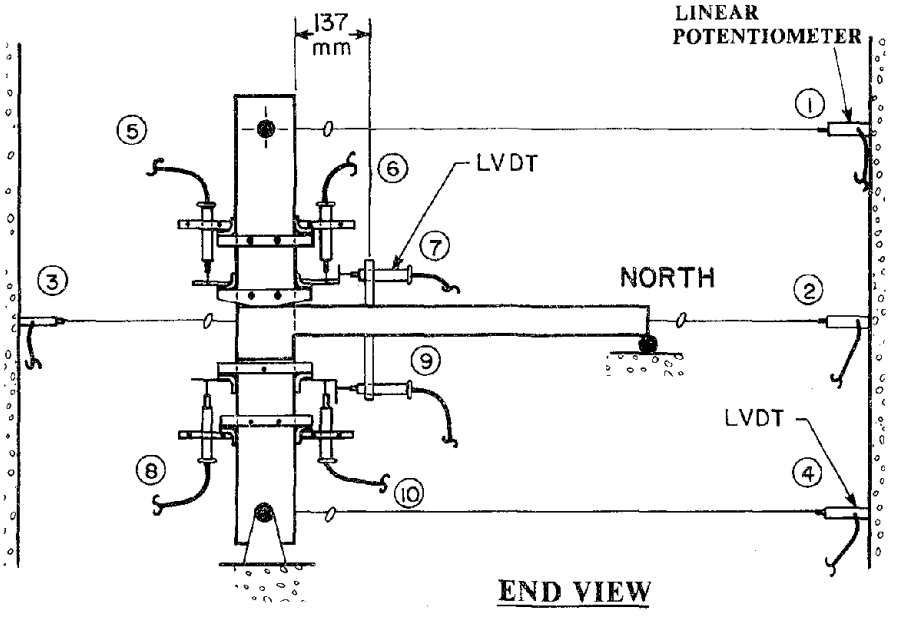

END VIEW

SET SCREWS FOR COLLARS AT
20mm & 150mm ABOVE SLAB SURFACE
AND
14mm & 155mm BELOW SLAB SURFACE

(b) EXTERIOR SPECIMEN

FIG. 3.12 Continued

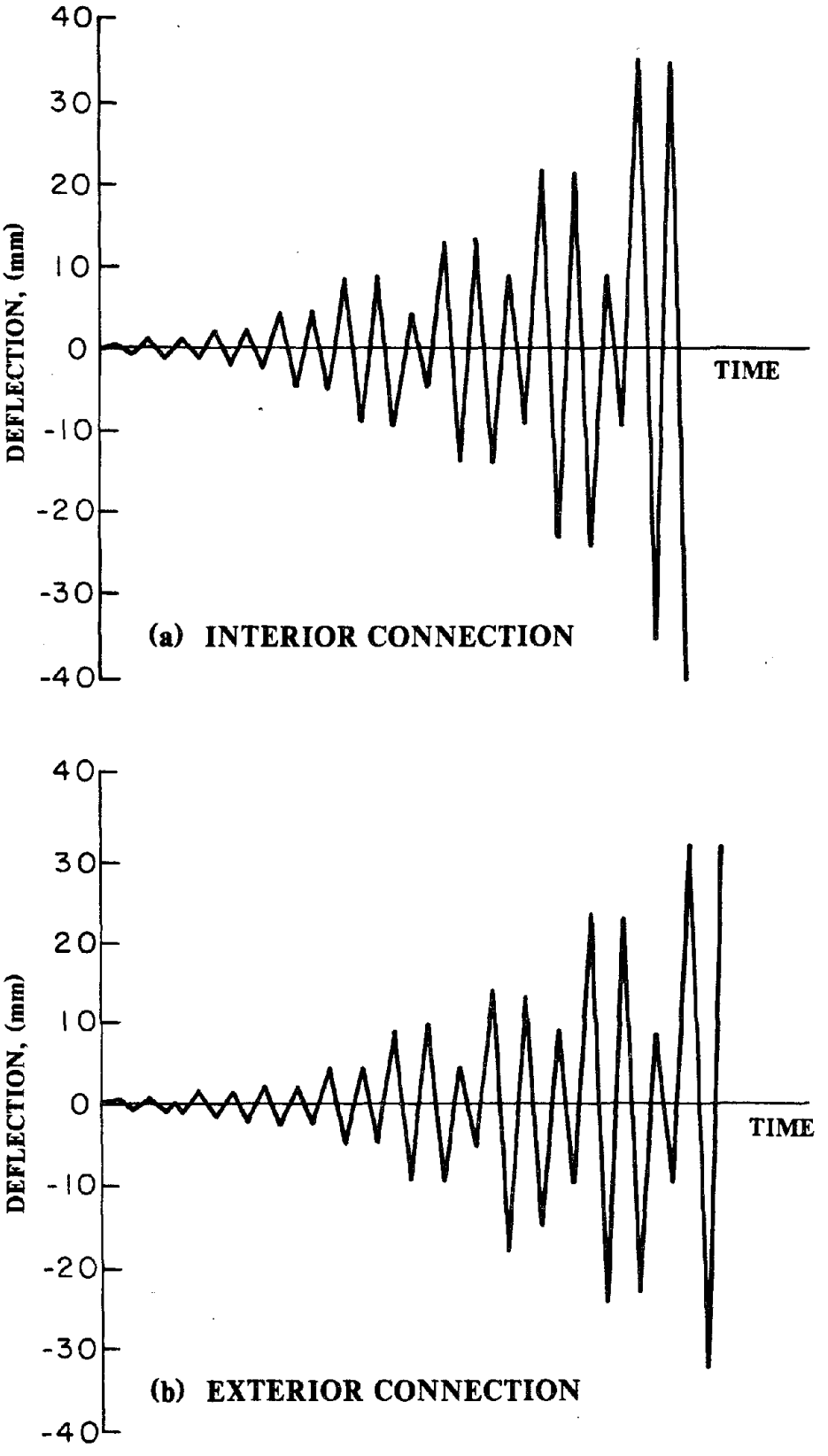

FIG. 4.1 Lateral Deflection Histories

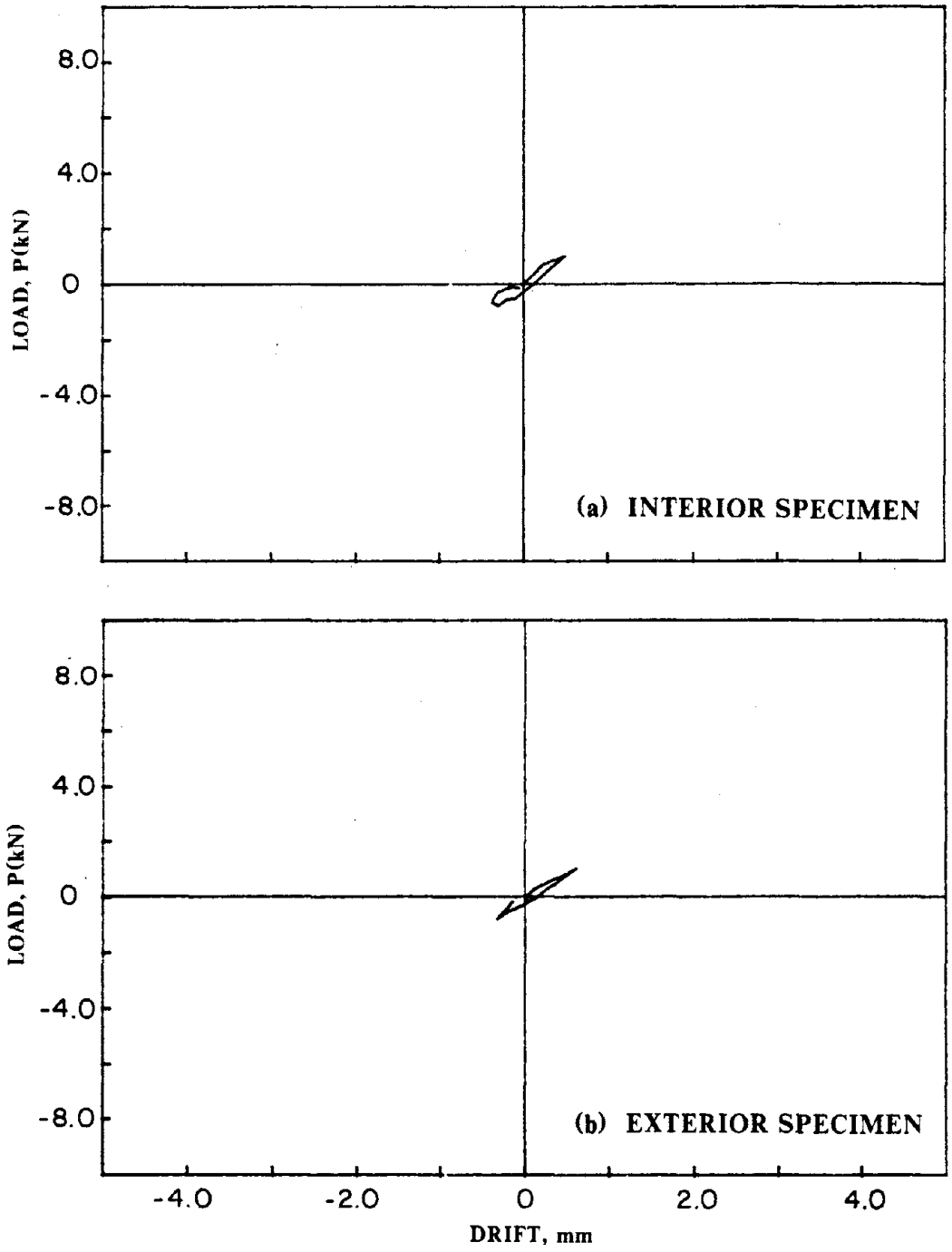

FIG. 4.2 Preliminary Load-Deflection Response

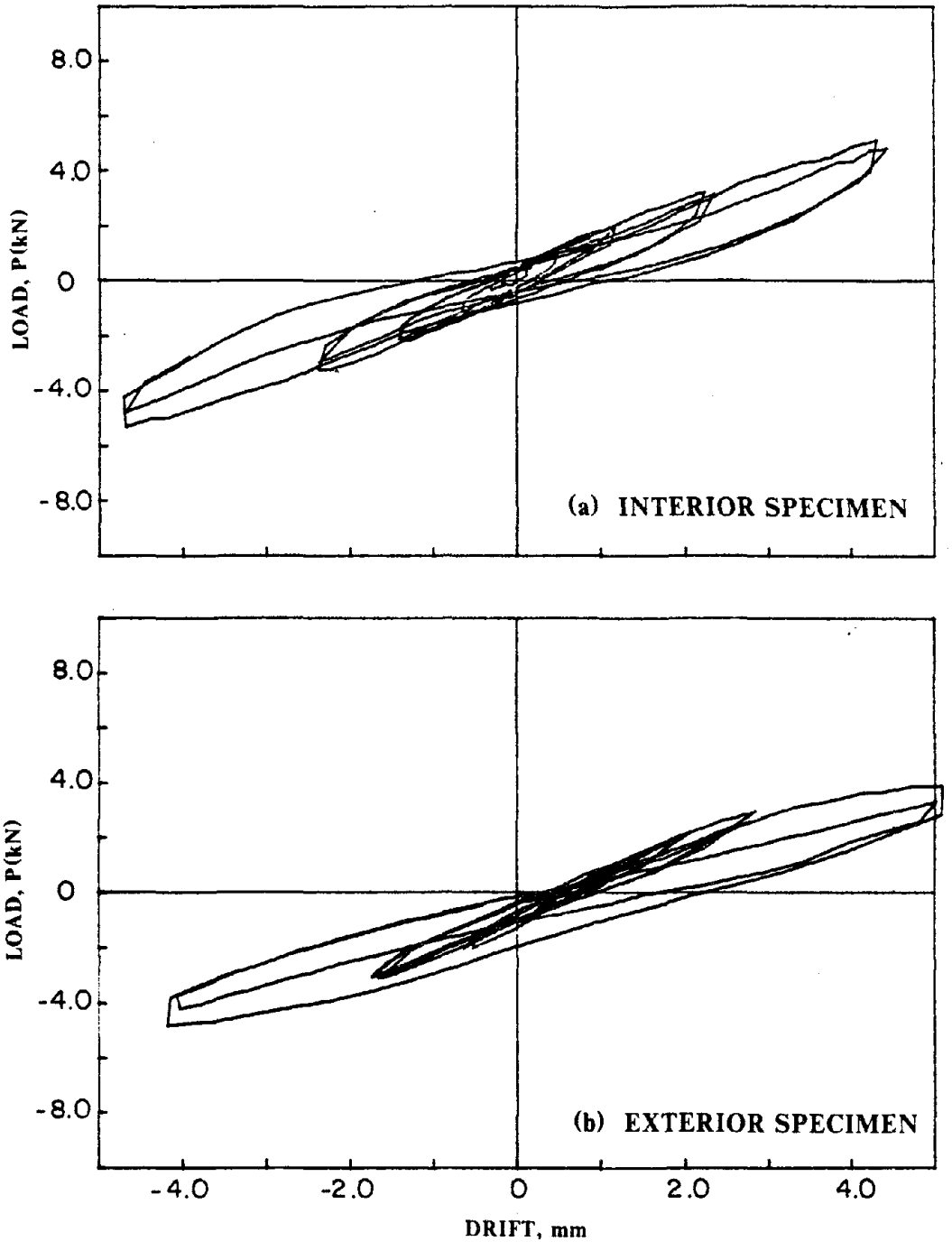

FIG. 4.3 Load-Deflection Response Up To Half Percent Of Interstory Drift

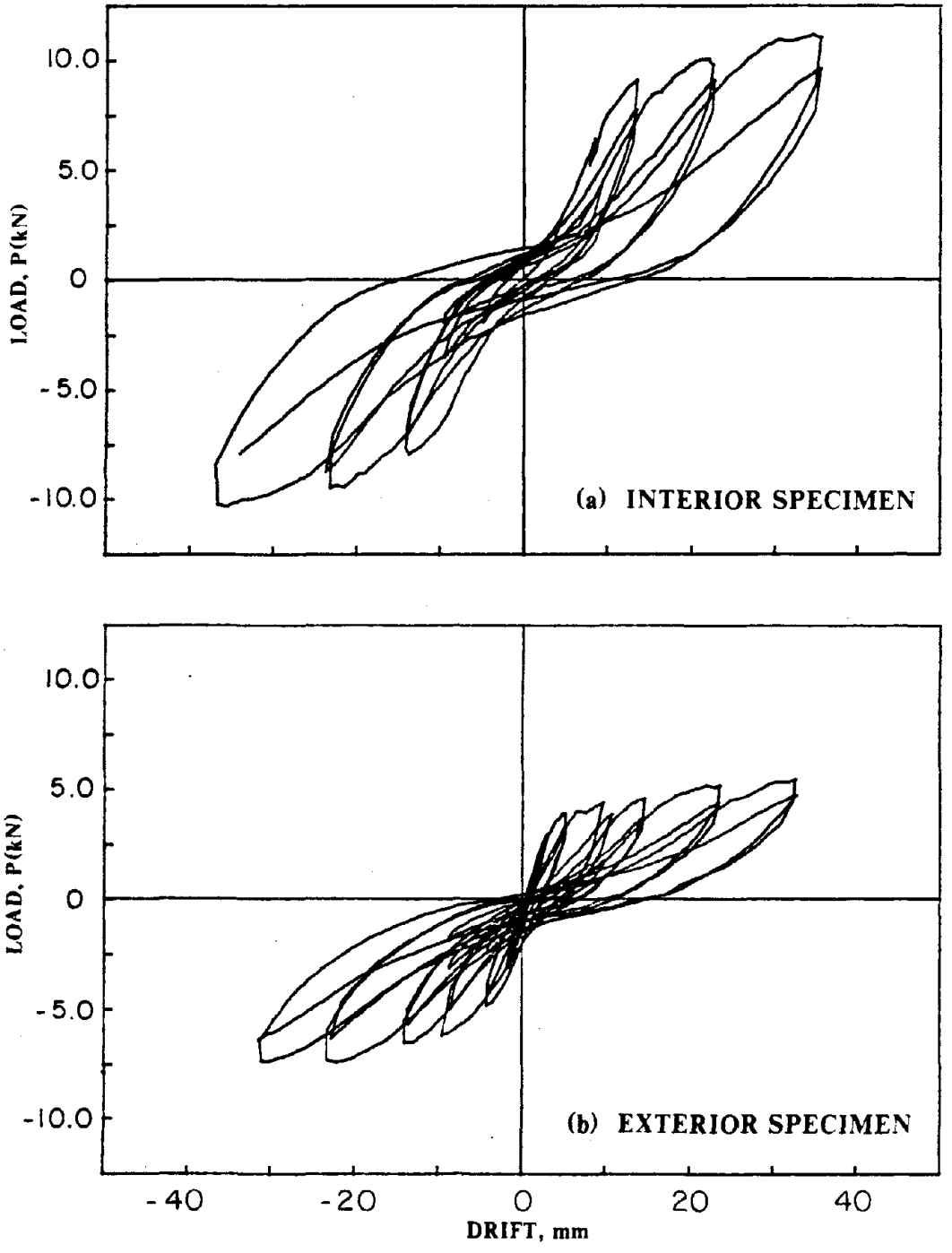

FIG. 4.4 Load-Deflection Response To Failure

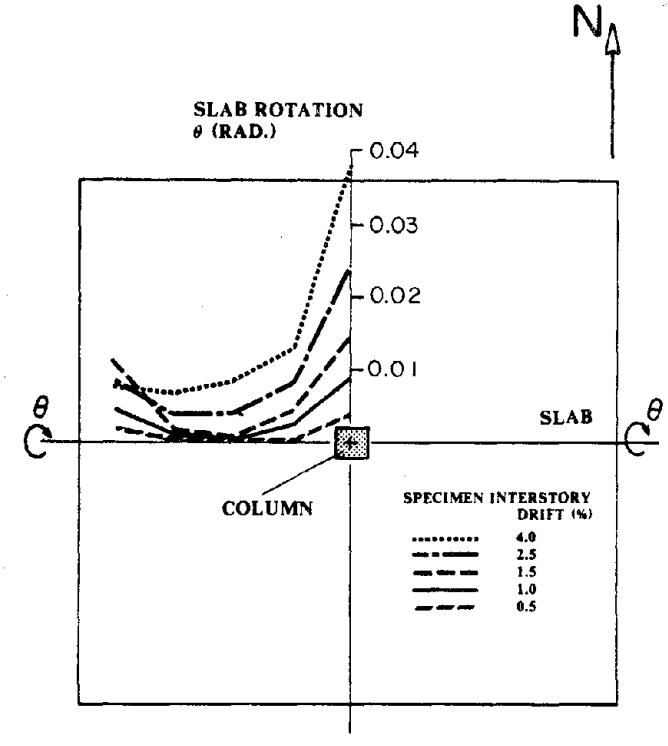

(a) INTERIOR CONNECTION

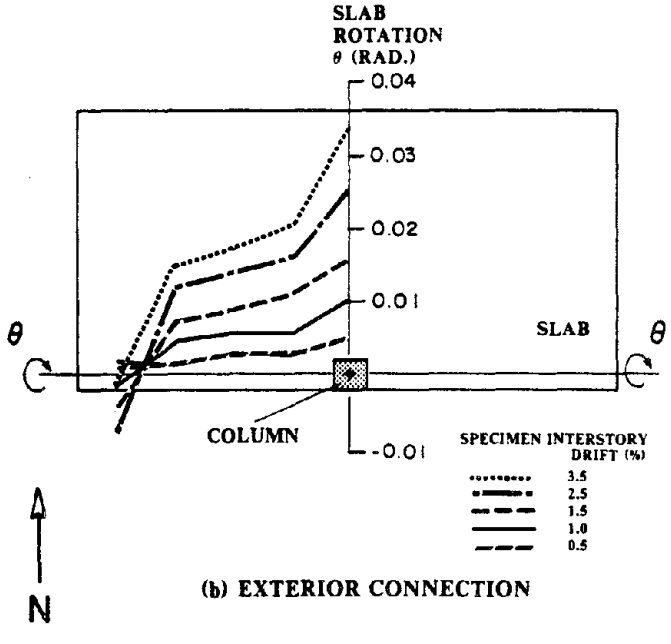

(b) EXTERIOR CONNECTION

FIG. 4.5 Slab Rotation Profiles For Selected Interstory Drifts

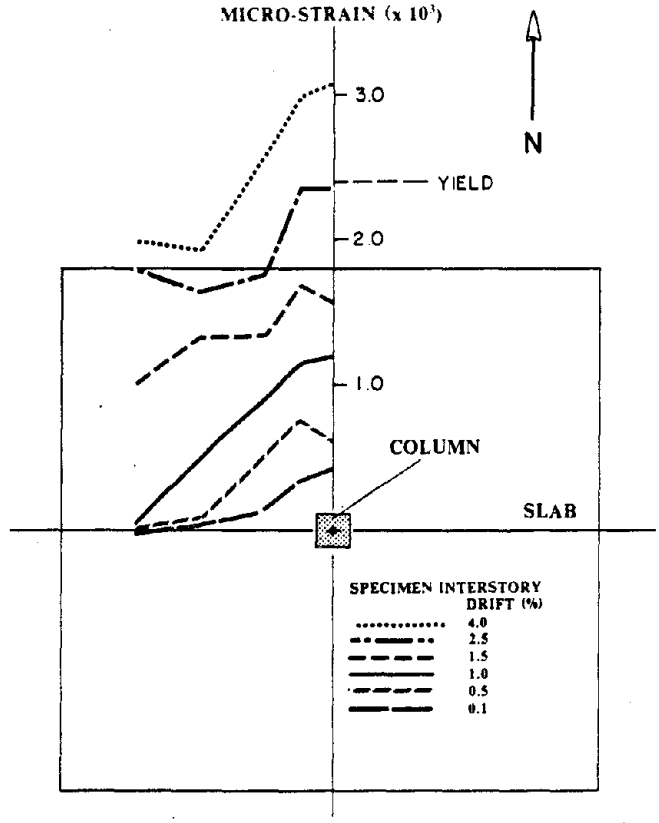

(a) INTERIOR CONNECTION

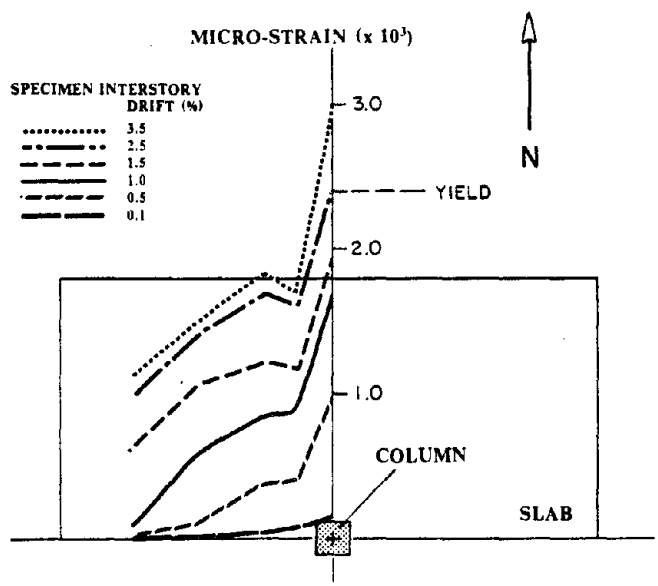

(b) EXTERIOR CONNECTION

FIG. 4.6 Strain Profiles For Top Layer Slab Reinforcement

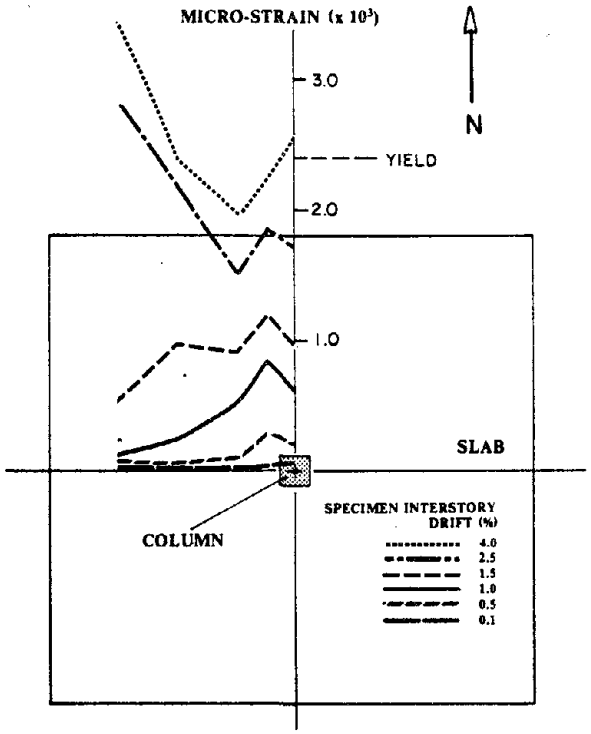

(a) INTERIOR CONNECTION

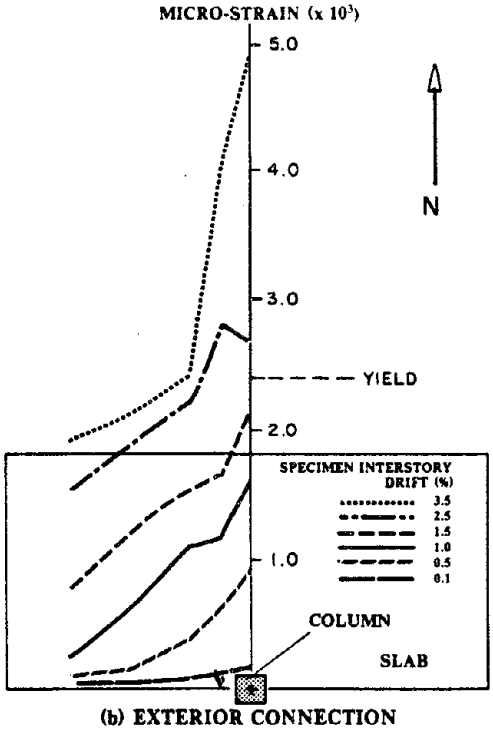

(b) EXTERIOR CONNECTION

FIG. 4.7 Strain Profiles For Bottom Layer Slab Reinforcement

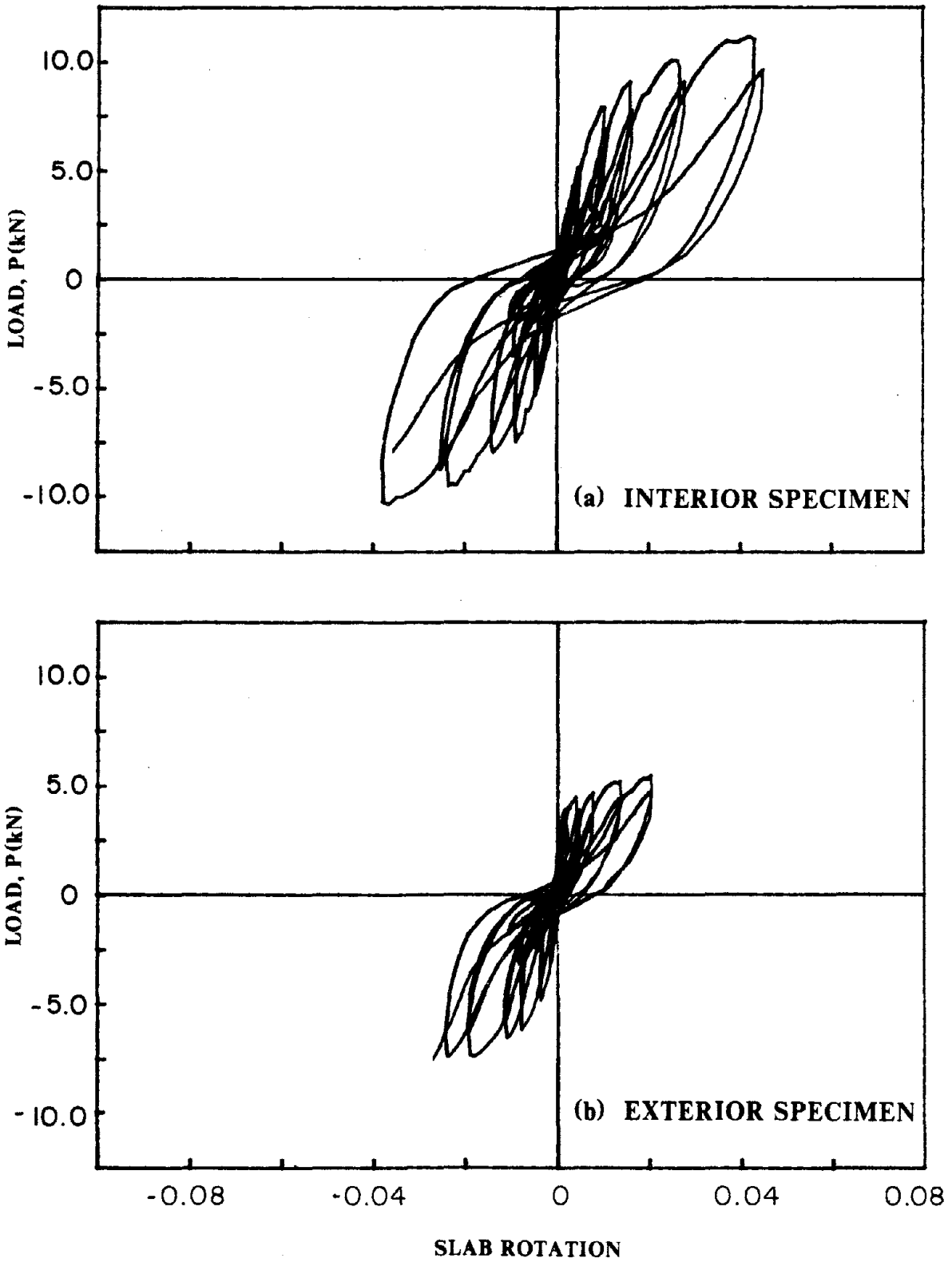

FIG. 4.8 Measured Rotational Slab Deformations Relative To The Column

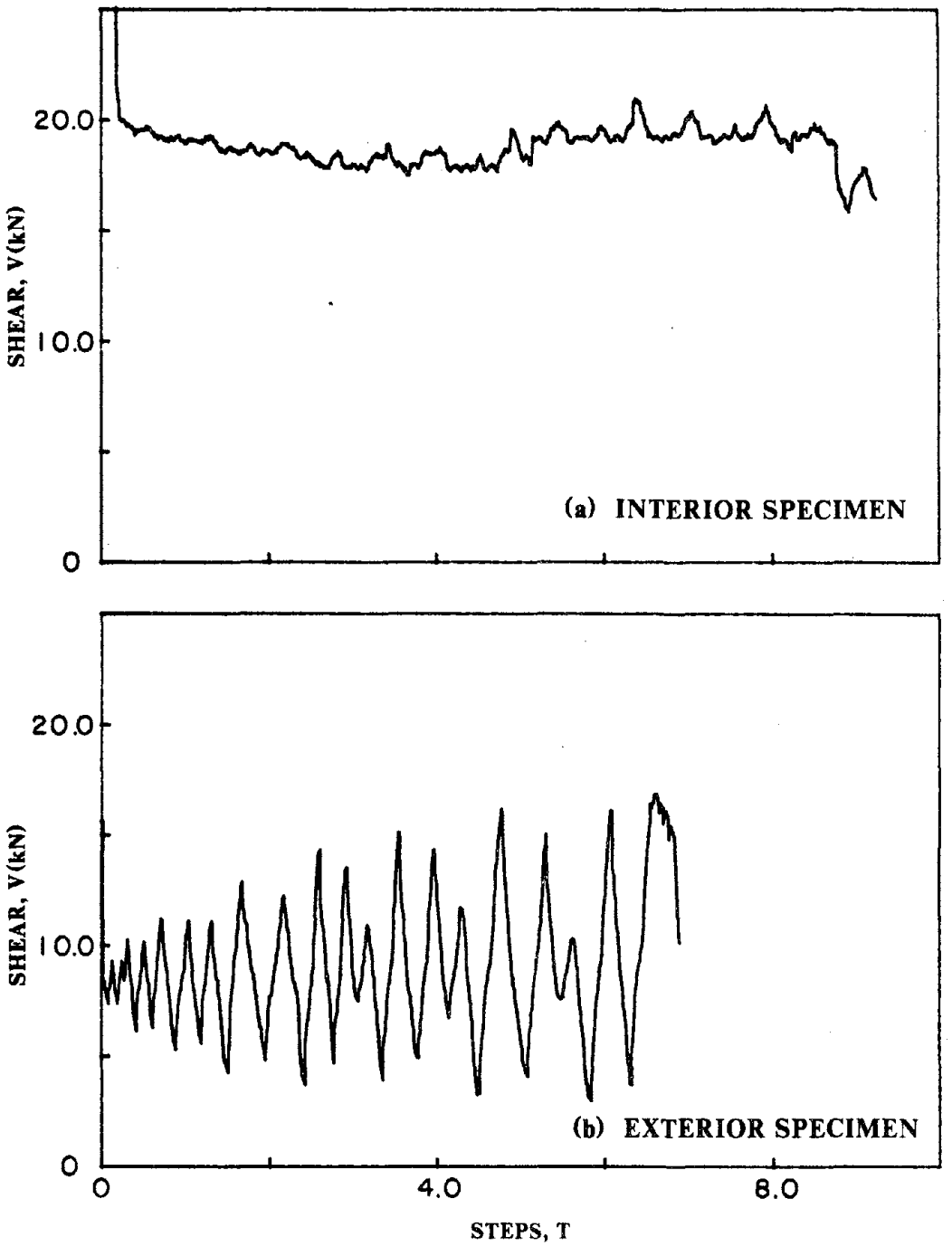

FIG. 4.9 Shear Histories

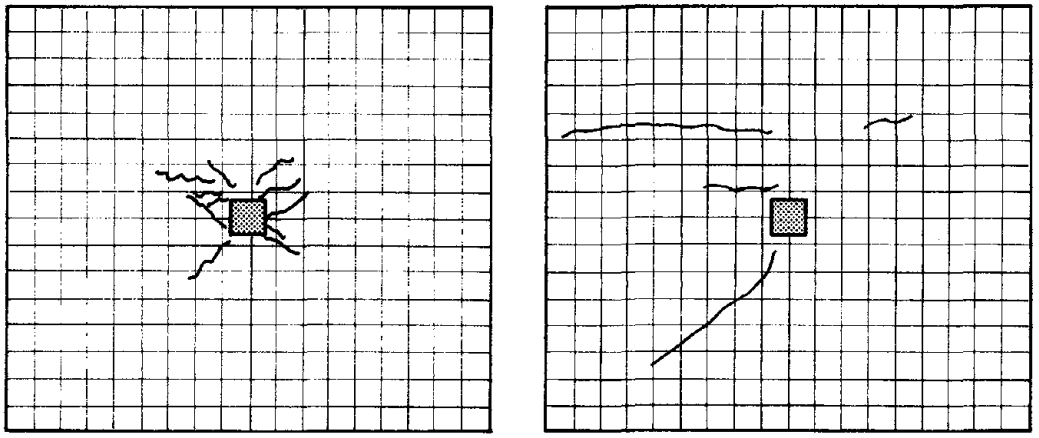

TOP SURFACE at 1% DRIFT

BOTTOM SURFACE at 1% DRIFT

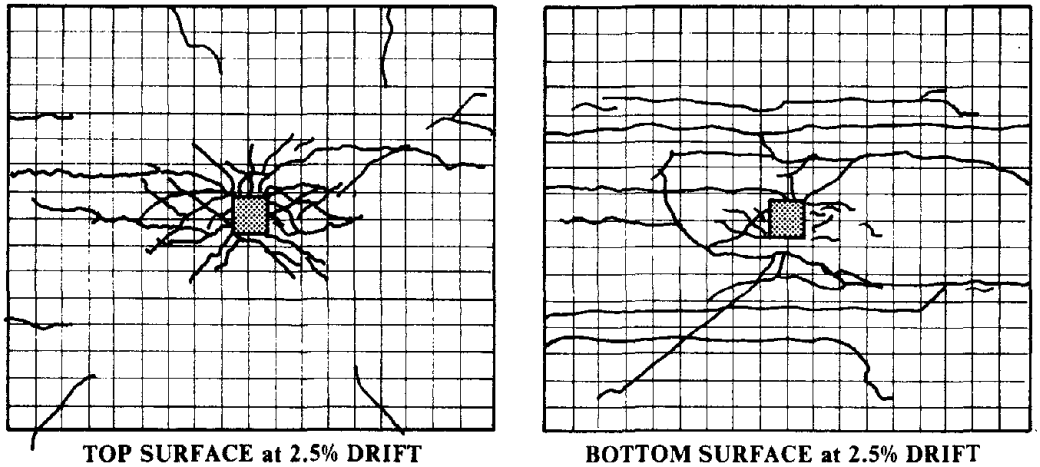

TOP SURFACE at 2.5% DRIFT

BOTTOM SURFACE at 2.5% DRIFT

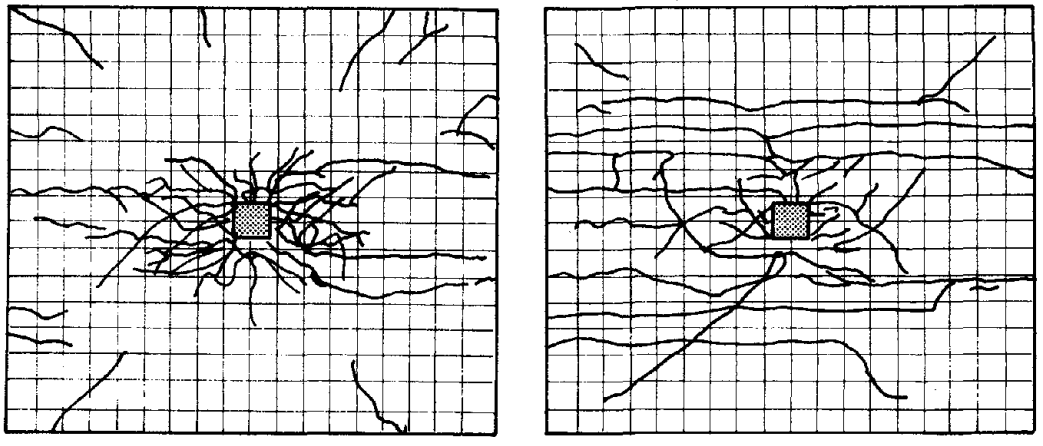

TOP SURFACE at 3.5% DRIFT

BOTTOM SURFACE at 3.5% DRIFT

COLUMN

(a) INTERIOR SPECIMEN

FIG. 4.10 Crack Patterns

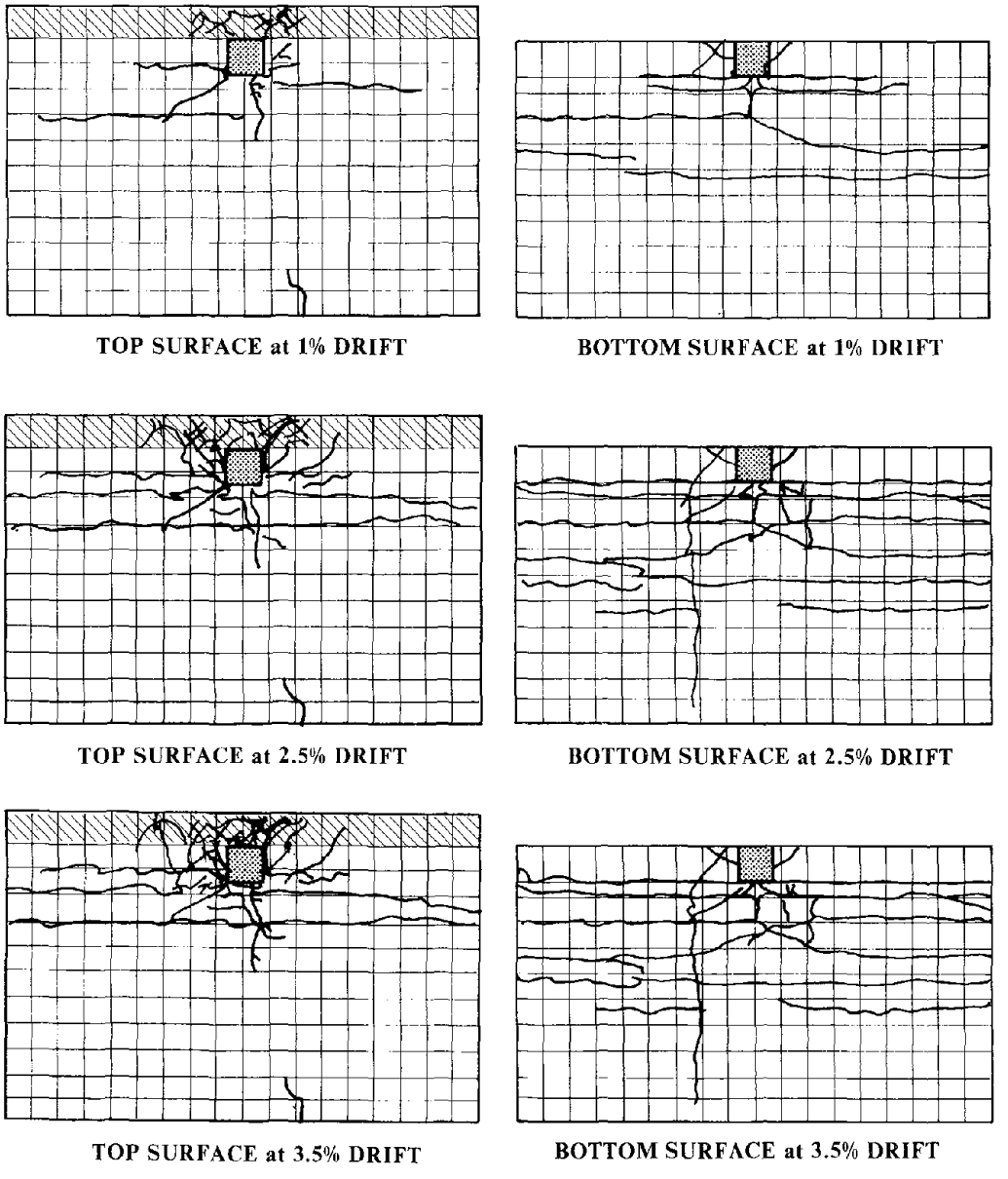

(b) EXTERIOR SPECIMEN

FIG. 4.10 Continued

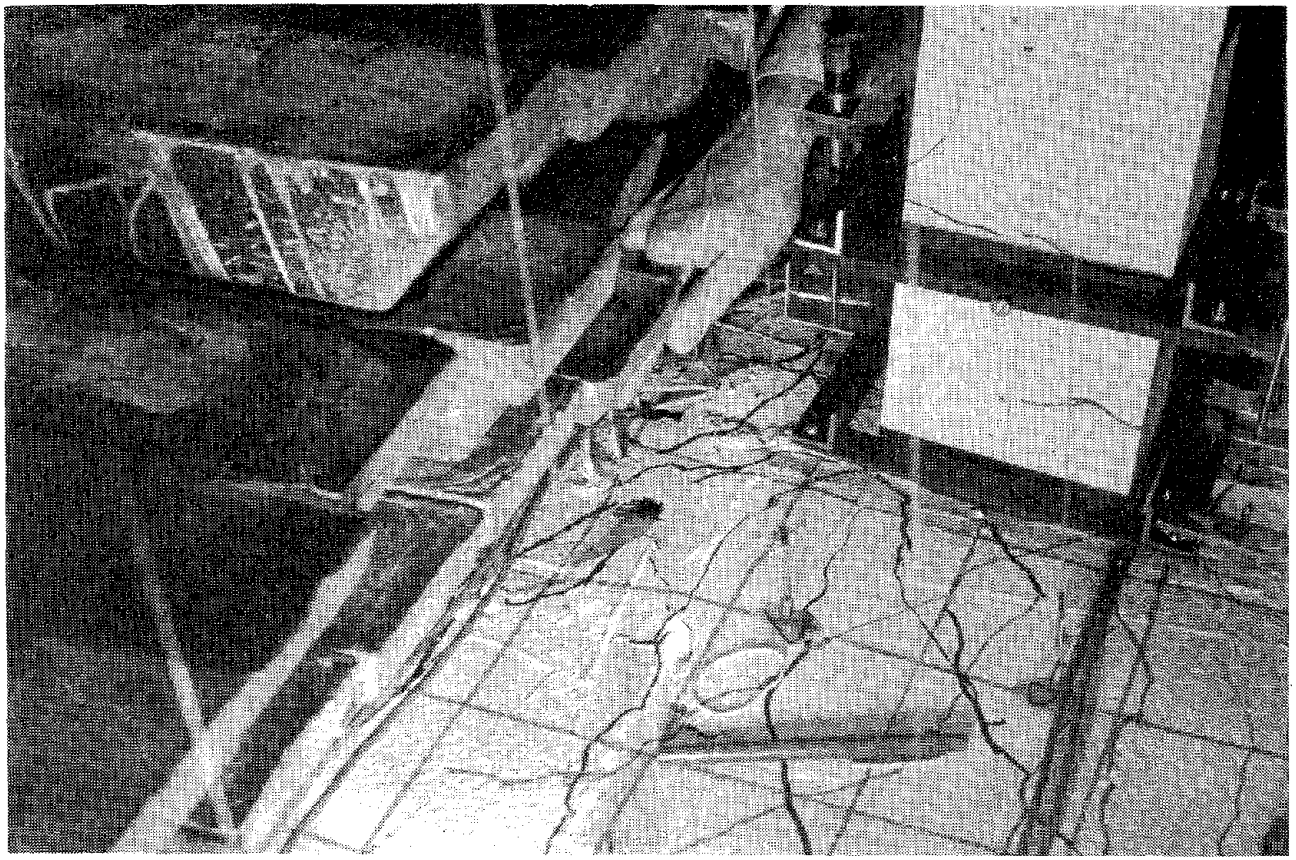

(a) INTERIOR SPECIMEN

FIG. 4.11 Specimen Damage

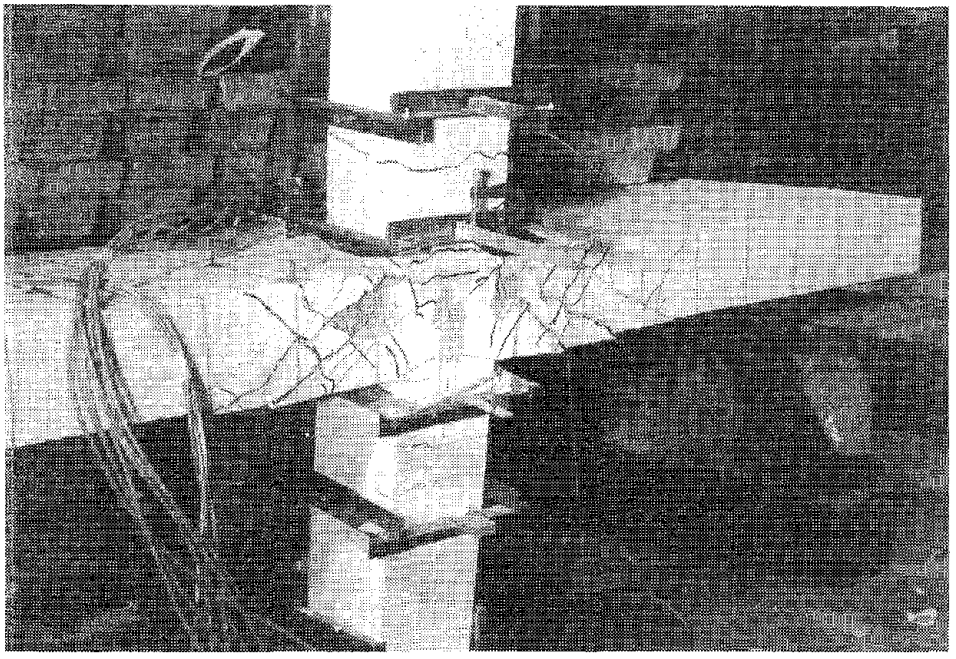

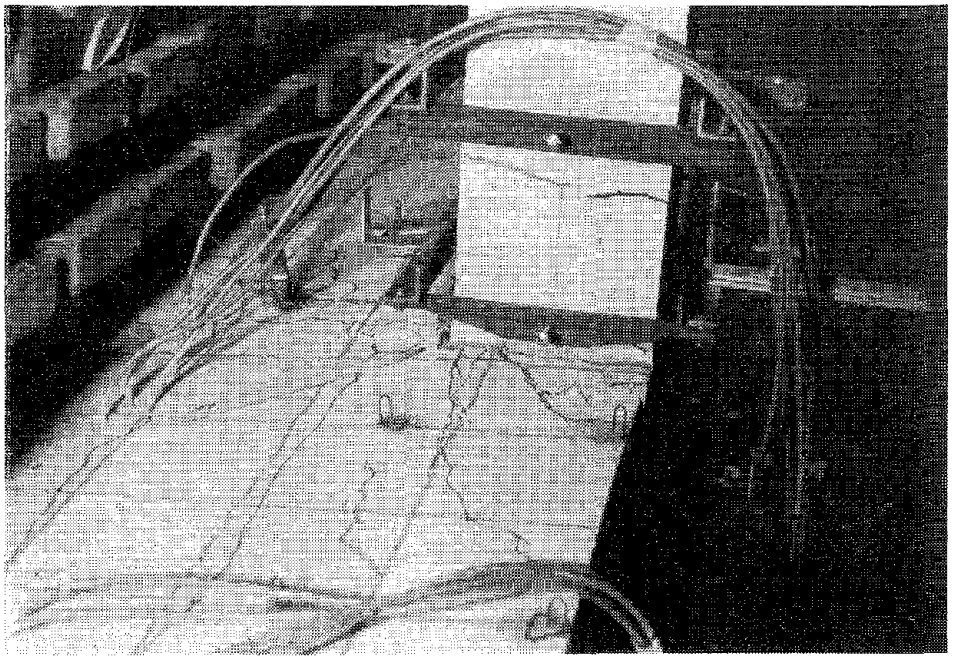

(b) EXTERIOR SPECIMEN

FIG. 4.11 Continued

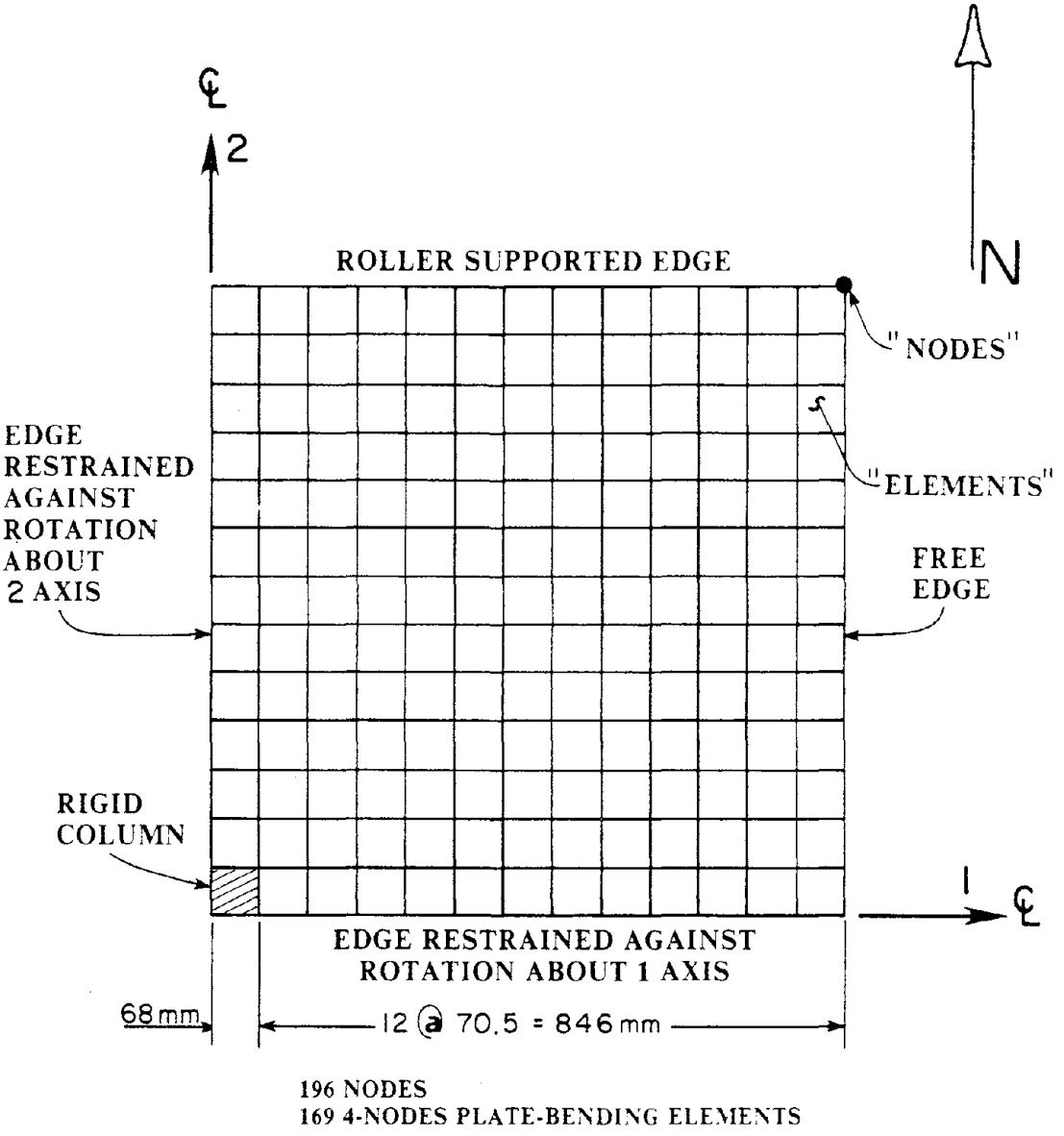

FIG. 5.1 Finite Element Mesh For Quarter Of Slab Panel

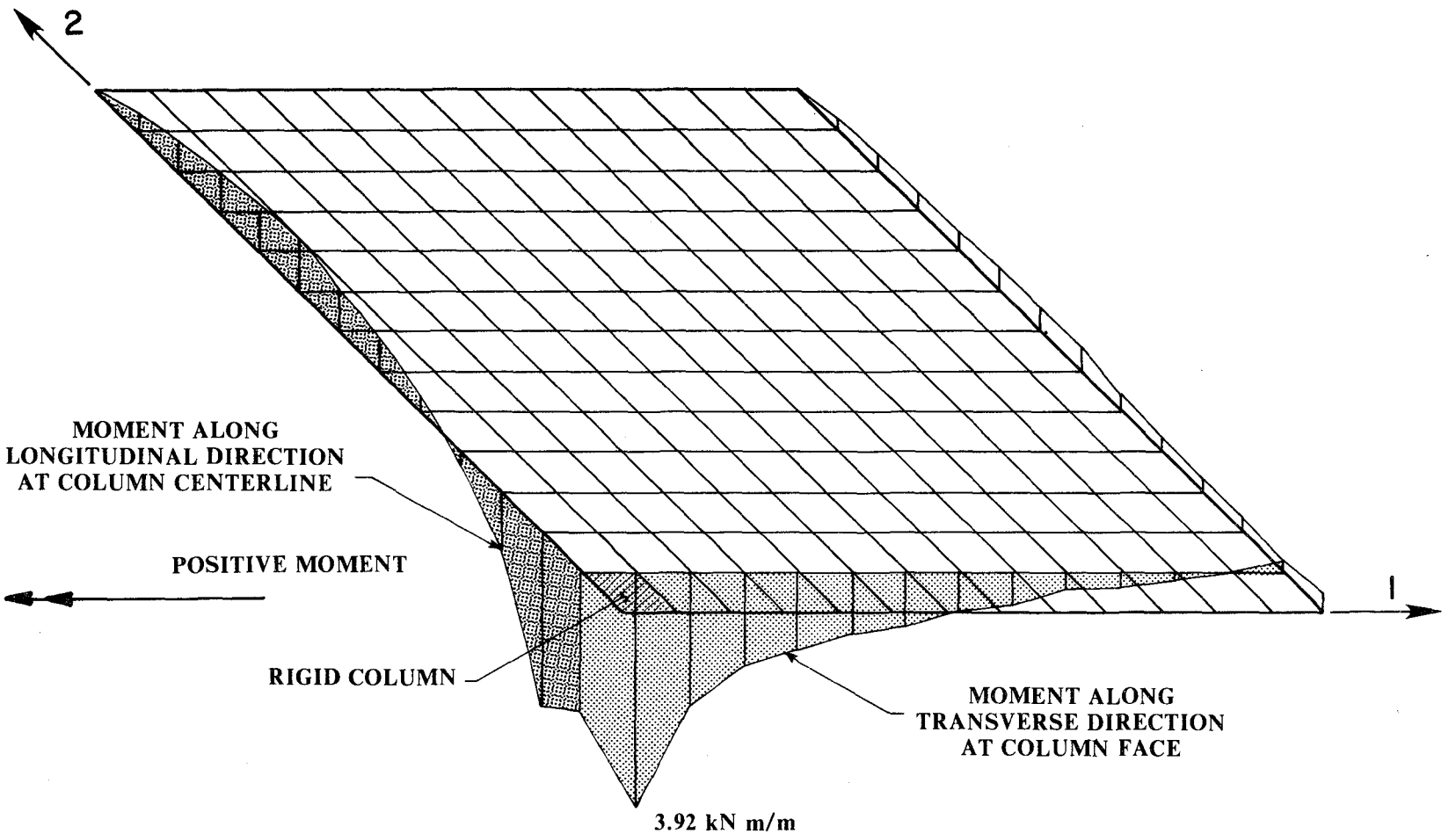

FIG. 5.2 Distribution Of Moments From Finite Element Analysis Of Quarter Panel

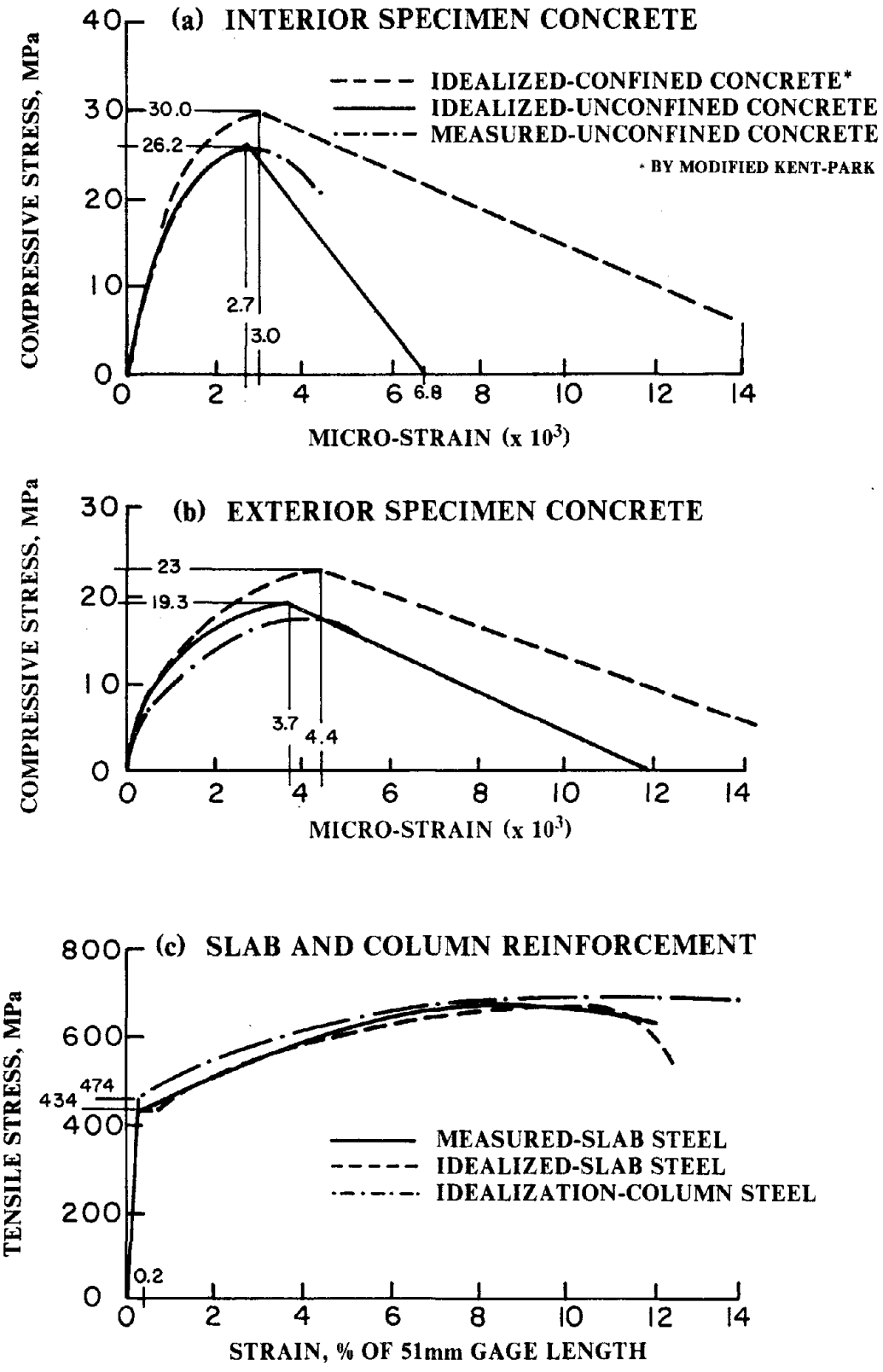

FIG. 5.3 Idealized Material Properties
For Moment-Curvature Analysis

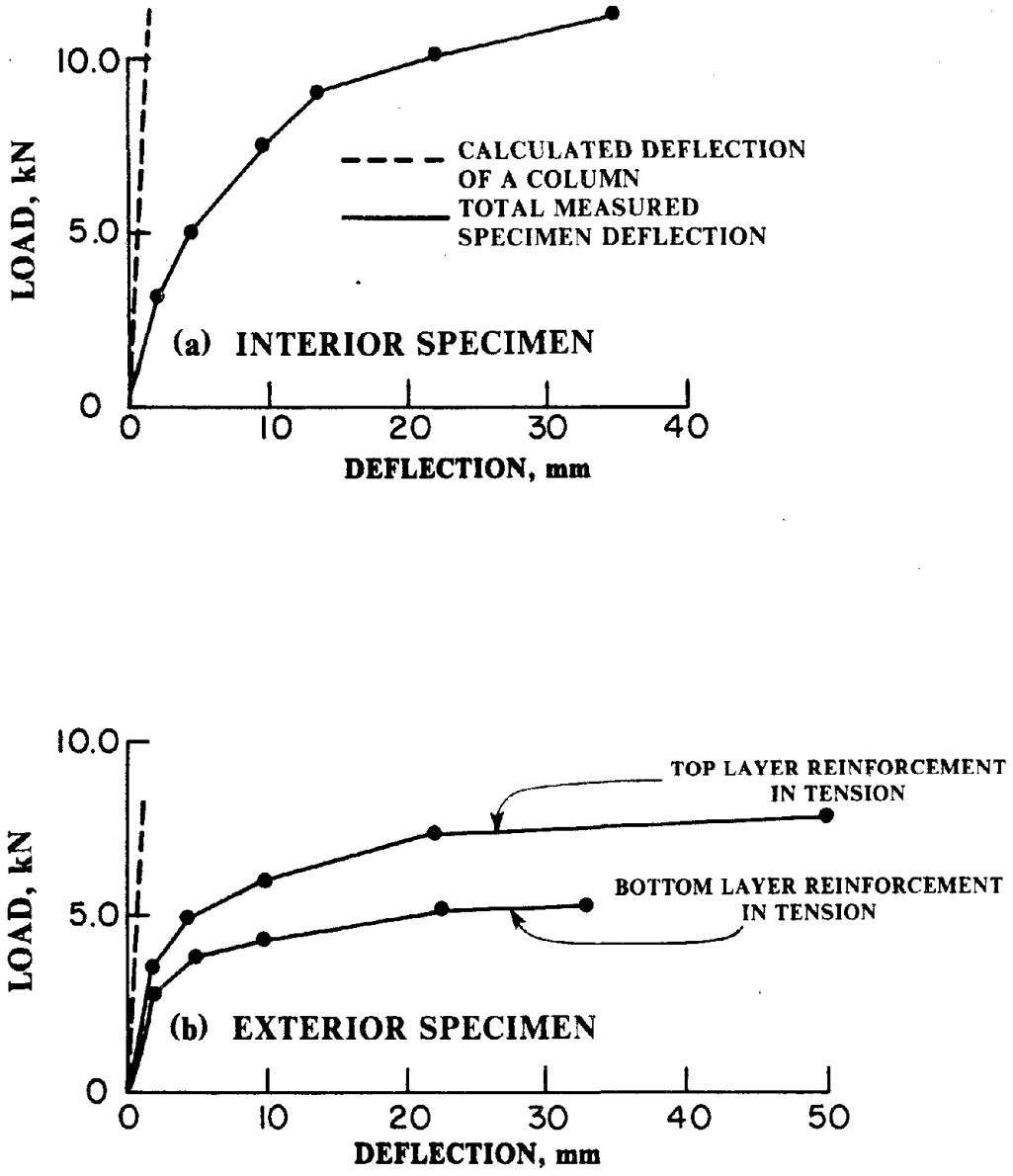

FIG. 5.4 Comparison Between Calculated Column Deflection And Measured Total Deflection

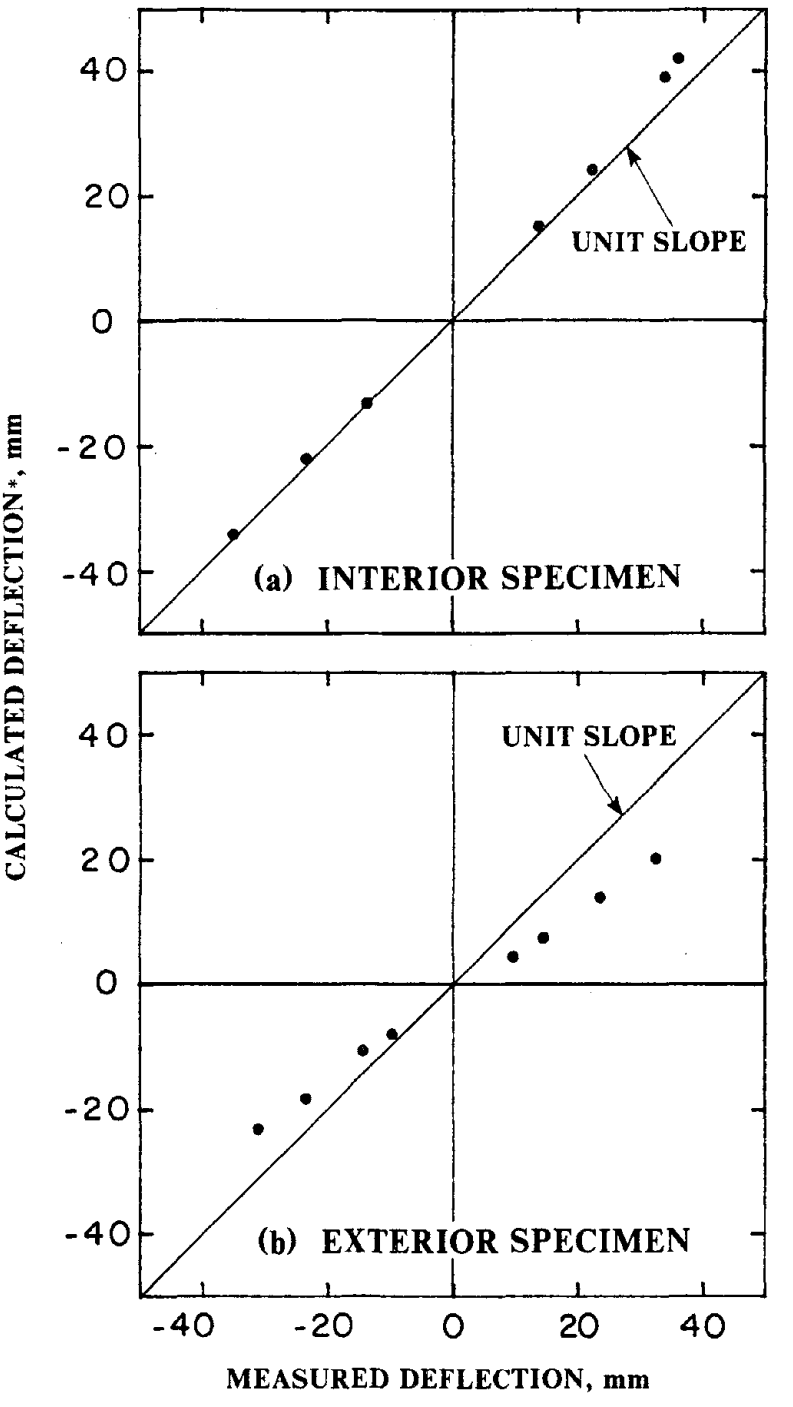

* CALCULATED CONTRIBUTION OF SLAB DEFORMATION TO MEASURED TOTAL SPECIMEN DEFLECTION

FIG. 5.5 Comparison Between Measured Drift And Calculated Slab Contribution

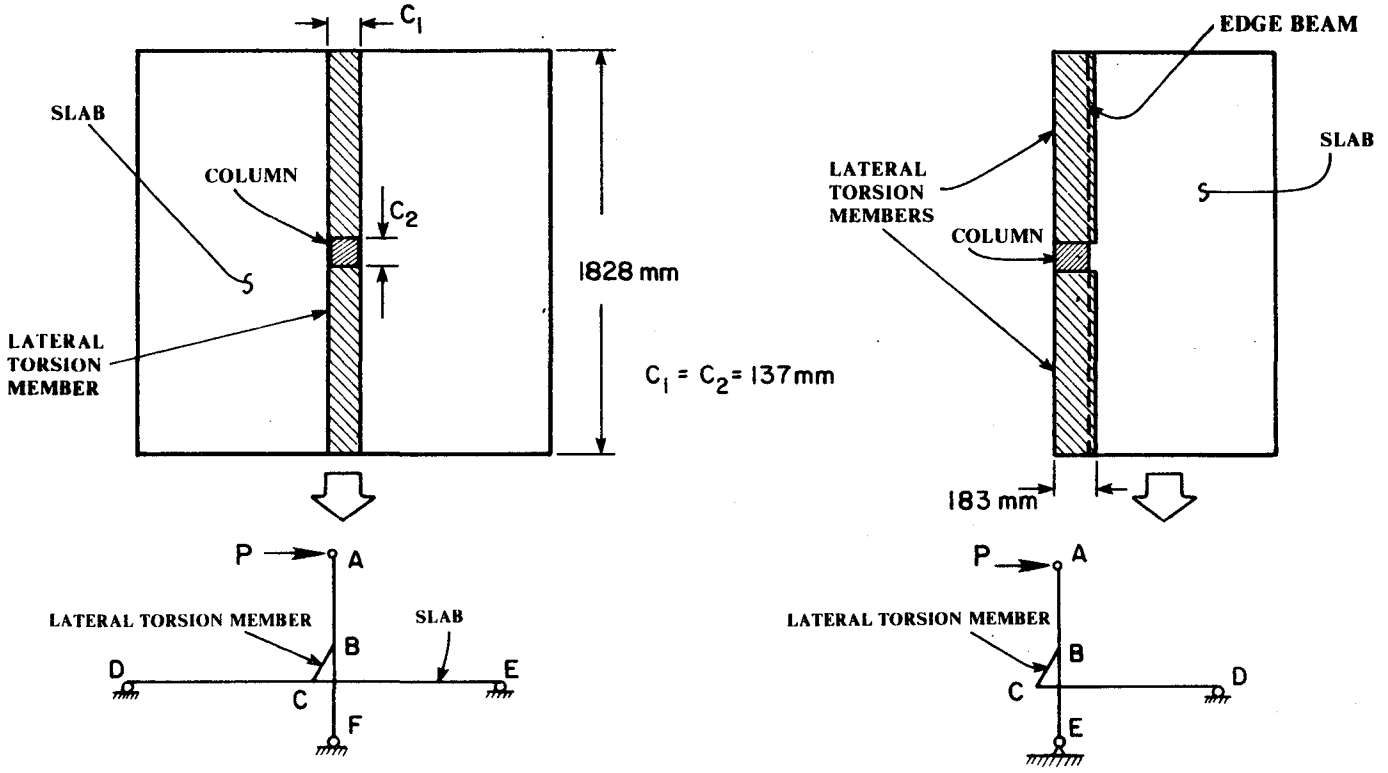

(a) INTERIOR SPECIMEN

(b) EXTERIOR SPECIMEN

FIG. 5.6 Idealizations Of Equivalent Frame Models

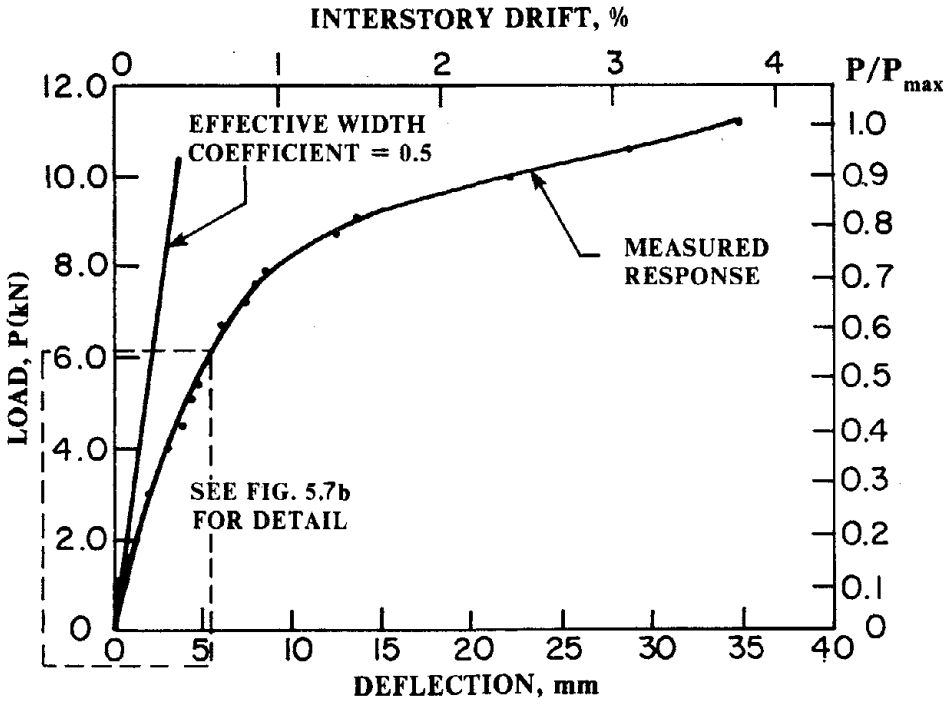

(a) ENTIRE HISTORY

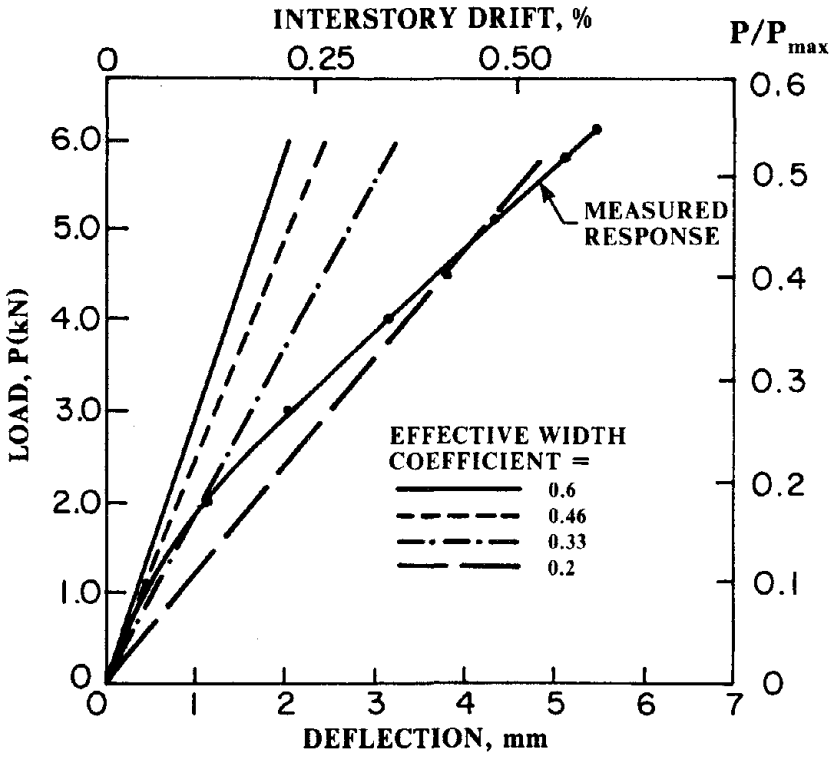

(b) DETAIL OF INITIAL BEHAVIOR

FIG. 5.7 Equivalent Beam Width Modeling Of Interior Specimen

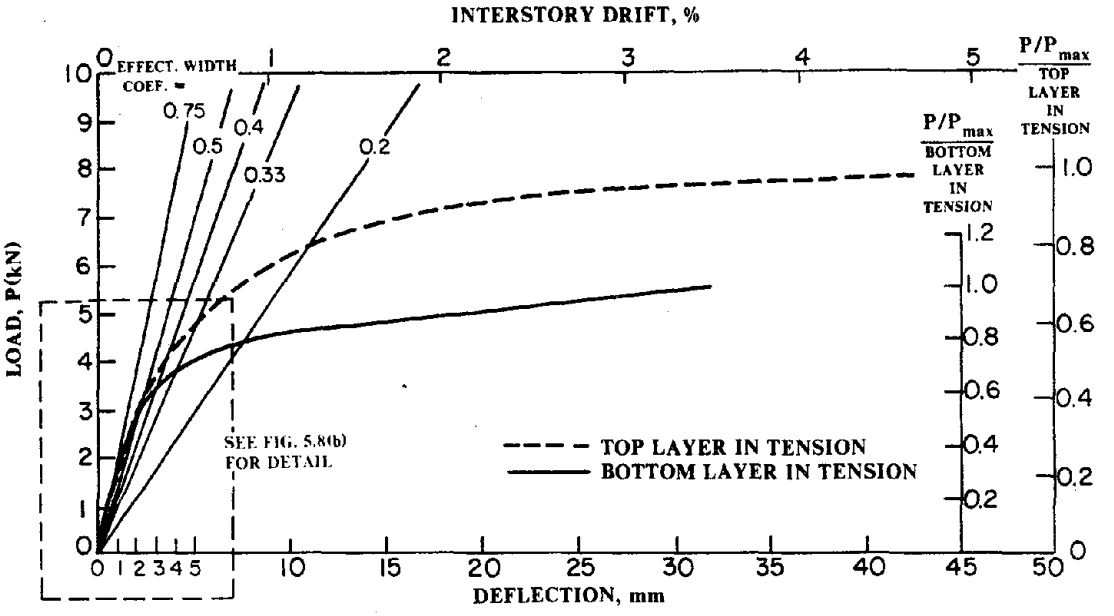

(a) ENTIRE HISTORY

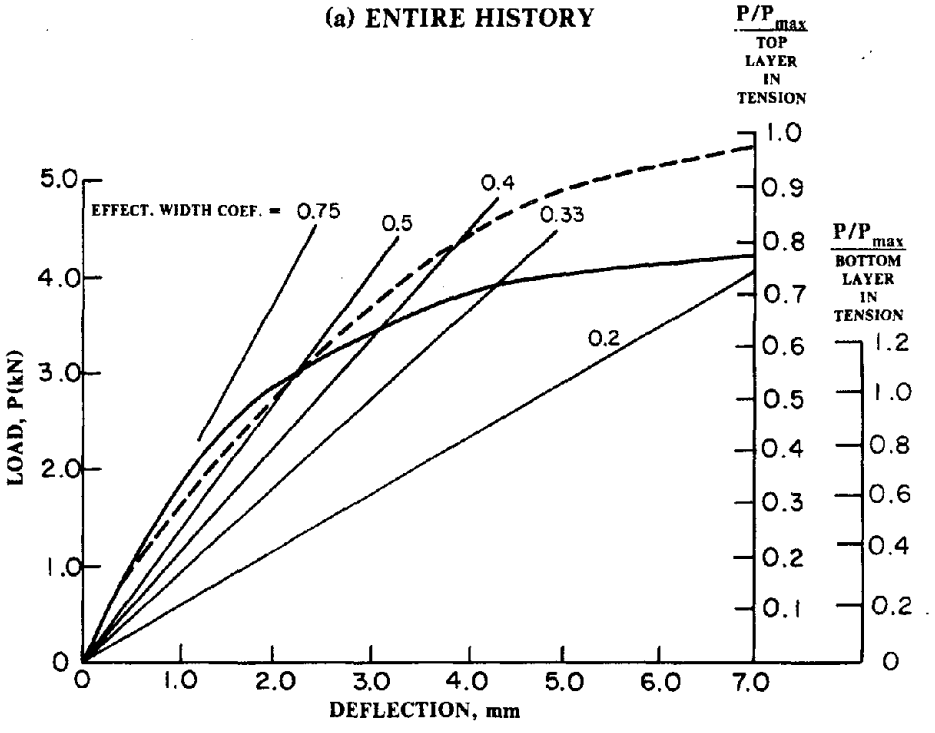

(b) DETAIL OF INITIAL BEHAVIOR

FIG. 5.8 Equivalent Beam Width Modeling Of Exterior Specimen

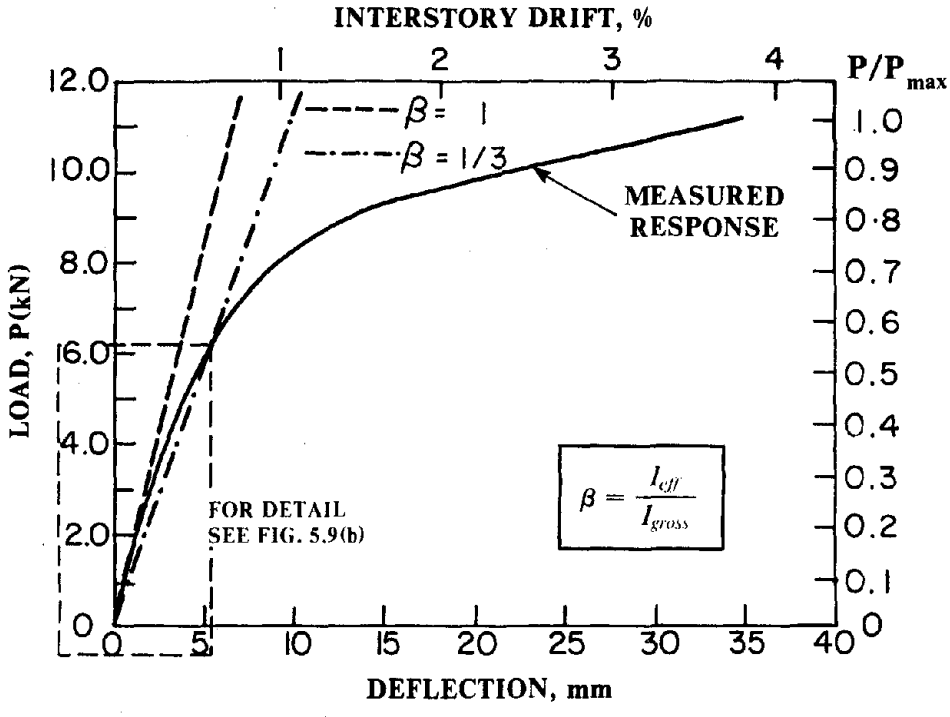

(a) ENTIRE HISTORY

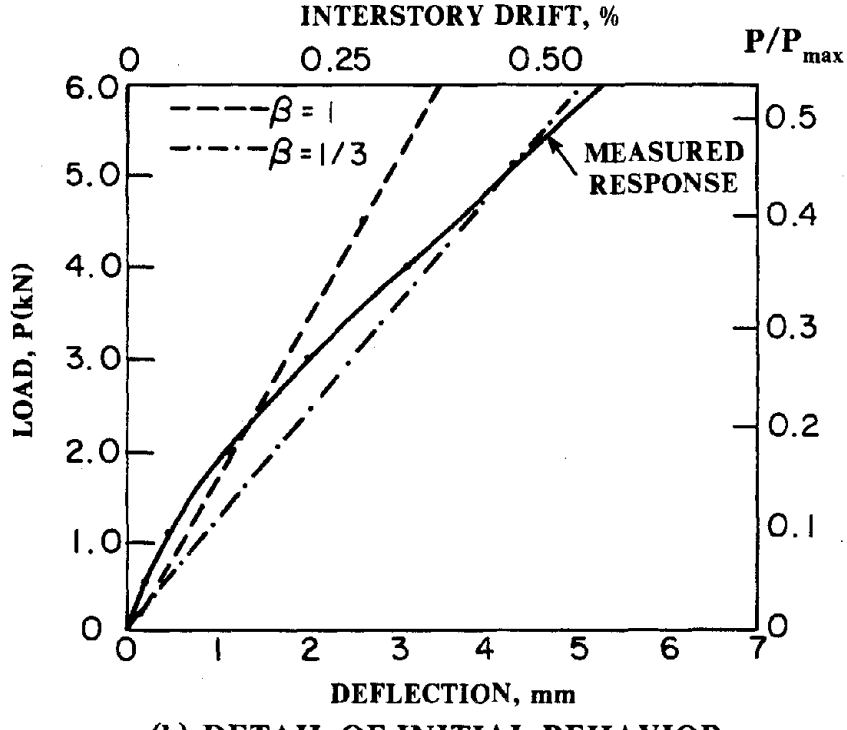

(b) DETAIL OF INITIAL BEHAVIOR

FIG. 5.9 Equivalent Frame Modeling Of Interior Specimen

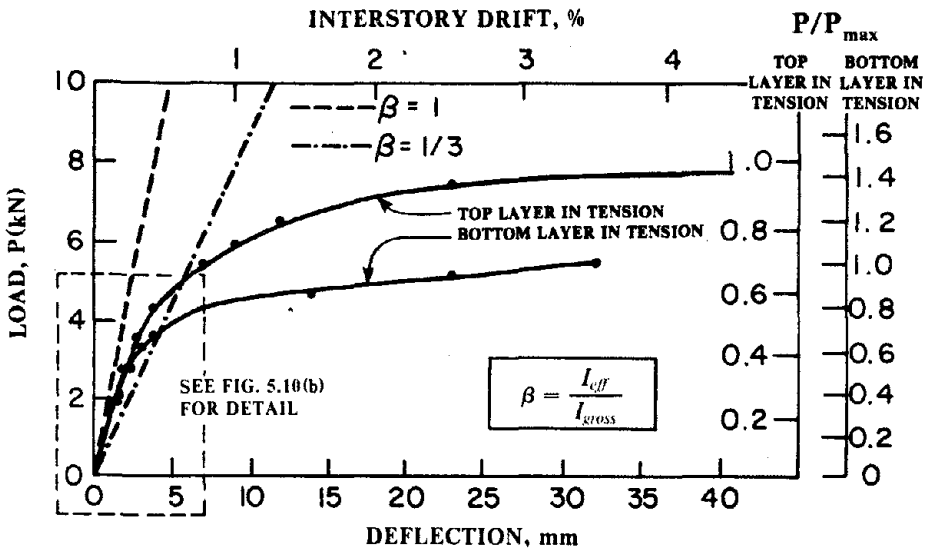

(a) ENTIRE HISTORY

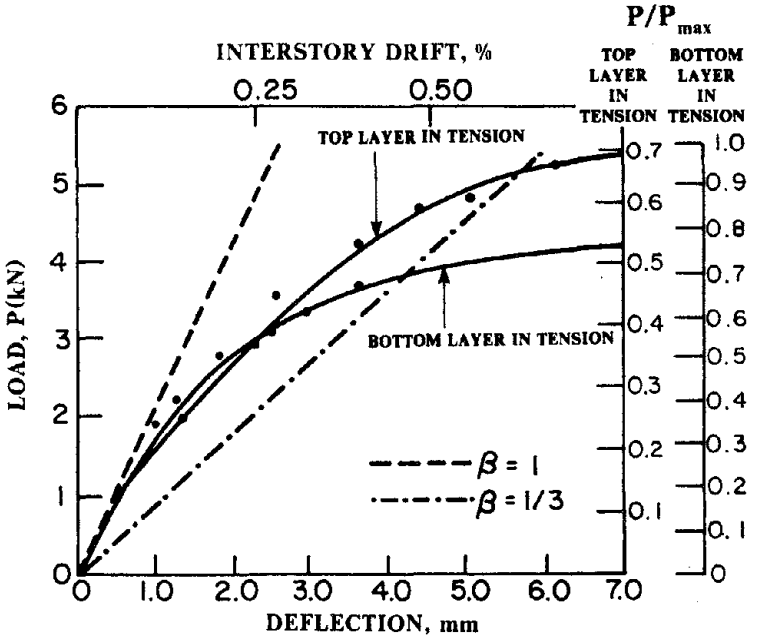

(b) DETAIL OF INITIAL BEHAVIOR

FIG. 5.10 Equivalent Frame Modeling Of Exterior Specimen

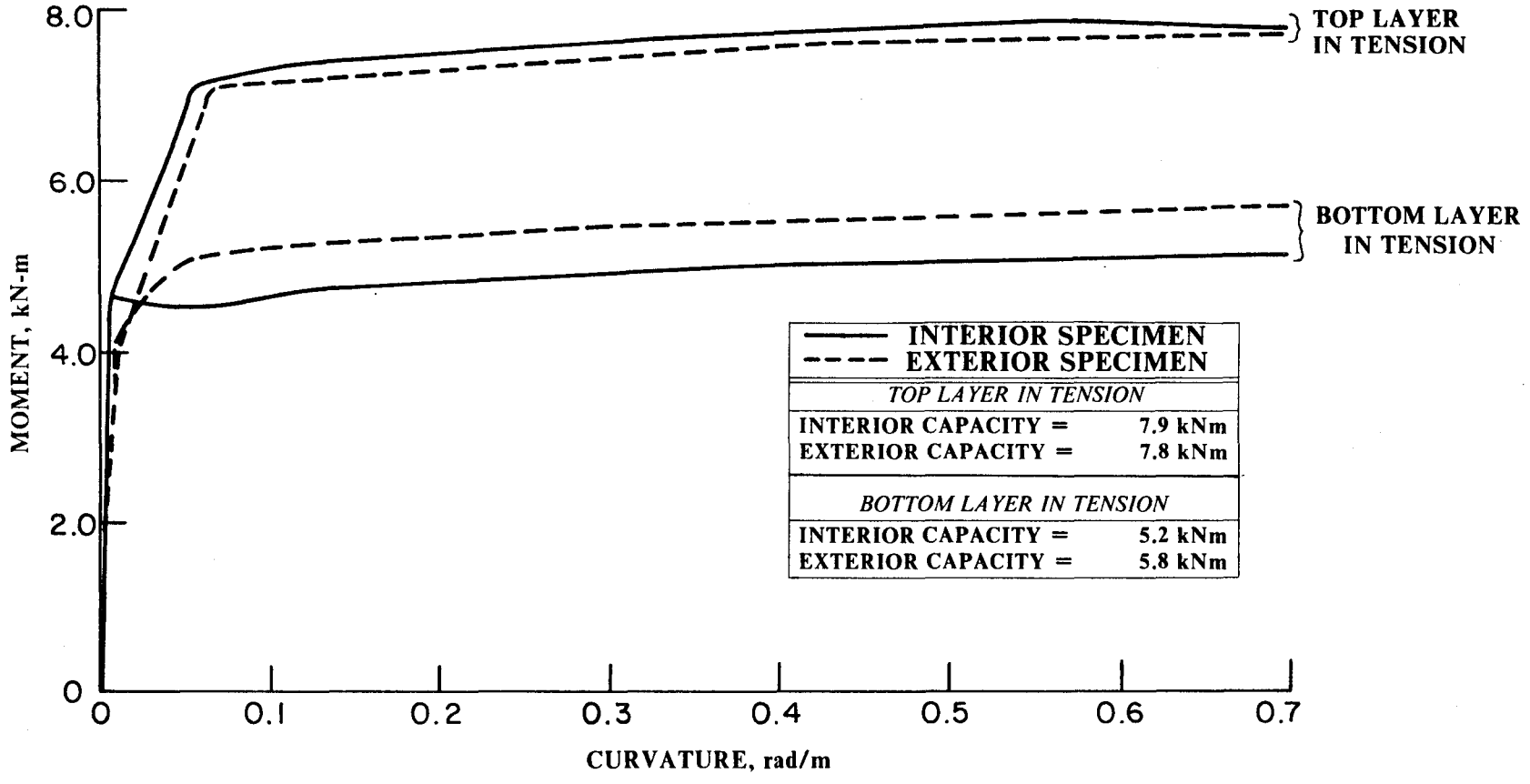

FIG. 5.11 Moment Curvature Response For Slab Sections Remaining Plane

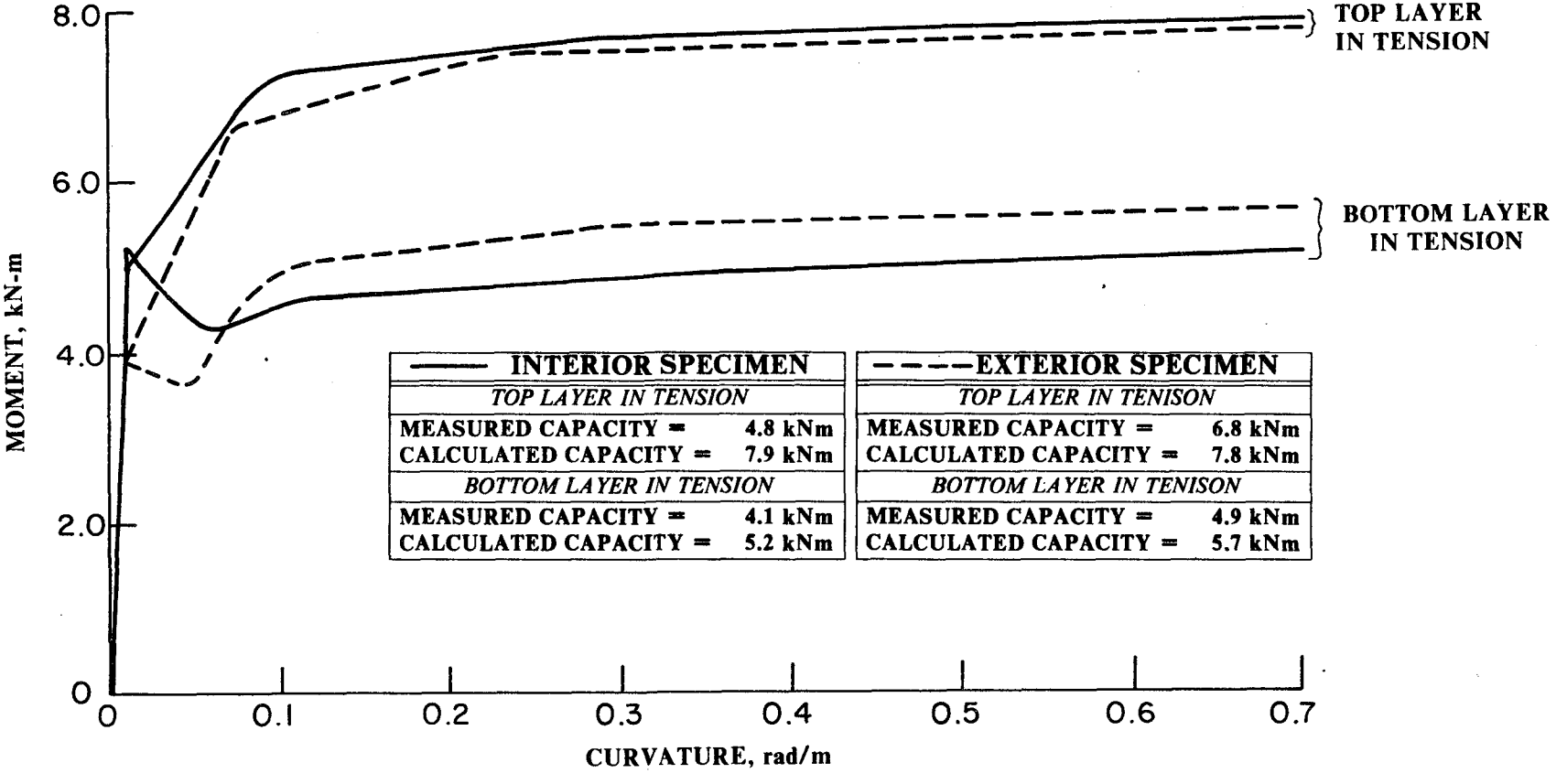

FIG. 5.12 Refined Moment-Curvature Response Of Specimen Slabs

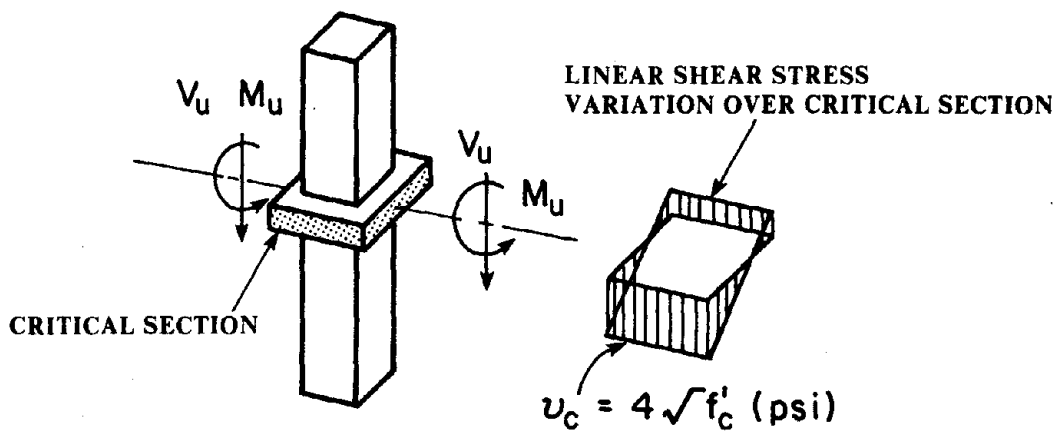

ACI 318–83 UNBALANCED CAPACITY = 8.2*kNm*

MEASURED = 10.3*kNm*

$$\frac{ACI\ 318\text{–}83}{MEASURED} = 0.8$$

FIG. 5.13 Strength Of Interior Connection By ACI Method

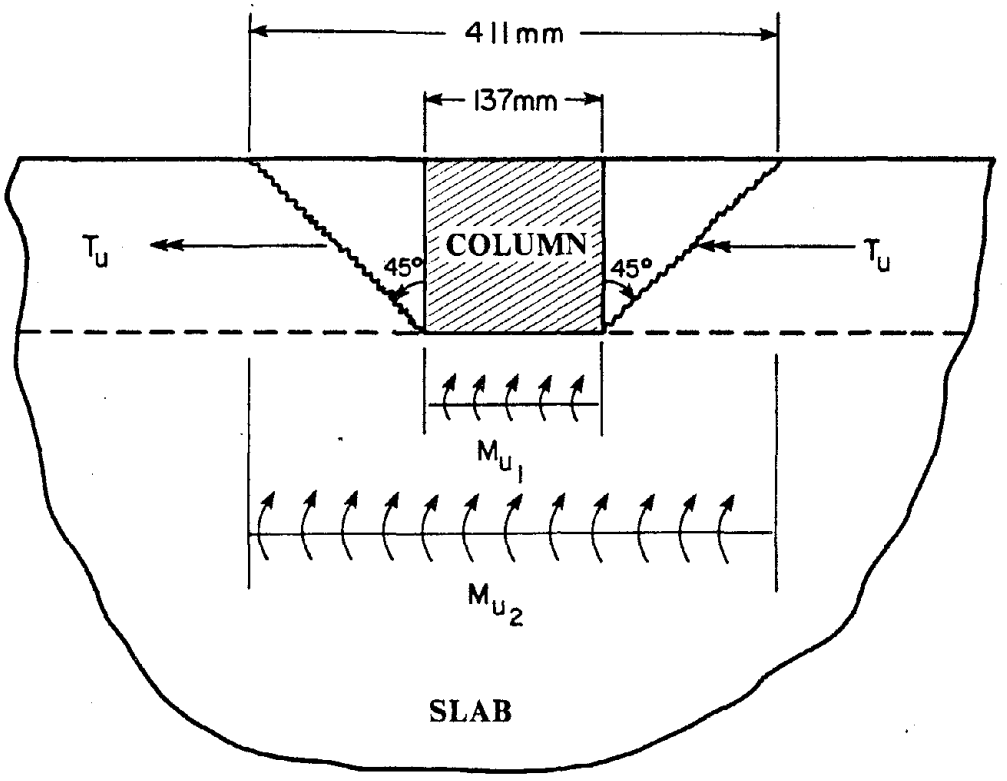

STRENGTH OF CONNECTION IS EITHER:

(i) $(Mu_1 \times 137) + 2Tu$

OR

(ii) $(Mu_2 \times 411) + 2Tu$

WHERE Mu_1 *&* Mu_2 *ARE FLEXURAL CAPACITIES*

AND Tu IS TORSIONAL CAPACITY OF EDGE BEAM

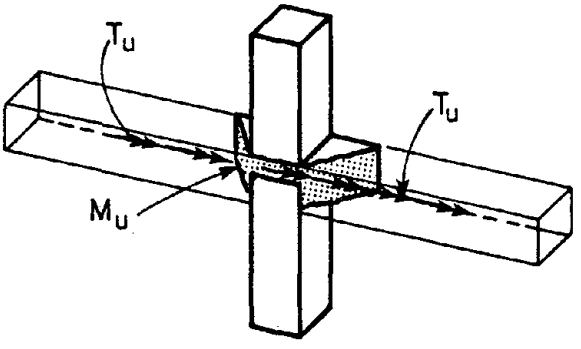

NEGATIVE MOMENT:

$$\frac{CALCULATED}{MEASURED} = \frac{6.6kNm}{7.3kNm} = 0.90$$

POSITIVE MOMENT:

$$\frac{CALCULATED}{MEASURED} = \frac{5.8kNm}{4.9kNm} = 1.18$$

FIG. 5.14 Strength Of Exterior Connection

APPENDIX A

PULLOUT TESTS

Eight specimens for pullout tests were prepared and tested. The purpose of the tests was to investigate bond characteristics between small-scale steel and concrete used slabs of the slab-column connections. The specimens and tests are described in this appendix.

A.1 Specimen Description

Each test specimen was a 76 by 76 by 280 mm concrete prism with a length of small-diameter reinforcing bar embedded in the prism and protruding from each end (Fig. A.1). The reinforcement was allowed to bond to the concrete in the central region of the prism along the length l_o shown in the figure. Polyethylene tubing, sealed at the ends, prevented bond outside of the region l_o. Specimens P-1-1, P-1-2, and P-1-3 all had nominal bond lengths l_o equal to 30 mm, while specimens P-2-1, P-2-2, and P-2-3 had nominal bond lengths equal to 60 mm. Specimens P-4-1 and P-4-2 both had nominal bond lengths of 100 mm. Actual bond lengths are in Table A1.

The specimens were cast in steel forms with reinforcing bars in a horizontal position. They were rodded and tamped in accordance with ASTM Specification C192. Immediately thereafter, the specimens were placed in a "fog" room for curing. Except for form removal 24 hours after casting, the specimens were cured

continuously in the fog room for 28 days. On day 29, the specimens were removed from the fog room and stored at 68°F and low humidity until testing. Nine 76 by 152 mm test cylinders received identical treatment.

Steel and concrete material properties were nominally the same as those for the slab-column specimens. Heights of deformations at opposite ends and at the center of the bond length of each specimen were measured. Average height of deformation values for the specimens are in Table A1. Compression and splitting tension tests were performed on the cylinders the same day the pullout tests were performed. The average compressive strength was 40.5 MPa (5.9 ksi) and the average tensile strength was 2.98 MPa (0.4 ksi).

A.2 Test Procedure

Pullout tests were performed with a 60-kip Baldwin hydraulic testing machine at a constant loading rate of 22.2 N/sec (5 lb/sec). The specimens were tested in a vertical position (Fig. A.2). One of the protruding ends of the embedded reinforcement was passed through a hole in the lower, stationary head of the testing machine and gripped by a gripping device which had been attached to the upper, movable loading head. The movable head loaded the specimen by pulling the protruding end up through the stationary head and bringing the end face of the prism to bear flush against the bottom of the stationary head. A 13-mm (0.5-in.) thick steel plate was placed between the prism and the stationary head to ensure a uniform bearing surface. A steel "cradle", lightly clamped onto the prism, supported the prism in

the event of bar failure (Fig. A.2).

A steel frame attached to the unloaded end of the specimen served as the reference frame for slip measurements (Fig. A2). Slip of the unloaded end of the reinforcement relative to this frame was measured by two linear variable displacement transducers (LVDT). One LVDT was attached to each side of the protruding bar, and slip was taken as the average of the two measurements. Measurements of applied load versus slip was plotted continuously by an X-Y recorder.

A.3 Results

Specimens P-1-1, P-1-2, and P-1-3 failed by pullout without bar failure. P-2-2 and P-2-3 failed by bar failure after some initial slippage. P-4-1 and P-4-2 failed by bar fracture with no measureable slip at the unloaded end. Plots of slip at the unloaded end are plotted in Figure A.3. The load at which the bars yielded in tension is also indicated in the figure.

The load-slip curves indicate that all test specimens achieved the yield strength of the reinforcement. However, specimens with nominal bondlengths of 30 mm (1.18 in.) sustained significant slip at the unloaded end. Slip at the loaded end was not measured directly.

To obtain a measure of slip at the loaded end for specimens P-1-1, P-1-2, and P-1-3, a uniform bond stress was assumed over the bonded length. Using this assumption, slip at the loaded end was computed for loads below the yield level load of the reinforcement. Computed relationships at the loaded end are compared with measured relations at the unloaded end in Figure

A.4. Similar relations could not be obtained for the other specimens because they yielded before any slip was measured at the unloaded end.

Average bond stress is calculated by dividing the load (P) by the area of the bonding surface. The ultimate average bond stress is defined here as the maximum average bond stress sustained by the specimen. Both the average bond stress at first slip (u_s) and the ultimate average bond stress (u_{ult}) decreased with increasing actual bond lengths. Values of load at first slip (P_s) and maximum load (P_{ult}), as well as average bond stresses, for each of the specimens are in Table A2.

Table A1 Details of Specimen Descriptions

Specimen	Nominal Diameter	Actual Bond Length	Avg. Height of Deform. Over Bond Length
P-1-1	4.52 mm	31.75 mm	0.15 mm
P-1-2	4.52	31.75	0.38
P-1-3	4.52	34.14	0.23
P-2-1	4.52	65.89	0.33
P-2-2	4.52	57.94	0.30
P-2-3	4.52	57.15	0.28
P-4-1	4.52	93.68	0.43
P-4-2	4.52	108.74	0.38

f_y = 455 MPa (66 ksi)
Nominal Area = 16.13 mm^2 (0.025 $in.^2$)
1 in. = 25.4 mm

Table A2 Average Bond Stresses

Specimen	L_o, mm	P_s, N	P_{max}, N	u_s, MPa	u_{ult}, MPa
P-1-1	31.75	5940	8760	13.2	19.4
P-1-2	31.75	6230	9120	13.8	20.2
P-1-3	34.14	4450	7430	9.2	15.3
P-2-1	65.89	--	10320	--	11.0
P-2-2	57.94	9560	10450	11.6	12.7
P-2-3	57.15	8250	10630	10.2	13.1
P-4-1	93.63	--	10450	--	7.8
P-4-2	108.74	--	10610	--	6.9

$u_s = P_s / d_o L_o$ = average bond stress at first slip

$u_{ult} = P_{max} / d_o L_o$ = maximum average bond stress

d_o = nominal diameter, mm

L_o = bond length, mm

1 lb = 4.448 N

1 MPa = 145 psi

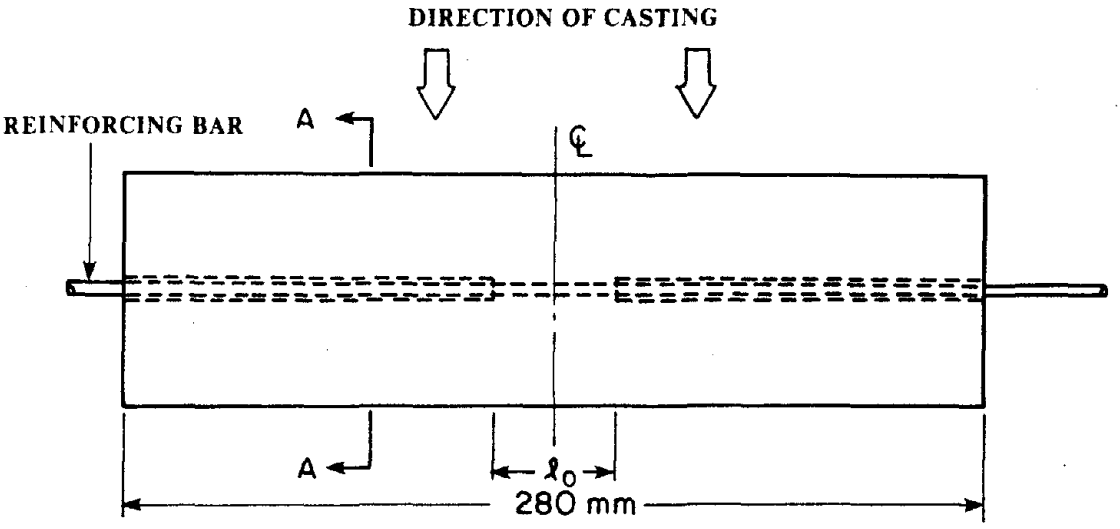

ELEVATION VIEW

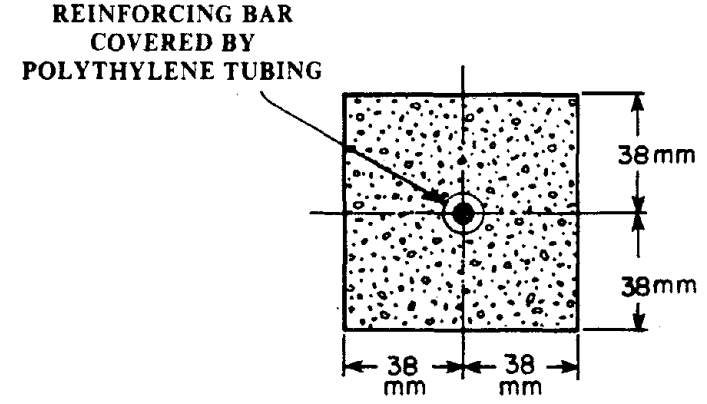

SECTION A-A

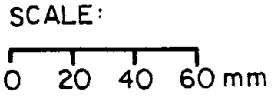

FIG. A1 Specimen For Pullout Test

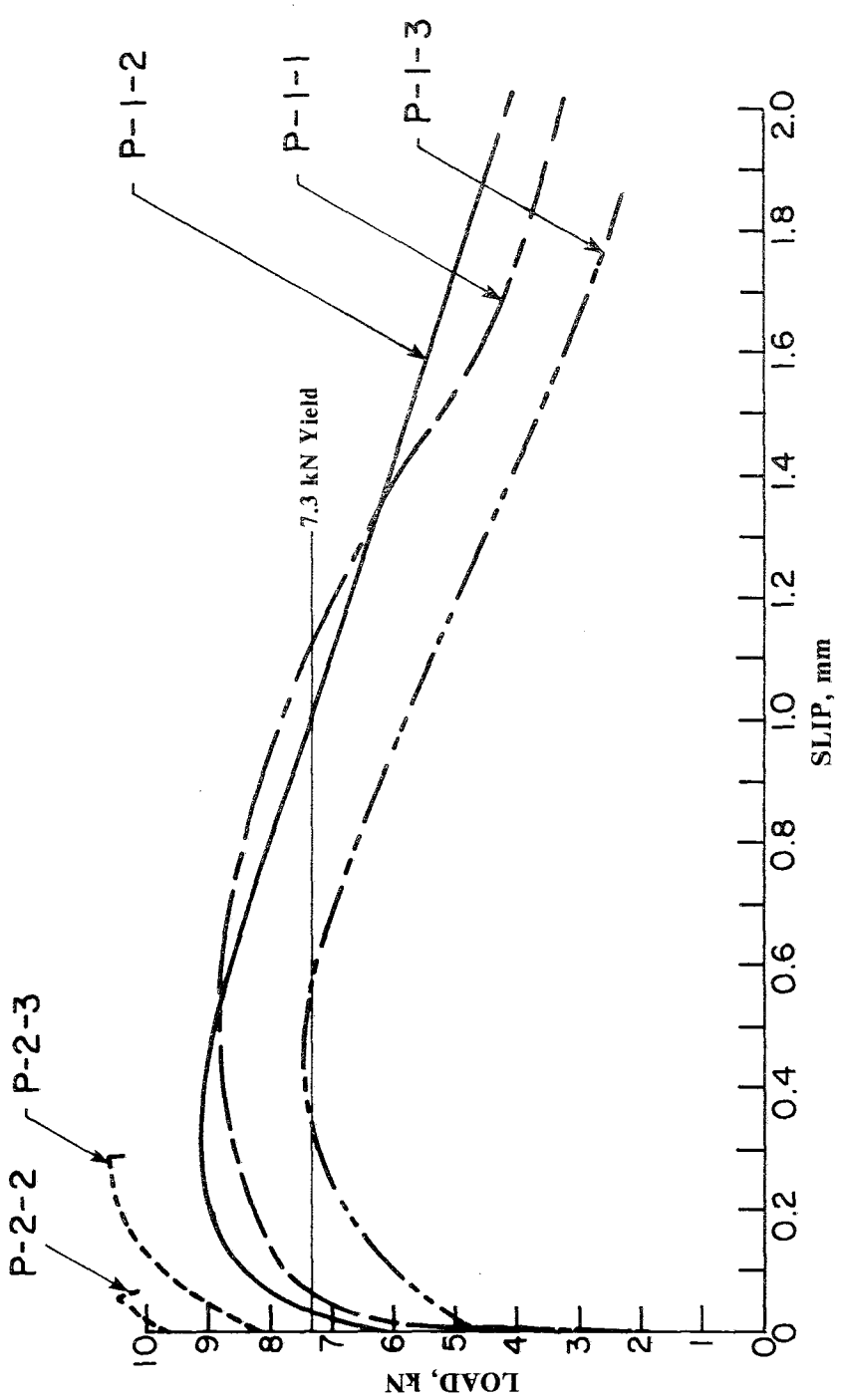

FIG. A2 Slip At Unloaded End Of Specimen

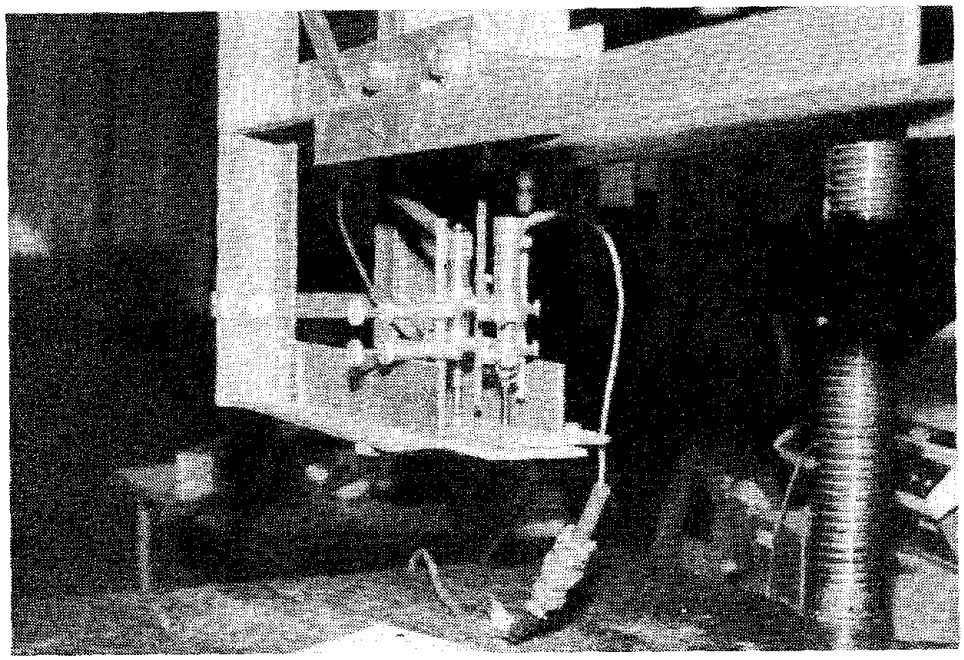

(a) INSTRUMENTATION

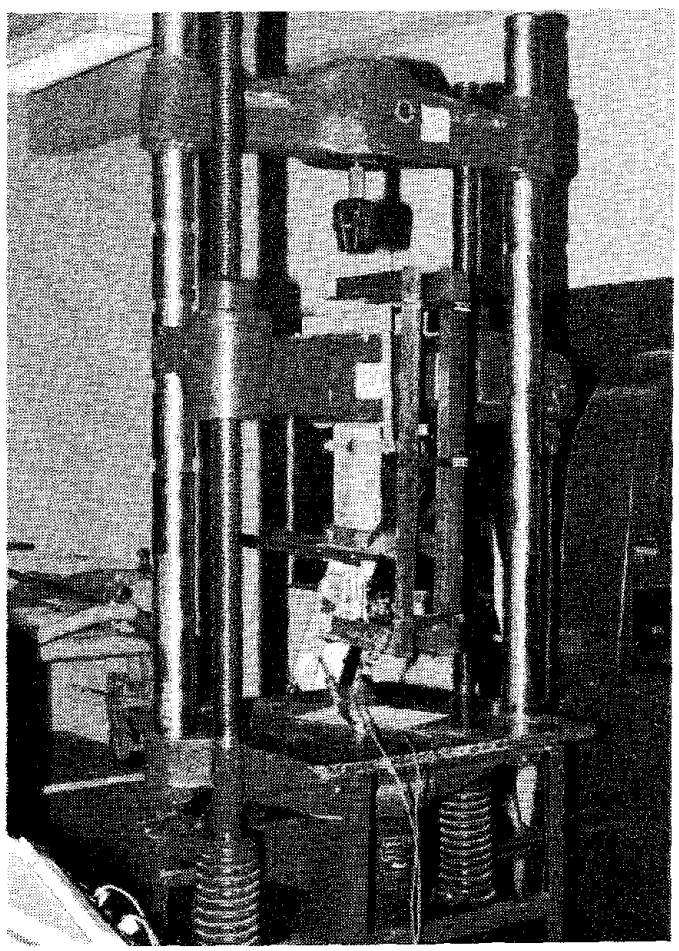

(b) APPARATUS

FIG. A3 Test Set-up

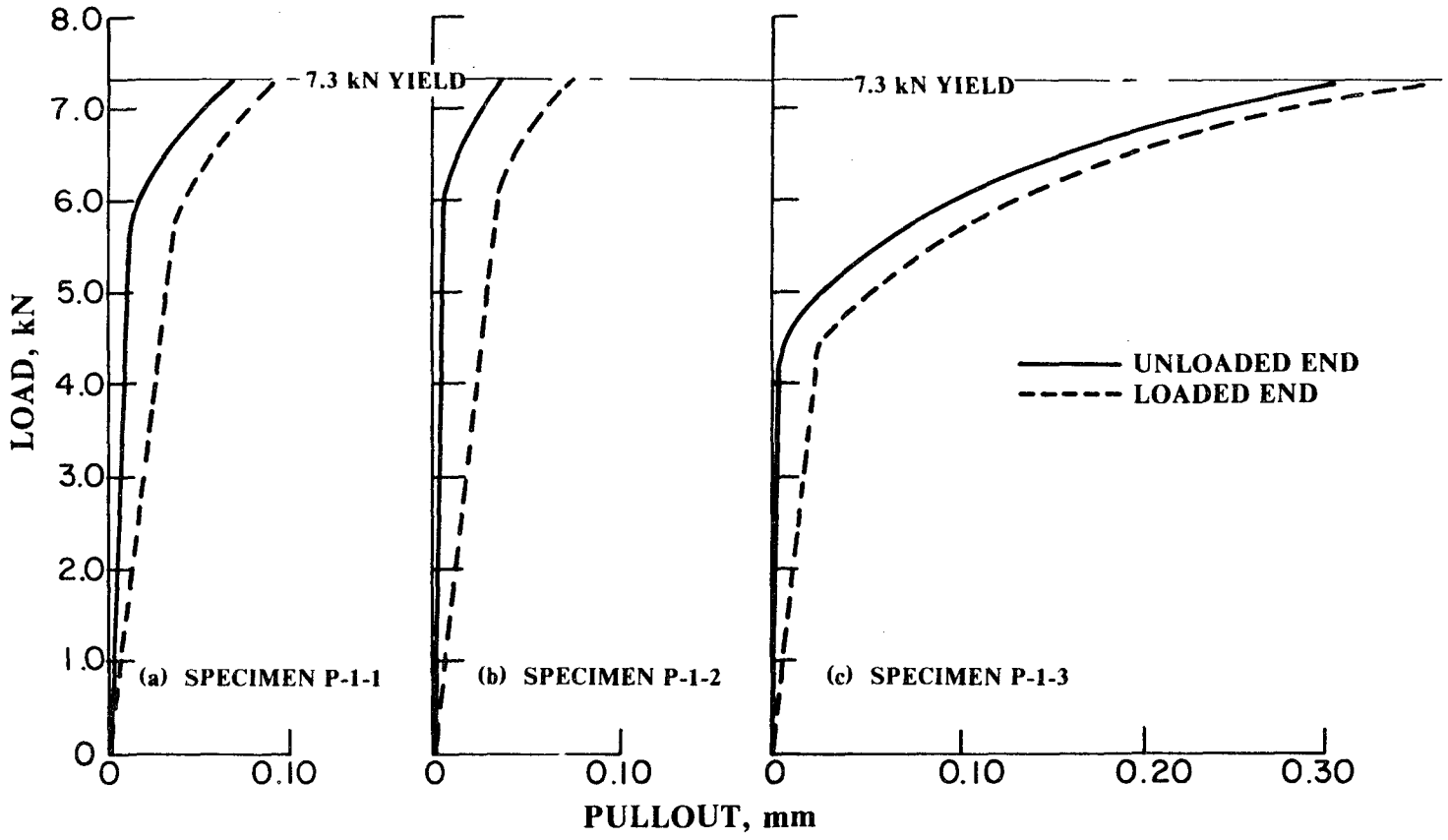

$$\Delta = \frac{1}{2}\,\sigma\frac{}{E}\Delta = \frac{1}{2}\,\frac{\sigma}{E}l_0 + \Delta_0 = \frac{Pl_0}{2EA} + \Delta_0$$

Δ = *PULLOUT @ LOADED END*

Δ_0 = *PULLOUT @ UNLOADED END*

$A = 16.13\ mm^2$

$E = 2 \times 10^{11}\ Pa$

FIG. A4 Pullout At Loaded & Unloaded Ends For Specimens P-1-1, P-1-2, P-1-3

NOTE: Numbers in parentheses are Accession Numbers assigned by the National Technical Information Service; these are followed by a price code. Copies of the reports may be ordered from the National Technical Information Service, 5285 Port Royal Road, Springfield, Virginia, 22161. Accession Numbers should be quoted on orders for reports (PB --- ---) and remittance must accompany each order. Reports without this information were not available at time of printing. The complete list of EERC reports (from EERC 67-1) is available upon request from the Earthquake Engineering Research Center, University of California, Berkeley, 47th Street and Hoffman Boulevard, Richmond, California 94804.

UCB/EERC-77/01 "PLUSH - A Computer Program for Probabilistic Finite Element Analysis of Seismic Soil-Structure Interaction," by M.P. Romo Organista, J. Lysmer and H.B. Seed - 1977 (PB81 177 651)A05

UCB/EERC-77/02 "Soil-Structure Interaction Effects at the Humboldt Bay Power Plant in the Ferndale Earthquake of June 7, 1975," by J.E. Valera, H.B. Seed, C.F. Tsai and J. Lysmer - 1977 (PB 265 795)A04

UCB/EERC-77/03 "Influence of Sample Disturbance on Sand Response to Cyclic Loading," by K. Mori, H.B. Seed and C.K. Chan - 1977 (PB 267 352)A04

UCB/EERC-77/04 "Seismological Studies of Strong Motion Records," by J. Shoja-Taheri - 1977 (PB 269 655)A10

UCB/EERC-77/05 Unassigned

UCB/EERC-77/06 "Developing Methodologies for Evaluating the Earthquake Safety of Existing Buildings," by No. 1 - B. Bresler; No. 2 - B. Bresler, T. Okada and D. Zisling; No. 3 - T. Okada and B. Bresler; No. 4 - V.V. Bertero and B. Bresler - 1977 (PB 267 354)A08

UCB/EERC-77/07 "A Literature Survey - Transverse Strength of Masonry Walls," by Y. Omote, R.L. Mayes, S.W. Chen and R.W. Clough - 1977 (PB 277 933)A07

UCB/EERC-77/08 "DRAIN-TABS: A Computer Program for Inelastic Earthquake Response of Three Dimensional Buildings," by R. Guendelman-Israel and G.H. Powell - 1977 (PB 270 693)A07

UCB/EERC-77/09 "SUBWALL: A Special Purpose Finite Element Computer Program for Practical Elastic Analysis and Design of Structural Walls with Substructure Option," by D.Q. Le, H. Peterson and E.P. Popov - 1977 (PB 270 567)A05

UCB/EERC-77/10 "Experimental Evaluation of Seismic Design Methods for Broad Cylindrical Tanks," by D.P. Clough (PB 272 280)A13

UCB/EERC-77/11 "Earthquake Engineering Research at Berkeley - 1976," - 1977 (PB 273 507)A09

UCB/EERC-77/12 "Automated Design of Earthquake Resistant Multistory Steel Building Frames," by N.D. Walker, Jr. - 1977 (PB 276 526)A09

UCB/EERC-77/13 "Concrete Confined by Rectangular Hoops Subjected to Axial Loads," by J. Vallenas, V.V. Bertero and E.P. Popov - 1977 (PB 275 165)A06

UCB/EERC-77/14 "Seismic Strain Induced in the Ground During Earthquakes," by Y. Sugimura - 1977 (PB 284 201)A04

UCB/EERC-77/15 Unassigned

UCB/EERC-77/16 "Computer Aided Optimum Design of Ductile Reinforced Concrete Moment Resisting Frames," by S.W. Zagajeski and V.V. Bertero - 1977 (PB 280 137)A07

UCB/EERC-77/17 "Earthquake Simulation Testing of a Stepping Frame with Energy-Absorbing Devices," by J.M. Kelly and D.F. Tsztoo - 1977 (PB 273 506)A04

UCB/EERC-77/18 "Inelastic Behavior of Eccentrically Braced Steel Frames under Cyclic Loadings," by C.W. Roeder and E.P. Popov - 1977 (PB 275 526)A15

UCB/EERC-77/19 "A Simplified Procedure for Estimating Earthquake-Induced Deformations in Dams and Embankments," by F.I. Makdisi and H.B. Seed - 1977 (PB 276 820)A04

UCB/EERC-77/20 "The Performance of Earth Dams during Earthquakes," by H.B. Seed, F.I. Makdisi and P. de Alba - 1977 (PB 276 821)A04

UCB/EERC-77/21 "Dynamic Plastic Analysis Using Stress Resultant Finite Element Formulation," by P. Lukkunapvasit and J.M. Kelly - 1977 (PB 275 453)A04

UCB/EERC-77/22 "Preliminary Experimental Study of Seismic Uplift of a Steel Frame," by R.W. Clough and A.A. Huckelbridge 1977 (PB 278 769)A08

UCB/EERC-77/23 "Earthquake Simulator Tests of a Nine-Story Steel Frame with Columns Allowed to Uplift," by A.A. Huckelbridge - 1977 (PB 277 944)A09

UCB/EERC-77/24 "Nonlinear Soil-Structure Interaction of Skew Highway Bridges," by M.-C. Chen and J. Penzien - 1977 (PB 276 176)A07

UCB/EERC-77/25 "Seismic Analysis of an Offshore Structure Supported on Pile Foundations," by D.D.-N. Liou and J. Penzien 1977 (PB 283 180)A06

UCB/EERC-77/26 "Dynamic Stiffness Matrices for Homogeneous Viscoelastic Half-Planes," by G. Dasgupta and A.K. Chopra - 1977 (PB 279 654)A06

UCB/EERC-77/27 "A Practical Soft Story Earthquake Isolation System," by J.M. Kelly, J.M. Eidinger and C.J. Derham - 1977 (PB 276 914)A07

UCB/EERC-77/28 "Seismic Safety of Existing Buildings and Incentives for Hazard Mitigation in San Francisco: An Exploratory Study," by A.J. Meltsner - 1977 (PB 281 970)A05

UCB/EERC-77/29 "Dynamic Analysis of Electrohydraulic Shaking Tables," by D. Rea, S. Abedi-Hayati and Y. Takahashi 1977 (PB 282 569)A04

UCB/EERC-77/30 "An Approach for Improving Seismic - Resistant Behavior of Reinforced Concrete Interior Joints," by B. Galunic, V.V. Bertero and E.P. Popov - 1977 (PB 290 870)A06

UCB/EERC-78/01 "The Development of Energy-Absorbing Devices for Aseismic Base Isolation Systems," by J.M. Kelly and D.F. Tsztoo - 1978 (PB 284 978)A04

UCB/EERC-78/02 "Effect of Tensile Prestrain on the Cyclic Response of Structural Steel Connections, by J.G. Bouwkamp and A. Mukhopadhyay - 1978

UCB/EERC-78/03 "Experimental Results of an Earthquake Isolation System using Natural Rubber Bearings," by J.M. Eidinger and J.M. Kelly - 1978 (PB 281 686)A04

UCB/EERC-78/04 "Seismic Behavior of Tall Liquid Storage Tanks," by A. Niwa - 1978 (PB 284 017)A14

UCB/EERC-78/05 "Hysteretic Behavior of Reinforced Concrete Columns Subjected to High Axial and Cyclic Shear Forces," by S.W. Zagajeski, V.V. Bertero and J.G. Bouwkamp - 1978 (PB 283 858)A13

UCB/EERC-78/06 "Three Dimensional Inelastic Frame Elements for the ANSR-I Program," by A. Riahi, D.G. Row and G.H. Powell - 1978 (PB 295 755)A04

UCB/EERC-78/07 "Studies of Structural Response to Earthquake Ground Motion," by O.A. Lopez and A.K. Chopra - 1978 (PB 282 790)A05

UCB/EERC-78/08 "A Laboratory Study of the Fluid-Structure Interaction of Submerged Tanks and Caissons in Earthquakes," by R.C. Byrd - 1978 (PB 284 957)A08

UCB/EERC-78/09 Unassigned

UCB/EERC-78/10 "Seismic Performance of Nonstructural and Secondary Structural Elements," by I. Sakamoto - 1978 (PB81 154 593)A05

UCB/EERC-78/11 "Mathematical Modelling of Hysteresis Loops for Reinforced Concrete Columns," by S. Nakata, T. Sproul and J. Penzien - 1978 (PB 298 274)A05

UCB/EERC-78/12 "Damageability in Existing Buildings," by T. Blejwas and B. Bresler - 1978 (PB 80 166 978)A05

UCB/EERC-78/13 "Dynamic Behavior of a Pedestal Base Multistory Building," by R.M. Stephen, E.L. Wilson, J.G. Bouwkamp and M. Button - 1978 (PB 286 650)A08

UCB/EERC-78/14 "Seismic Response of Bridges - Case Studies," by R.A. Imbsen, V. Nutt and J. Penzien - 1978 (PB 286 503)A10

UCB/EERC-78/15 "A Substructure Technique for Nonlinear Static and Dynamic Analysis," by D.G. Row and G.H. Powell - 1978 (PB 288 077)A10

UCB/EERC-78/16 "Seismic Risk Studies for San Francisco and for the Greater San Francisco Bay Area," by C.S. Oliveira - 1978 (PB 81 120 115)A07

UCB/EERC-78/17 "Strength of Timber Roof Connections Subjected to Cyclic Loads," by P. Gülkan, R.L. Mayes and R.W. Clough - 1978 (HUD-000 1491)A07

UCB/EERC-78/18 "Response of K-Braced Steel Frame Models to Lateral Loads," by J.G. Bouwkamp, R.M. Stephen and E.P. Popov - 1978

UCB/EERC-78/19 "Rational Design Methods for Light Equipment in Structures Subjected to Ground Motion," by J.L. Sackman and J.M. Kelly - 1978 (PB 292 357)A04

UCB/EERC-78/20 "Testing of a Wind Restraint for Aseismic Base Isolation," by J.M. Kelly and D.E. Chitty - 1978 (PB 292 833)A03

UCB/EERC-78/21 "APOLLO - A Computer Program for the Analysis of Pore Pressure Generation and Dissipation in Horizontal Sand Layers During Cyclic or Earthquake Loading," by P.P. Martin and H.B. Seed - 1978 (PB 292 835)A04

UCB/EERC-78/22 "Optimal Design of an Earthquake Isolation System," by M.A. Bhatti, K.S. Pister and E. Polak - 1978 (PB 294 735)A06

UCB/EERC-78/23 "MASH - A Computer Program for the Non-Linear Analysis of Vertically Propagating Shear Waves in Horizontally Layered Deposits," by P.P. Martin and H.B. Seed - 1978 (PB 293 101)A05

UCB/EERC-78/24 "Investigation of the Elastic Characteristics of a Three Story Steel Frame Using System Identification," by I. Kaya and H.D. McNiven - 1978 (PB 296 225)A06

UCB/EERC-78/25 "Investigation of the Nonlinear Characteristics of a Three-Story Steel Frame Using System Identification," by I. Kaya and H.D. McNiven - 1978 (PB 301 363)A05

UCB/EERC-78/26 "Studies of Strong Ground Motion in Taiwan," by Y.M. Hsiung, B.A. Bolt and J. Penzien - 1978 (PB 298 436)A06

UCB/EERC-78/27 "Cyclic Loading Tests of Masonry Single Piers: Volume 1 - Height to Width Ratio of 2," by P.A. Hidalgo, R.L. Mayes, H.D. McNiven and R.W. Clough - 1978 (PB 296 211)A07

UCB/EERC-78/28 "Cyclic Loading Tests of Masonry Single Piers: Volume 2 - Height to Width Ratio of 1," by S.-W.J. Chen, P.A. Hidalgo, R.L. Mayes, R.W. Clough and H.D. McNiven - 1978 (PB 296 212)A09

UCB/EERC-78/29 "Analytical Procedures in Soil Dynamics," by J. Lysmer - 1978 (PB 298 445)A06

UCB/EERC-79/01 "Hysteretic Behavior of Lightweight Reinforced Concrete Beam-Column Subassemblages," by B. Forzani, E.P. Popov and V.V. Bertero - April 1979(PB 298 267)A06

UCB/EERC-79/02 "The Development of a Mathematical Model to Predict the Flexural Response of Reinforced Concrete Beams to Cyclic Loads, Using System Identification," by J. Stanton & H. McNiven - Jan. 1979(PB 295 875)A10

UCB/EERC-79/03 "Linear and Nonlinear Earthquake Response of Simple Torsionally Coupled Systems," by C.L. Kan and A.K. Chopra - Feb. 1979(PB 298 262)A06

UCB/EERC-79/04 "A Mathematical Model of Masonry for Predicting its Linear Seismic Response Characteristics," by Y. Mengi and H.D. McNiven - Feb. 1979(PB 298 266)A06

UCB/EERC-79/05 "Mechanical Behavior of Lightweight Concrete Confined by Different Types of Lateral Reinforcement," by M.A. Manrique, V.V. Bertero and E.P. Popov - May 1979(PB 301 114)A06

UCB/EERC-79/06 "Static Tilt Tests of a Tall Cylindrical Liquid Storage Tank," by R.W. Clough and A. Niwa - Feb. 1979 (PB 301 167)A06

UCB/EERC-79/07 "The Design of Steel Energy Absorbing Restrainers and Their Incorporation into Nuclear Power Plants for Enhanced Safety: Volume 1 - Summary Report," by P.N. Spencer, V.F. Zackay, and E.R. Parker - Feb. 1979(UCB/EERC-79/07)A09

UCB/EERC-79/08 "The Design of Steel Energy Absorbing Restrainers and Their Incorporation into Nuclear Power Plants for Enhanced Safety: Volume 2 - The Development of Analyses for Reactor System Piping,""Simple Systems" by M.C. Lee, J. Penzien, A.K. Chopra and K. Suzuki "Complex Systems" by G.H. Powell, E.L. Wilson, R.W. Clough and D.G. Row - Feb. 1979(UCB/EERC-79/08)A10

UCB/EERC-79/09 "The Design of Steel Energy Absorbing Restrainers and Their Incorporation into Nuclear Power Plants for Enhanced Safety: Volume 3 - Evaluation of Commercial Steels," by W.S. Owen, R.M.N. Pelloux, R.O. Ritchie, M. Faral, T. Ohhashi, J. Toplosky, S.J. Hartman, V.F. Zackay and E.R. Parker - Feb. 1979(UCB/EERC-79/09)A04

UCB/EERC-79/10 "The Design of Steel Energy Absorbing Restrainers and Their Incorporation into Nuclear Power Plants for Enhanced Safety: Volume 4 - A Review of Energy-Absorbing Devices," by J.M. Kelly and M.S. Skinner - Feb. 1979(UCB/EERC-79/10)A04

UCB/EERC-79/11 "Conservatism In Summation Rules for Closely Spaced Modes," by J.M. Kelly and J.L. Sackman - May 1979(PB 301 328)A03

UCB/EERC-79/12 "Cyclic Loading Tests of Masonry Single Piers; Volume 3 - Height to Width Ratio of 0.5," by P.A. Hidalgo, R.L. Mayes, H.D. McNiven and R.W. Clough - May 1979(PB 301 321)A08

UCB/EERC-79/13 "Cyclic Behavior of Dense Course-Grained Materials in Relation to the Seismic Stability of Dams," by N.G. Banerjee, H.B. Seed and C.K. Chan - June 1979(PB 301 373)A13

UCB/EERC-79/14 "Seismic Behavior of Reinforced Concrete Interior Beam-Column Subassemblages," by S. Viwathanatepa, E.P. Popov and V.V. Bertero - June 1979(PB 301 326)A10

UCB/EERC-79/15 "Optimal Design of Localized Nonlinear Systems with Dual Performance Criteria Under Earthquake Excitations," by M.A. Bhatti - July 1979(PB 80 167 109)A06

UCB/EERC-79/16 "OPTDYN - A General Purpose Optimization Program for Problems with or without Dynamic Constraints," by M.A. Bhatti, E. Polak and K.S. Pister - July 1979(PB 80 167 091)A05

UCB/EERC-79/17 "ANSR-II, Analysis of Nonlinear Structural Response, Users Manual," by D.P. Mondkar and G.H. Powell July 1979(PB 80 113 301)A05

UCB/EERC-79/18 "Soil Structure Interaction in Different Seismic Environments," A. Gomez-Masso, J. Lysmer, J.-C. Chen and H.B. Seed - August 1979(PB 80 101 520)A04

UCB/EERC-79/19 "ARMA Models for Earthquake Ground Motions," by M.K. Chang, J.W. Kwiatkowski, R.F. Nau, R.M. Oliver and K.S. Pister - July 1979(PB 301 166)A05

UCB/EERC-79/20 "Hysteretic Behavior of Reinforced Concrete Structural Walls," by J.M. Vallenas, V.V. Bertero and E.P. Popov - August 1979(PB 80 165 905)A12

UCB/EERC-79/21 "Studies on High-Frequency Vibrations of Buildings - 1: The Column Effect," by J. Lubliner - August 1979 (PB 80 158 553)A03

UCB/EERC-79/22 "Effects of Generalized Loadings on Bond Reinforcing Bars Embedded in Confined Concrete Blocks," by S. Viwathanatepa, E.P. Popov and V.V. Bertero - August 1979(PB 81 124 018)A14

UCB/EERC-79/23 "Shaking Table Study of Single-Story Masonry Houses, Volume 1: Test Structures 1 and 2," by P. Gülkan, R.L. Mayes and R.W. Clough - Sept. 1979 (HUD-000 1763)A12

UCB/EERC-79/24 "Shaking Table Study of Single-Story Masonry Houses, Volume 2: Test Structures 3 and 4," by P. Gülkan, R.L. Mayes and R.W. Clough - Sept. 1979 (HUD-000 1836)A12

UCB/EERC-79/25 "Shaking Table Study of Single-Story Masonry Houses, Volume 3: Summary, Conclusions and Recommendations," by R.W. Clough, R.L. Mayes and P. Gülkan - Sept. 1979 (HUD-000 1837)A06

UCB/EERC-79/26 "Recommendations for a U.S.-Japan Cooperative Research Program Utilizing Large-Scale Testing Facilities," by U.S.-Japan Planning Group - Sept. 1979(PB 301 407)A06

UCB/EERC-79/27 "Earthquake-Induced Liquefaction Near Lake Amatitlan, Guatemala," by H.B. Seed, I. Arango, C.K. Chan, A. Gomez-Masso and R. Grant de Ascoli - Sept. 1979(NUREG-CR1341)A03

UCB/EERC-79/28 "Infill Panels: Their Influence on Seismic Response of Buildings," by J.W. Axley and V.V. Bertero Sept. 1979(PB 80 163 371)A10

UCB/EERC-79/29 "3D Truss Bar Element (Type 1) for the ANSR-II Program," by D.P. Mondkar and G.H. Powell - Nov. 1979 (PB 80 169 709)A02

UCB/EERC-79/30 "2D Beam-Column Element (Type 5 - Parallel Element Theory) for the ANSR-II Program," by D.G. Row, G.H. Powell and D.P. Mondkar - Dec. 1979(PB 80 167 224)A03

UCB/EERC-79/31 "3D Beam-Column Element (Type 2 - Parallel Element Theory) for the ANSR-II Program," by A. Riahi, G.H. Powell and D.P. Mondkar - Dec. 1979(PB 80 167 216)A03

UCB/EERC-79/32 "On Response of Structures to Stationary Excitation," by A. Der Kiureghian - Dec. 1979(PB 80166 929)A03

UCB/EERC-79/33 "Undisturbed Sampling and Cyclic Load Testing of Sands," by S. Singh, H.B. Seed and C.K. Chan Dec. 1979(ADA 087 298)A07

UCB/EERC-79/34 "Interaction Effects of Simultaneous Torsional and Compressional Cyclic Loading of Sand," by P.M. Griffin and W.N. Houston - Dec. 1979(ADA 092 352)A15

UCB/EERC-80/01 "Earthquake Response of Concrete Gravity Dams Including Hydrodynamic and Foundation Interaction Effects," by A.K. Chopra, P. Chakrabarti and S. Gupta - Jan. 1980(AD-A087297)A10

UCB/EERC-80/02 "Rocking Response of Rigid Blocks to Earthquakes," by C.S. Yim, A.K. Chopra and J. Penzien - Jan. 1980 (PB80 166 002)A04

UCB/EERC-80/03 "Optimum Inelastic Design of Seismic-Resistant Reinforced Concrete Frame Structures," by S.W. Zagajeski and V.V. Bertero - Jan. 1980(PB80 164 635)A06

UCB/EERC-80/04 "Effects of Amount and Arrangement of Wall-Panel Reinforcement on Hysteretic Behavior of Reinforced Concrete Walls," by R. Iliya and V.V. Bertero - Feb. 1980(PB81 122 525)A09

UCB/EERC-80/05 "Shaking Table Research on Concrete Dam Models," by A. Niwa and R.W. Clough - Sept. 1980(PB81 122 368)A06

UCB/EERC-80/06 "The Design of Steel Energy-Absorbing Restrainers and their Incorporation into Nuclear Power Plants for Enhanced Safety (Vol 1A): Piping with Energy Absorbing Restrainers: Parameter Study on Small Systems," by G.H. Powell, C. Oughourlian and J. Simons - June 1980

UCB/EERC-80/07 "Inelastic Torsional Response of Structures Subjected to Earthquake Ground Motions," by Y. Yamazaki April 1980(PB81 122 327)A08

UCB/EERC-80/08 "Study of X-Braced Steel Frame Structures Under Earthquake Simulation," by Y. Ghanaat - April 1980 (PB81 122 335)A11

UCB/EERC-80/09 "Hybrid Modelling of Soil-Structure Interaction," by S. Gupta, T.W. Lin, J. Penzien and C.S. Yeh May 1980(PB81 122 319)A07

UCB/EERC-80/10 "General Applicability of a Nonlinear Model of a One Story Steel Frame," by B.I. Sveinsson and H.D. McNiven - May 1980(PB81 124 877)A06

UCB/EERC-80/11 "A Green-Function Method for Wave Interaction with a Submerged Body," by W. Kioka - April 1980 (PB81 122 269)A07

UCB/EERC-80/12 "Hydrodynamic Pressure and Added Mass for Axisymmetric Bodies," by F. Nilrat - May 1980(PB81 122 343)A08

UCB/EERC-80/13 "Treatment of Non-Linear Drag Forces Acting on Offshore Platforms," by B.V. Dao and J. Penzien May 1980(PB81 153 413)A07

UCB/EERC-80/14 "2D Plane/Axisymmetric Solid Element (Type 3 - Elastic or Elastic-Perfectly Plastic) for the ANSR-II Program," by D.P. Mondkar and G.H. Powell - July 1980(PB81 122 350)A03

UCB/EERC-80/15 "A Response Spectrum Method for Random Vibrations," by A. Der Kiureghian - June 1980(PB81 122 301)A03

UCB/EERC-80/16 "Cyclic Inelastic Buckling of Tubular Steel Braces," by V.A. Zayas, E.P. Popov and S.A. Mahin June 1980(PB81 124 885)A10

UCB/EERC-80/17 "Dynamic Response of Simple Arch Dams Including Hydrodynamic Interaction," by C.S. Porter and A.K. Chopra - July 1980(PB81 124 000)A13

UCB/EERC-80/18 "Experimental Testing of a Friction Damped Aseismic Base Isolation System with Fail-Safe Characteristics," by J.M. Kelly, K.E. Beucke and M.S. Skinner - July 1980(PB81 148 595)A04

UCB/EERC-80/19 "The Design of Steel Energy-Absorbing Restrainers and their Incorporation into Nuclear Power Plants for Enhanced Safety (Vol 1B): Stochastic Seismic Analyses of Nuclear Power Plant Structures and Piping Systems Subjected to Multiple Support Excitations," by M.C. Lee and J. Penzien - June 1980

UCB/EERC-80/20 "The Design of Steel Energy-Absorbing Restrainers and their Incorporation into Nuclear Power Plants for Enhanced Safety (Vol 1C): Numerical Method for Dynamic Substructure Analysis," by J.M. Dickens and E.L. Wilson - June 1980

UCB/EERC-80/21 "The Design of Steel Energy-Absorbing Restrainers and their Incorporation into Nuclear Power Plants for Enhanced Safety (Vol 2): Development and Testing of Restraints for Nuclear Piping Systems," by J.M. Kelly and M.S. Skinner - June 1980

UCB/EERC-80/22 "3D Solid Element (Type 4-Elastic or Elastic-Perfectly-Plastic) for the ANSR-II Program," by D.P. Mondkar and G.H. Powell - July 1980(PB81 123 242)A03

UCB/EERC-80/23 "Gap-Friction Element (Type 5) for the ANSR-II Program," by D.P. Mondkar and G.H. Powell - July 1980 (PB81 122 285)A03

UCB/EERC-80/24 "U-Bar Restraint Element (Type 11) for the ANSR-II Program," by C. Oughourlian and G.H. Powell July 1980(PB81 122 293)A03

UCB/EERC-80/25 "Testing of a Natural Rubber Base Isolation System by an Explosively Simulated Earthquake," by J.M. Kelly - August 1980(PB81 201 360)A04

UCB/EERC-80/26 "Input Identification from Structural Vibrational Response," by Y. Hu - August 1980(PB81 152 308)A05

UCB/EERC-80/27 "Cyclic Inelastic Behavior of Steel Offshore Structures," by V.A. Zayas, S.A. Mahin and E.P. Popov August 1980(PB81 196 180)A15

UCB/EERC-80/28 "Shaking Table Testing of a Reinforced Concrete Frame with Biaxial Response," by M.G. Oliva October 1980(PB81 154 304)A10

UCB/EERC-80/29 "Dynamic Properties of a Twelve-Story Prefabricated Panel Building," by J.G. Bouwkamp, J.P. Kollegger and R.M. Stephen - October 1980(PB82 117 128)A06

UCB/EERC-80/30 "Dynamic Properties of an Eight-Story Prefabricated Panel Building," by J.G. Bouwkamp, J.P. Kollegger and R.M. Stephen - October 1980(PB81 200 313)A05

UCB/EERC-80/31 "Predictive Dynamic Response of Panel Type Structures Under Earthquakes," by J.P. Kollegger and J.G. Bouwkamp - October 1980(PB81 152 316)A04

UCB/EERC-80/32 "The Design of Steel Energy-Absorbing Restrainers and their Incorporation into Nuclear Power Plants for Enhanced Safety (Vol 3): Testing of Commercial Steels in Low-Cycle Torsional Fatigue," by P. Spencer, E.R. Parker, E. Jongewaard and M. Drory

UCB/EERC-80/33 "The Design of Steel Energy-Absorbing Restrainers and their Incorporation into Nuclear Power Plants for Enhanced Safety (Vol 4): Shaking Table Tests of Piping Systems with Energy-Absorbing Restrainers," by S.F. Stiemer and W.G. Godden - Sept. 1980

UCB/EERC-80/34 "The Design of Steel Energy-Absorbing Restrainers and their Incorporation into Nuclear Power Plants for Enhanced Safety (Vol 5): Summary Report," by P. Spencer

UCB/EERC-80/35 "Experimental Testing of an Energy-Absorbing Base Isolation System," by J.M. Kelly, M.S. Skinner and K.E. Beucke - October 1980(PB81 154 072)A04

UCB/EERC-80/36 "Simulating and Analyzing Artificial Non-Stationary Earthquake Ground Motions," by R.F. Nau, R.M. Oliver and K.S. Pister - October 1980(PB81 153 397)A04

UCB/EERC-80/37 "Earthquake Engineering at Berkeley - 1980," - Sept. 1980(PB81 205 674)A09

UCB/EERC-80/38 "Inelastic Seismic Analysis of Large Panel Buildings," by V. Schricker and G.H. Powell - Sept. 1980 (PB81 154 338)A13

UCB/EERC-80/39 "Dynamic Response of Embankment, Concrete-Gravity and Arch Dams Including Hydrodynamic Interaction," by J.F. Hall and A.K. Chopra - October 1980(PB81 152 324)A11

UCB/EERC-80/40 "Inelastic Buckling of Steel Struts Under Cyclic Load Reversal," by R.G. Black, W.A. Wenger and E.P. Popov - October 1980(PB81 154 312)A08

UCB/EERC-80/41 "Influence of Site Characteristics on Building Damage During the October 3, 1974 Lima Earthquake," by P. Repetto, I. Arango and H.B. Seed - Sept. 1980(PB81 161 739)A05

UCB/EERC-80/42 "Evaluation of a Shaking Table Test Program on Response Behavior of a Two Story Reinforced Concrete Frame," by J.M. Blondet, R.W. Clough and S.A. Mahin

UCB/EERC-80/43 "Modelling of Soil-Structure Interaction by Finite and Infinite Elements," by F. Medina - December 1980(PB81 229 270)A04

UCB/EERC-81/01 "Control of Seismic Response of Piping Systems and Other Structures by Base Isolation," edited by J.M. Kelly - January 1981 (PB81 200 735)A05

UCB/EERC-81/02 "OPTNSR - An Interactive Software System for Optimal Design of Statically and Dynamically Loaded Structures with Nonlinear Response," by M.A. Bhatti, V. Ciampi and K.S. Pister - January 1981 (PB81 218 851)A09

UCB/EERC-81/03 "Analysis of Local Variations in Free Field Seismic Ground Motions," by J.-C. Chen, J. Lysmer and H.B. Seed - January 1981 (AD-A099508)A13

UCB/EERC-81/04 "Inelastic Structural Modeling of Braced Offshore Platforms for Seismic Loading," by V.A. Zayas, P.-S.B. Shing, S.A. Mahin and E.P. Popov - January 1981(PB82 138 777)A07

UCB/EERC-81/05 "Dynamic Response of Light Equipment in Structures," by A. Der Kiureghian, J.L. Sackman and B. Nour-Omid - April 1981 (PB81 218 497)A04

UCB/EERC-81/06 "Preliminary Experimental Investigation of a Broad Base Liquid Storage Tank," by J.G. Bouwkamp, J.P. Kollegger and R.M. Stephen - May 1981(PB82 140 385)A03

UCB/EERC-81/07 "The Seismic Resistant Design of Reinforced Concrete Coupled Structural Walls," by A.E. Aktan and V.V. Bertero - June 1981(PB82 113 358)A11

UCB/EERC-81/08 "The Undrained Shearing Resistance of Cohesive Soils at Large Deformations," by M.R. Pyles and H.B. Seed - August 1981

UCB/EERC-81/09 "Experimental Behavior of a Spatial Piping System with Steel Energy Absorbers Subjected to a Simulated Differential Seismic Input," by S.F. Stiemer, W.G. Godden and J.M. Kelly - July 1981

UCB/EERC-81/10 "Evaluation of Seismic Design Provisions for Masonry in the United States," by B.I. Sveinsson, R.L. Mayes and H.D. McNiven - August 1981 (PB82 166 075)A08

UCB/EERC-81/11 "Two-Dimensional Hybrid Modelling of Soil-Structure Interaction," by T.-J. Tzong, S. Gupta and J. Penzien - August 1981(PB82 142 118)A04

UCB/EERC-81/12 "Studies on Effects of Infills in Seismic Resistant R/C Construction," by S. Brokken and V.V. Bertero - September 1981 (PB82 166 190)A09

UCB/EERC-81/13 "Linear Models to Predict the Nonlinear Seismic Behavior of a One-Story Steel Frame," by H. Valdimarsson, A.H. Shah and H.D. McNiven - September 1981(PB82 138 793)A07

UCB/EERC-81/14 "TLUSH: A Computer Program for the Three-Dimensional Dynamic Analysis of Earth Dams," by T. Kagawa, L.H. Mejia, H.B. Seed and J. Lysmer - September 1981(PB82 139 940)A06

UCB/EERC-81/15 "Three Dimensional Dynamic Response Analysis of Earth Dams," by L.H. Mejia and H.B. Seed - September 1981 (PB82 137 274)A12

UCB/EERC-81/16 "Experimental Study of Lead and Elastomeric Dampers for Base Isolation Systems," by J.M. Kelly and S.B. Hodder - October 1981 (PB82 166 182)A05

UCB/EERC-81/17 "The Influence of Base Isolation on the Seismic Response of Light Secondary Equipment," by J.M. Kelly - April 1981 (PB82 255 266)A04

UCB/EERC-81/18 "Studies on Evaluation of Shaking Table Response Analysis Procedures," by J. Marcial Blondet - November 1981 (PB82 197 278)A10

UCB/EERC-81/19 "DELIGHT.STRUCT: A Computer-Aided Design Environment for Structural Engineering," by R.J. Balling, K.S. Pister and E. Polak - December 1981 (PB82 218 496)A07

UCB/EERC-81/20 "Optimal Design of Seismic-Resistant Planar Steel Frames," by R.J. Balling, V. Ciampi, K.S. Pister and E. Polak - December 1981 (PB82 220 179)A07

UCB/EERC-82/01 "Dynamic Behavior of Ground for Seismic Analysis of Lifeline Systems," by T. Sato and A. Der Kiureghian - January 1982 (PB82 218 926)A05

UCB/EERC-82/02 "Shaking Table Tests of a Tubular Steel Frame Model," by Y. Ghanaat and R. W. Clough - January 1982 (PB82 220 161)A07

UCB/EERC-82/03 "Behavior of a Piping System under Seismic Excitation: Experimental Investigations of a Spatial Piping System supported by Mechanical Shock Arrestors and Steel Energy Absorbing Devices under Seismic Excitation," by S. Schneider, H.-M. Lee and W. G. Godden - May 1982 (PB83 172 544)A09

UCB/EERC-82/04 "New Approaches for the Dynamic Analysis of Large Structural Systems," by E. L. Wilson - June 1982 (PB83 148 080)A05

UCB/EERC-82/05 "Model Study of Effects of Damage on the Vibration Properties of Steel Offshore Platforms," by F. Shahrivar and J. G. Bouwkamp - June 1982 (PB83 148 742)A10

UCB/EERC-82/06 "States of the Art and Practice in the Optimum Seismic Design and Analytical Response Prediction of R/C Frame-Wall Structures," by A. E. Aktan and V. V. Bertero - July 1982 (PB83 147 736)A05

UCB/EERC-82/07 "Further Study of the Earthquake Response of a Broad Cylindrical Liquid-Storage Tank Model," by G. C. Manos and R. W. Clough - July 1982 (PB83 147 744)A11

UCB/EERC-82/08 "An Evaluation of the Design and Analytical Seismic Response of a Seven Story Reinforced Concrete Frame - Wall Structure," by F. A. Charney and V. V. Bertero - July 1982(PB83 157 628)A09

UCB/EERC-82/09 "Fluid-Structure Interactions: Added Mass Computations for Incompressible Fluid," by J. S.-H. Kuo - August 1982 (PB83 156 281)A07

UCB/EERC-82/10 "Joint-Opening Nonlinear Mechanism: Interface Smeared Crack Model," by J. S.-H. Kuo - August 1982 (PB83 149 195)A05

UCB/EERC-82/11 "Dynamic Response Analysis of Techi Dam," by R. W. Clough, R. M. Stephen and J. S.-H. Kuo - August 1982 (PB83 147 496)A06

UCB/EERC-82/12 "Prediction of the Seismic Responses of R/C Frame-Coupled Wall Structures," by A. E. Aktan, V. V. Bertero and M. Piazza - August 1982 (PB83 149 203)A09

UCB/EERC-82/13 "Preliminary Report on the SMART 1 Strong Motion Array in Taiwan," by B. A. Bolt, C. H. Loh, J. Penzien, Y. B. Tsai and Y. T. Yeh - August 1982 (PB83 159 400)A10

UCB/EERC-82/14 "Shaking-Table Studies of an Eccentrically X-Braced Steel Structure," by M. S. Yang - September 1982 (PB83 260 778)A12

UCB/EERC-82/15 "The Performance of Stairways in Earthquakes," by C. Roha, J. W. Axley and V. V. Bertero - September 1982 (PB83 157 693)A07

UCB/EERC-82/16 "The Behavior of Submerged Multiple Bodies in Earthquakes," by W.-G. Liao - Sept. 1982 (PB83 158 709)A07

UCB/EERC-82/17 "Effects of Concrete Types and Loading Conditions on Local Bond-Slip Relationships," by A. D. Cowell, E. P. Popov and V. V. Bertero - September 1982 (PB83 153 577)A04

UCB/EERC-82/18 "Mechanical Behavior of Shear Wall Vertical Boundary Members: An Experimental Investigation," by M. T. Wagner and V. V. Bertero - October 1982 (PB83 159 764)A05

UCB/EERC-82/19 "Experimental Studies of Multi-support Seismic Loading on Piping Systems," by J. M. Kelly and A. D. Cowell - November 1982

UCB/EERC-82/20 "Generalized Plastic Hinge Concepts for 3D Beam-Column Elements," by P. F.-S. Chen and G. H. Powell - November 1982 (PB83 247 981)A13

UCB/EERC-82/21 "ANSR-III: General Purpose Computer Program for Nonlinear Structural Analysis," by C. V. Oughourlian and G. H. Powell - November 1982 (PB83 251 330)A12

UCB/EERC-82/22 "Solution Strategies for Statically Loaded Nonlinear Structures," by J. W. Simons and G. H. Powell - November 1982 (PB83 197 970)A06

UCB/EERC-82/23 "Analytical Model of Deformed Bar Anchorages under Generalized Excitations," by V. Ciampi, R. Eligehausen, V. V. Bertero and E. P. Popov - November 1982 (PB83 169 532)A06

UCB/EERC-82/24 "A Mathematical Model for the Response of Masonry Walls to Dynamic Excitations," by H. Sucuoğlu, Y. Mengi and H. D. McNiven - November 1982 (PB83 169 011)A07

UCB/EERC-82/25 "Earthquake Response Considerations of Broad Liquid Storage Tanks," by F. J. Cambra - November 1982 (PB83 251 215)A09

UCB/EERC-82/26 "Computational Models for Cyclic Plasticity, Rate Dependence and Creep," by B. Mosaddad and G. H. Powell - November 1982 (PB83 245 829)A08

UCB/EERC-82/27 "Inelastic Analysis of Piping and Tubular Structures," by M. Mahasuverachai and G. H. Powell - November 1982 (PB83 249 987)A07

UCB/EERC-83/01 "The Economic Feasibility of Seismic Rehabilitation of Buildings by Base Isolation," by J. M. Kelly - January 1983 (PB83 197 988)A05

UCB/EERC-83/02 "Seismic Moment Connections for Moment-Resisting Steel Frames," by E. P. Popov - January 1983 (PB83 195 412)A04

UCB/EERC-83/03 "Design of Links and Beam-to-Column Connections for Eccentrically Braced Steel Frames," by E. P. Popov and J. O. Malley - January 1983 (PB83 194 811)A04

UCB/EERC-83/04 "Numerical Techniques for the Evaluation of Soil-Structure Interaction Effects in the Time Domain," by E. Bayo and E. L. Wilson - February 1983 (PB83 245 605)A09

UCB/EERC-83/05 "A Transducer for Measuring the Internal Forces in the Columns of a Frame-Wall Reinforced Concrete Structure," by R. Sause and V. V. Bertero - May 1983 (PB84 119 494)A06

UCB/EERC-83/06 "Dynamic Interactions between Floating Ice and Offshore Structures," by P. Croteau - May 1983 (PB84 119 486)A16

UCB/EERC-83/07 "Dynamic Analysis of Multiply Tuned and Arbitrarily Supported Secondary Systems," by T. Igusa and A. Der Kiureghian - June 1983 (PB84 118 272)A11

UCB/EERC-83/08 "A Laboratory Study of Submerged Multi-body Systems in Earthquakes," by G. R. Ansari - June 1983 (PB83 261 842)A17

UCB/EERC-83/09 "Effects of Transient Foundation Uplift on Earthquake Response of Structures," by C.-S. Yim and A. K. Chopra - June 1983 (PB83 261 396)A07

UCB/EERC-83/10 "Optimal Design of Friction-Braced Frames under Seismic Loading," by M. A. Austin and K. S. Pister - June 1983 (PB84 119 288)A06

UCB/EERC-83/11 "Shaking Table Study of Single-Story Masonry Houses: Dynamic Performance under Three Component Seismic Input and Recommendations," by G. C. Manos, R. W. Clough and R. L. Mayes - June 1983

UCB/EERC-83/12 "Experimental Error Propagation in Pseudodynamic Testing," by P. B. Shing and S. A. Mahin - June 1983 (PB84 119 270)A09

UCB/EERC-83/13 "Experimental and Analytical Predictions of the Mechanical Characteristics of a 1/5-scale Model of a 7-story R/C Frame-Wall Building Structure," by A. E. Aktan, V. V. Bertero, A. A. Chowdhury and T. Nagashima - August 1983 (PB84 119 213)A07

UCB/EERC-83/14 "Shaking Table Tests of Large-Panel Precast Concrete Building System Assemblages," by M. G. Oliva and R. W. Clough - August 1983

UCB/EERC-83/15 "Seismic Behavior of Active Beam Links in Eccentrically Braced Frames," by K. D. Hjelmstad and E. P. Popov - July 1983 (PB84 119 676)A09

UCB/EERC-83/16 "System Identification of Structures with Joint Rotation," by J. S. Dimsdale and H. D. McNiven - July 1983

UCB/EERC-83/17 "Construction of Inelastic Response Spectra for Single-Degree-of-Freedom Systems," by S. Mahin and J. Lin - July 1983

UCB/EERC-83/18 "Interactive Computer Analysis Methods for Predicting the Inelastic Cyclic Behaviour of Structural Sections," by S. Kaba and S. Mahin - July 1983 (PB84 192 012) A06

UCB/EERC-83/19 "Effects of Bond Deterioration on Hysteretic Behavior of Reinforced Concrete Joints," by F.C. Filippou, E.P. Popov and V.V. Bertero - August 1983 (PB84 192 020) A10

UCB/EERC-83/20 "Analytical and Experimental Correlation of Large-Panel Precast Building System Performance," by M.G. Oliva, R.W. Clough, M. Velkov, P. Gavrilovic and J. Petrovski - November 1983

UCB/EERC-83/21 "Mechanical Characteristics of Materials Used in a 1/5 Scale Model of a 7-Story Reinforced Concrete Test Structure," by V.V. Bertero, A.E. Aktan, H.G. Harris and A.A. Chowdhury - September 1983 (PB84 193 697) A05

UCB/EERC-83/22 "Hybrid Modelling of Soil-Structure Interaction in Layered Media," by T.-J. Tzong and J. Penzien - October 1983 (PB84 192 178) A08

UCB/EERC-83/23 "Local Bond Stress-Slip Relationships of Deformed Bars under Generalized Excitations," by R. Eligehausen, E.P. Popov and V.V. Bertero - October 1983 (PB84 192 848) A09

UCB/EERC-83/24 "Design Considerations for Shear Links in Eccentrically Braced Frames," by J.O. Malley and E.P. Popov - November 1983 (PB84 192 186) A07

UCB/EERC-84/01 "Pseudodynamic Test Method for Seismic Performance Evaluation: Theory and Implementation," by P.-S. B. Shing and S. A. Mahin - January 1984 (PB84 190 644) A08

UCB/EERC-84/02 "Dynamic Response Behavior of Xiang Hong Dian Dam," by R.W. Clough, K.-T. Chang, H.-Q. Chen, R.M. Stephen, G.-L. Wang, and Y. Ghanaat - April 1984

UCB/EERC-84/03 "Refined Modelling of Reinforced Concrete Columns for Seismic Analysis," by S.A. Kaba and S.A. Mahin - April, 1984

UCB/EERC-84/04 "A New Floor Response Spectrum Method for Seismic Analysis of Multiply Supported Secondary Systems," by A. Asfura and A. Der Kiureghian - June 1984

UCB/EERC-84/05 "Earthquake Simulation Tests and Associated Studies of a 1/5th-scale Model of a 7-Story R/C Frame-Wall Test Structure," by V.V. Bertero, A.E. Aktan, F.A. Charney and R. Sause - June 1984

UCB/EERC-84/06 "R/C Structural Walls: Seismic Design for Shear," by A.E. Aktan and V.V. Bertero

UCB/EERC-84/07 "Behavior of Interior and Exterior Flat-Plate Connections subjected to Inelastic Load Reversals," by H.L. Zee and J.P. Moehle